Università degli Studi di Cagliari

DOTTORATO DI RICERCA

In Scienze e Tecnologie Chimiche

Ciclo XXX

# TITOLO TESI

Immobilization of enzymes on SBA-15 and ZIF-8

for biocatalytic applications

Settore scientifico disciplinari di afferenza

CHIM/02


| | |
|---|---|
| Presentata da: | Federica Pitzalis |
| Coordinatore Dottorato | Prof. Stefano Enzo |
| Tutor | Prof. Andrea Salis |


Esame finale anno accademico 2016 – 2017

Tesi discussa nella sessione d'esame Marzo 2018

Dedicated to Riccardo, my husband

and to Vitalia and Raimondo, my parents

# Acknowledgements

Thanks are due to Agenzia delle Dogane e dei Monopoli for financing this PhD work.
I thank the Senior Manager and all the collegues of Laboratori e Servizi Chimici of Genova, and special thanks are due to Mr Savino Disanti and Dr. Luca Mogavero.

Foremost I am grateful to Prof. Andrea Salis and Prof. Maura Monduzzi for having included me in their research group and for their valuable and irreplaceable advice and precious encouragement.

Furthermore I am grateful to Prof. Davide Carboni, Prof. Luca Malfatti and Dr. Barbara Lasio for the support received during the collaboration with the "Laboratorio di Scienza dei Materiali e Nanotecnologie", Università degli Studi di Sassari.

Moreover, a special thanks is due to senior researchers Dr. Martina Pilloni and Dr. Francesco Secci for their precious advice.

Special acknowledgments are dedicated to my colleague and officemate Valentina Nairi for all the good and bad moments we shared, to senior researchers Dr. Francesca Cugia and Dr. Luca Medda, and Dr. Valentina Cabras for their kindness, their friendship and help, and the colleagues Cristina Carucci and Maryam Naseri and are thanked for their fundamental contribution to this work.

Also, I would like to thank all my relatives and friends who helped and supported me, each one in different ways.

Special thanks are due to my parents for their love, their kindness, their patience, and their help in home management, and for their example of solidity.

Lastly, my dearest thanks goes to my husband, who gave to me strength, support, help and comfort whenever I needed, and shared with me all the difficulties of this hard work.

# List of abbreviations

ABTS = 2,2'-azino-bis 3-ethylbenzthiazoline-6-sulphonic acid

AKL = Lipase AK from *Pseudomonas fluorescens*

APTES = 3-aminopropyltrimethoxysilane

Asp = Aspartate

Bes= N,N-bis-(2-hydroxyethyl)-2-aminoethanesulfonic acid

CMC =critical micellar concentration

CTAB = cetyltrimethylammonium bromide

EE%=Encapsulation efficiency percent

GA = glutaraldehyde

GOx = Glucose Oxidase

GPTMS = Glycidoxypropyltrimethoxysilane

HRP = Horseradish peroxidase

His = Histidine

L = loading, mg of protein per g of catalyst

LE% = Loading efficiency percent

LYZ = lysozyme

MCF/MSF = Mesocellular foam/ Mesoporous Silica Foam

MCM-41 = Mobile Composition of Matter n. 41

MOF = Metal Organic Framework

OMS =ordered mesoporous silica

PEO-PPO-PEO /Pluronic = polymer of polyethylene oxide polypropylene oxide

p*I*= isoelectric point

PNPB = paranitro phenyl butyrate

PNPh = paranitro phenol

PO = Peroxidase

PZC =potential of zero charge

RML = Lipase from *Rhizomucor miehei*

SAXS = Small Angle X-Rays Scattering

SBA-15 = Santa Barbara Amorphous n.15

SEM = Scanning Electron Microscopy

Ser = serine

TEM = Transmission Electron Microscopy

TEOS = Tetraethylorthosilicate

TGA = Thermo Gravimetric Analysis

TMB = 1,3, 5, trimethyl benzene

TMOS = Tetramethylorthosilicate

Tris = Tris(hydroxymethyl) aminomethane

U = enzymatic unit

XRD = X-Rays diffraction

ZIF = Zeolite Imidazolate Framework

Zn:L = Zinc: Ligand molar ratio

# List of publications

## Published papers

- Cugia, F., Sedda,S., **Pitzalis, F.**, Parsons, D.F. , Monduzzi M., Salis A. *"Are specific buffer effects the new frontier of Hofmeister phenomena? Insights from lysozyme adsorption on ordered mesoporous silica"* RSC Advances, 6 (2016) 94617-94621. **DOI:** 10.1039/C6RA17356J

- **Pitzalis,F.**, Monduzzi,M., Salis, A. *"A bienzymatic biocatalyst constituted by glucose oxidase and Horseradish peroxidase immobilized on ordered mesoporous silica"* Microporous and Mesoporous Materials 241 (2017) 145-154, **DOI:** 10.1016/j.micromeso.2016.12.023

- **Pitzalis, F**.; Carucci,C., Naseri, M., Magner,E., Fotohui, L., Salis A. *"Lipases encapsulation onto ZIF-8. A comparison of biocatalysts obtained at low and high zinc:2methyl-imidazole mole ratio in aqueous medium"* ChemCatChem (2018) In Press **DOI:** 10.1002/cctc.201701984

## Poster presentation at international conferences

- First European Conference on Physical and Theoretical Chemistry", Catania 14-18 Sept. 2015 *"An Enzymatic Tandem System constituted by Glucose oxidase and Horseradish Peroxidase immobilized on mesoporous silica films and particles"*

- ECIS 2016 Roma 4-9 Sept. 2016, "Simultaneous immobilization of Glucose Oxidase and Horseradish Peroxidase on SBA-15 mesoporous silica"

# Abstract

This study deals with the immobilization of enzymes on two different class of supports, namely: SBA-15 mesoporous silica and the metal organic framework named ZIF-8. The synthesis of the supports, their functionalization and characterization were studied. After the choice of the proper enzymes (lysozyme, glucose oxidase, horseradish peroxidase, and two lipases), the biocatalysts were designed and prepared through three different immobilization strategies (physical adsorption, covalent binding and encapsulation) as outlined by the following three tasks:

1. **Physical adsorption** of lysozyme (LYZ) on mesoporous silica SBA-15 and amino functionalized SBA-15-$NH_2$.
2. **Covalent binding** of glucose oxidase (GOx) and horseradish peroxidase (HRP) on SBA-15-$NH_2$ (amino-functionalized mesoporous silica) to obtain a bienzymatic system.
3. **Encapsulation** of lipase AK from *Pseudomonas fluorescens* (AKL) and lipase from *Rhizomucor miehei* (RML) on ZIF-8 by means of a biomimetic mineralization approach.

**Task 1. Specific buffer effects on the physical adsorption of LYZ on SBA-15 and SBA-15-$NH_2$**

The synthesis of mesoporous silica SBA-15 and the amino-functionalization to obtain SBA-15-$NH_2$, were carried out according to standard protocols. Lysozyme (LYZ) from hen egg white was physically adsorbed onto both supports at a fixed pH (7.15), and the loading was quantified. It is usually considered that pH affects the loading of the physisorbed enzyme, but no attention is paid on the chemical nature of the buffer used to fix pH. To this purpose LYZ immobilization was carried out in different buffers, namely Tris [tris(hydroxymethyl) amino methane], Bes [N,N-bis-(2-hydroxyethyl)-2-aminoethanesulfonic acid], phosphate and citrate. A specific buffer effect on LYZ loading was observed on SBA-15, while this effect was negligible for SBA-15-$NH_2$. Moreover, for Tris and citrate buffers, the presence of strong electrolytes was found to significantly affect the loading according to the Hofmeister series. The effect of buffer and salts (weak and strong electrolytes) was also investigated towards electrophoretic mobility of the free LYZ, SBA-15 and SBA-15-$NH_2$. Also for this property, specific buffer effects and the synergistic action of salts were observed, suggesting that Hofmeister phenomena occur for both strong and weak electrolytes.

**Task 2. Covalent binding of GOx and HRP on SBA-15$NH_2$**

The tandem cascade reaction catalyzed by GOx and HRP consists of two reactions. Firstly the oxidation of glucose to gluconolactone and the reduction of oxygen to hydrogen peroxide is carried out by GOx. Then, HRP uses the hydrogen peroxide produced in the first step, to oxidize different kind of substrates, such as phenolic compounds. The "*in situ"* generation of $H_2O_2$, provided by GOx, is useful to avoid a possible irreversible deactivation of HRP. Herein, the covalent immobilization of GOx

and HRP on amino-functionalized mesoporous silica SBA-15 was investigated. The silica support was first synthesized and then functionalized and characterized. The binding of the enzymes on the surface was performed using the bifunctional linker glutaraldehyde (GA). The two enzymes were immobilized simultaneously and separately, and the loading kinetics were followed. The kinetic models of pseudo-second order, and intraparticle diffusion were applied to estimate the loading. The activities were significantly influenced by the drying process. Storage stability and recycling tests were performed. In order to test the possible effectiveness of the biocatalysts on the degradation of phenolic pollutants, the oxidation of the model molecules ferulic acid and caffeic acid was investigated.

**Task 3. Encapsulation of AKL and RML on ZIF-8.**

Lipases AKL and RML were encapsulated in the Zeolite Imidazolate Framework ZIF-8, via a biomimetic mineralization approach, in a "*one pot*" synthesis. The synthesis was carried out by using two Zinc: 2-methylimidazol molar ratios (Zn:L ratio1:4 vs 1:40). The structural and textural parameters were investigated by means of X-rays diffraction and $N_2$ physisorption. The obtained biocatalysts were significantly different in terms of crystal structure and surface area. In particular, a sodalite-like crystal structure of ZIF-8 was obtained for the Zn:L ratio 1:40, while a different phase was obtained at Zn:L ratio 1:4. Moreover, adsorption-desorption isotherms of the Zn:L=1:40 ratios were associated with the type I isotherms, typical of microporous materials with high surface areas (600-900 $m^2/g$). Whereas isotherms obtained from low Zn:L ratio =1:4 resulted in low values of surface areas (30-80 $m^2/g$). The activity of the encapsulated enzymes was tested by means of the p-nitro phenyl butyrate assay. The biocatalysts obtained by means of the Zn:L ratio 1:4 displayed a higher specific activity than those obtained by Zn:L ratio 1:40. Thus, in order to improve the activity of the biocatalysts obtained by Zn:L ratio 1:40, a series of synthesis with a control of pH was carried out. It was observed that the decrease of pH ligand solution before the addition of the lipase, led to the reduction of surface areas of the lipase@ZIF-8 biocatalysts. The most active biocatalyst was that obtained by means of Zn:L ratio 1:4. The storage stability at 15 days was tested and A high retention of activity was detected for both AK@ZIF-$8_{1:4}$ (99%) and RM@ZIF-$8_{1:4}$ (88%) Moreover the AK@ZIF-$8_{1:4}$ was recycled 5 times, while RM@ZIF-$8_{1:4}$ was recycled twice.

This topic was object of an accepted manuscript on ChemCatChem journal (**2018**).

# Summary

# **Chapter 1:** *Introduction*

## 1.1 Biocatalysis

Biocatalysis is the catalysis performed in biological systems, and according to the IUPAC, *Compendium of Chemical Terminology*, a biocatalyst is an enzyme, or a complex of enzymes that "catalyses metabolic reactions in living organisms and/or substrate conversions in various chemical reactions".[1] Nowadays, the development of new technological and industrial processes requires a particular attention towards energetic and environmental issues. Solutions that involve the use of increasingly innovative catalysts, with high attention to safer processes and waste reduction are desirable. Green Chemistry - developed in 1990 by Anastas and co-workers[2,3] - is defined as ''the design of chemical products and processes to reduce or eliminate the use and generation of hazardous substances"[2] by EPA (Environmental Protection Agency of United States). In agreement with the 9$^{th}$of the 12 principles of green chemistry,[2] biocatalysis can provide an increase of greenness to industrial processes. For these reasons the employment of enzymes in many chemical processes is becoming more and more important.[4] Indeed, biocatalysis offers a valid alternative to chemical catalysis, due to the high substrate specificity, that generally allows the formation of products, minimizing the formation of undesired byproducts. Moreover, enzymes require the use of mild reaction conditions, i.e. ambient temperature, atmospheric pressure and neutral pH, which are ideal for the design of eco-friendly industrial processes.[5–8]

Currently, biocatalysts are mainly used in the pharmaceutical industry.[9,10] This because most drugs are chiral molecules that can be produced in few enzymatic steps in comparison to the long routes used by traditional organic chemistry.[10] Biocatalysis is also used in the food industry, biosensing and wastewater treatment. I.e. lactose-free

products are prepared by the treatment of specific lactases (β-galactosidase). Lysozyme is commonly used as food preservative for its antibacterial activity.[11] Commercial glucometers are biosensors for glycemia measurement that work with strips based on glucose oxidase for the detection of glucose. The treatment of wastewaters from food or textile industry, particularly for the removal of recalcitrant pollutants,[12–14] involves the degradation of dyes by means of algae of fungi, often used combined with chemical degradation.[14] In addition to these applications already in use, others are subject to intense research, i.e. enzymatic biocatalysts are being investigated for the production of biofuels,[15] that is fuels obtained from renewable feedstock, by means of new environmentally friendly processes.

The main drawback of biocatalysts compared to traditional chemical catalysts is due to the high costs of enzyme production. Although many enzymes are being produced through the fermentation of solid waste as cheap culture media,[12] their cost is still higher than that of chemical catalysts. Many research efforts are being paid for the development of new, specific, and cheap biocatalysts that can provide high product yields. One strategy involves what is known as "enzyme engineering", that is the modification of the primary structure of enzymes based on the introduction of plasmids (DNA fragments) in the genome of bacteria or fungi. This procedure manipulates the sequence of genes resulting in a modification of the polypeptide chain to obtain more active or more stable enzymes.[16] Alternatively biocatalysts performance can be enhanced by means of enzyme immobilization. Immobilization is the “confinement of a biocatalyst inside a bio-reaction system with retention of its biocatalytic activity over several reaction cycles”.[6] The use of immobilized enzymes can provide significant advantages in all the processes that require the use of a biocatalyst.[12,15] This topic will

be discussed in chapter 2.

## 1.2 Enzymes

From the chemical point of view enzymes are essentially globular proteins, except for ribozymes, that are RNA molecules with catalytic properties.[17] The linear peptide sequence of amino acids constitutes the primary structure. The secondary structure, α-helix, β-sheet or random coil, is due to intra-chain hydrogen bonds. The tertiary structure is the final spatial conformation taken by proteins. Weak hydrophobic interactions, such as van der Waals forces, dipole-dipole interactions, London forces, and polar hydrogen bonds promote the arrangement of hydrophobic residues in the inner part (core) of the protein, and of hydrophilic residues on the external surface, in contact with aqueous media.[18] Also strong bonds such as disulfide bridges between cysteine amino acids are involved in tertiary structure. Finally, the quaternary structure consists in the assembly of two or more individual protein subunits. The catalytic function of enzymes is carried out by a so called "*active site*". The active site generally includes two main regions: i. a binding site and ii. a catalytic site.[19] In the binding site a reagent molecule, named substrate, is bound with a correct orientation for the successive action of the catalytic site. The catalytic site is the region where the substrate is converted into the products. The reaction is allowed by specific amino acid residues that decrease the activation energy of the reaction. Additionally, there might be allosteric sites that allow either enzyme activation or deactivation depending on the substrate or product concentrations.[19] Cofactors are often required for the enzymatic function. Cofactors can be metal ions (i.e. $Zn^{2+}$ in alcohol dehydrogenases, $Mg^{2+}$ in kinases, $Cu^{2+}$ in laccases), or organic/metal-organic compounds (i.e. heme groups, nicotinamide adenine dinucleotide, NAD, flavin adenine dinucleotide, FAD, bound to

the enzyme. Cofactors include prosthetic groups and coenzymes. The former are strongly bound to the enzyme (low dissociation constant, FAD is a typical prosthetic group), the latter are weakly bound to the enzyme (high dissociation constant, NAD is a typical coenzyme).[20]

According with the "Nomenclature Committee of the International Union of Biochemistry and Molecular Biology" (NC-IUBMB), enzymes are classified in function of the reactions they catalyze.[21]

**Tab.1.1** classification of enzymes

| **Class**<br>**EC number** | **Name** | **Reaction** | **Effect** |
|---|---|---|---|
| 1 | Oxidoreductase | $AH_2 + B \rightarrow A + BH_2$<br>$AH_2 + B^+ \rightarrow A + BH + H^+$ | Oxidation or reduction of functional groups |
| 2 | Transferase | $AX+B \rightarrow A+BX$ | Transfer of functional groups |
| 3 | Hydrolase | $AB + H_2O \rightarrow AH+BOH$ | Hydrolysis |
| 4 | Lyase | $A\text{-}B + X\text{-}Y \rightarrow X\text{-}A\text{-}B\text{-}Y$ | Addition or removal of functional groups |
| 5 | Isomerase | $A \rightarrow B$ | Formation of isomers |
| 6 | Ligase | $X+Y+ATP \rightarrow XY+ADP+Pi$ | Formation of new bonds C-C; C-N; C-O; C-S |

### 1.2.1 Enzyme activity

The enzymatic activity and the protein content are important parameters that need to be specified in biocatalysis. The activity of an enzyme can be detected by monitoring the rate of its typical reaction. According to the International Union of Biochemistry the standard unit (U) of enzyme activity is the amount that catalyses the transformation of 1 micromole of the substrate per minute, under standard conditions and through a specified standard assay.[22] In terms of International System of Units (SI), the enzymatic activity should be expressed in Katal (kat), namely moles per second (mol/s). However in the practical use, the activity is expressed in micromoles of

substrate/product per minute. The International Union of Biochemistry defines the relation between standard Units and kat as follows:[22]

"1U corresponds to a rate of 1 µmol/min = 1/60 µmol/s ≈ 16.67 nmol/s; 16.67 nkat catalyse a rate of 16.67 nmol/s. Therefore 1 U corresponds to 16.67 nkat."

Two derived quantities are the *specific catalytic activity* of an enzyme, expressed in kat /kg and the *molar catalytic activity*, kat/mol.[22] In this work enzymatic activity is expressed as U = µmol/min of substrate/product, and specific activity is expressed in micromoles per minute per milligram of protein (µmol $min^{-1}$ $mg^{-1}$, or U/mg). Specific activity is an important parameter that allows the comparison among different enzymes because it is referred to the unitary amount of enzyme (mg), while the activity do not take in to account the amount of enzyme involved in the reaction. The reaction rate is measured by the appearance of product or the disappearance of substrate at the start of the reaction. An example scheme is given below (Fig.1.1) where the appearance of the product is reported as a function of time.

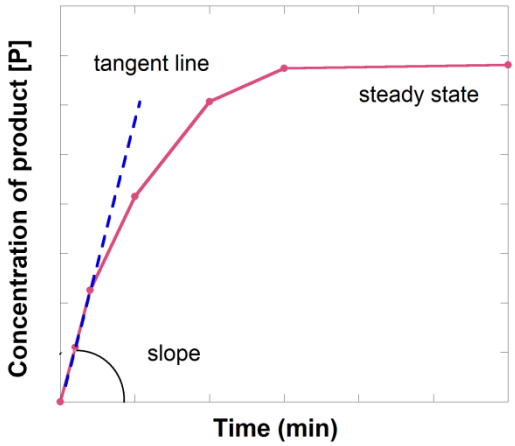


**Fig. 1.1** the slope of the tangent line passing through the zero is the value of enzymatic activity.

The concentration of the enzymatic product increases quickly at the start of the reaction, then slowly decreases until it reaches a steady state, when the maximum speed is achieved. The activity is the measurement of initial velocity, obtained by calculating the slope of the tangent line passing through the zero. All activity tests need specified conditions such as concentration of substrate, pH, and temperature.

The turnover number, indicated as $k_{cat}$ is another important parameter used in biocatalysis. $k_{cat}$ are the moles of product/substrate converted per mole of the enzyme per second at the steady state. In these conditions the enzyme is saturated by the substrate, and acts at its maximum speed, so that the velocity of conversion does not depend on concentration of substrate. $k_{cat}$ is measured in $s^{-1}$.[17]

The reaction between an enzyme E and its substrate S to give the product P, depends on the initial concentrations of the enzyme $[E]_0$ and the substrate $[S]_0$. At low substrate concentrations the formation rate of P is proportional to $[S]_0$. At high substrate concentrations enzyme-substrate complex [ES] reaches its maximum concentration, and the product formation rate is independent by $[S]_0$. Supposing that the formation of the ES complex is reversible and the formation of the product is irreversible, the reactions involved can be written as:

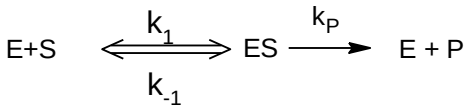


Where $k_1$ is the constant rate of the reaction E +S → ES

$k_{-1}$ is the constant rate of the reaction ES→ E+ S

$k_P$ is the constant rate of the reaction ES→ E+ P

At the equilibrium, the enzyme is saturated by the substrate, and works at its maximum speed and the product formation rate is not negligible. Namely the rate of formation of the complex ES, the disappearance of S and the formation of P reach their maximum with no further concentration changes during a time Δt. This condition is named steady-state.

The kinetics of the reaction rate variation as a function of the substrate concentration is expressed by the Micaelis-Menten equation, which relates the reaction rate of product appearance *v* to the substrate concentration $[S]_0$

$$V = \frac{d[P]}{dt} = \frac{V_{max}\,[S]_0}{K_M + [S]_0} \quad (1.1)$$

where $V_{max}$ is the maximum rate of the enzymatic reaction. $K_M$ is the Micaelis-Menten constant, corresponding to the substrate concentration that allows the achievement of a half of the $V_{max}$.[17] $K_M$ can be written as

$$K_M = \frac{k_{-1} + k_P}{k_1} \quad (1.2)$$

## 1.3 An overview of the chosen enzymes

In this work the immobilization of enzymes belonging to the class of hydrolases and oxidoreductases was investigated. Among hydrolases two lipases - from *Pseudomonas fluorescens* (Lipase AK), and from *Rhizomucor miehei* (lipase RM) - and lysozyme from hen egg white (LYZ) were used. Among oxidoreductases glucose oxidase from *Aspergillus niger* (GOx), horseradish peroxidase from *Armoracia rusticana* (HRP), were used.

The choice of these enzymes was related to some aspects of the immobilization procedures studied. Firstly, lysozyme from hen egg white was chosen for its high purity as a model enzyme, to study a still unexplored buffer specific effect on its physical adsorption on a mesoporous silica matrix. No activity measurements were carried out as the main goal was to investigate how weak and strong electrolytes modulate the phenomena occurring at the bio-nanointerface.

Another task of the work was to investigate the immobilization of a bienzymatic sequential system on silica amino-functionalized support. Therefore, glucose oxidase and horseradish peroxidase were chosen as their combined use is widely studied for cascade reactions. A study on the covalent immobilization procedure was the main goal in this part of the work.

Finally, the work focused on the immobilization of enzymes on new promising host materials, the Zeolite Imidazolate Frameworks, particularly the ZIF-8. For this purpose, the chosen enzymes were the two lipases, while the immobilization procedure was the encapsulation. This method was chosen as the pore dimensions of the supports are incompatible with enzyme dimensions, and thus a post-synthesis immobilization was not allowed.

Moreover, the choice of all these enzymes was due to their important applications in many (industrial, food, pharmaceuticals, bioanalytical, etc.) fields. Their main structural features are reported in detail in the following paragraphs, while an overview of this enzymes immobilized on ZIFs and Silica are reported in the following chapters.

### 1.3.1 Lipase

According to the Nomenclature Committee of International Union of Biochemistry and Molecular Biology (NC-IUBMB)[21] classification, lipases (triacylglycerol

acylhydrolases, E.C. 3.1.1.3.) are the enzymes the allow the hydrolysis of triacylglycerols in living organisms. Lipases are a subclass of esterases that hydrolyze the ester bond of lipids or phospholipids (phospholipases), according to the general reaction.

$$RCOOR' + H_2O \rightarrow RCOOH + R'OH$$

Almost every living organism or microorganism produces lipases. Their wide diffusion, the water solubility, but also the capability to work in non aqueous media, are quite interesting properties that make them useful enzymes for industrial purposes.[9] Hundreds of lipases, especially those obtained from microorganisms like fungi, that generally are more stable than lipases from plants or animals, are being investigated and used in the industry. Among different uses, lipases find application in biofuels production,[23] in food processing (modification of flavors, milk fats hydrolysis, cheese production),[9,24] in pharmaceutical industry (hydrolysis of 3-phenylglycidic acid ester, an intermediate used in synthesis of diltiazem hydrochloride,[9] racemic production of ibuprofene[6]) and detergent industry.[9,25] For these reasons lipases have nowadays a significant commercial importance.[7]

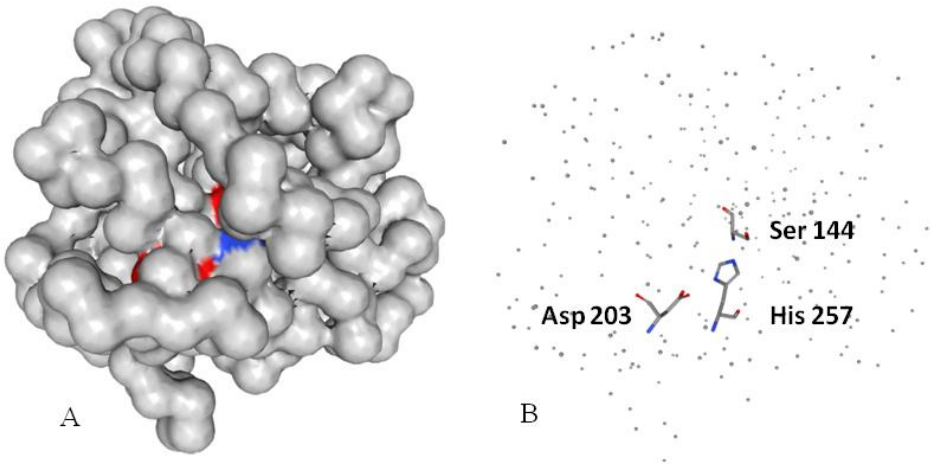

**Fig. 1.2** 3D representation of lipase from *Rhizomucor miehei.* A) The overall structure and B) a detail of the catalytic triad. The picture is adapted from the ref.[26] from a deposited PDB file 1TGL, using the NGL viewer from http://www.rcsb.org/pdb [27,28]

*Structural parameters of lipases*

Several lipases from different microorganisms have been purified and characterized.[29–32] Their molecular mass usually ranges from 30 to 50 kDa. Most lipases have an activity optimum in the pH range 7.5–9,[29] and an optimal temperature from 35 to 50°C.[7] For lipases from thermophilic microorganisms the optimal temperature can be around 60-80°C and even higher. Although lipases from different sources can significantly differ in many physical (i.e. size, isoelectric point) and structural aspects, there are some common features for all these enzymes. In most lipases the catalytic site is placed in the inner part of the enzyme and its accessibility is allowed by a mobile lid, constituted by α-helix loops.[33] In its closed conformation, the active site of a lipase is not accessible and no activity can be detected whereas, in the open conformation, the substrates can freely reach the active site. The change of between the closed and the open conformation occurs when a lipase is adsorbed at an oil interface. This mechanism is called "interfacial activation"[34–36]. In the active site of lipases the catalytic triad, constituted by the amino acids serine-histidine-aspartate/glutamate, is involved in the catalytic mechanism as described below. The scheme 1.1[37] shows the hydrolysis mechanism of lipases, also defined as a chymotrypsine-like mechanism.[32] From the chemical point of view, the mechanism of hydrolysis proceeds in two steps. Firstly, the -OH residue of serine makes a nucleofilic attack to the carbonyl group of the ester.

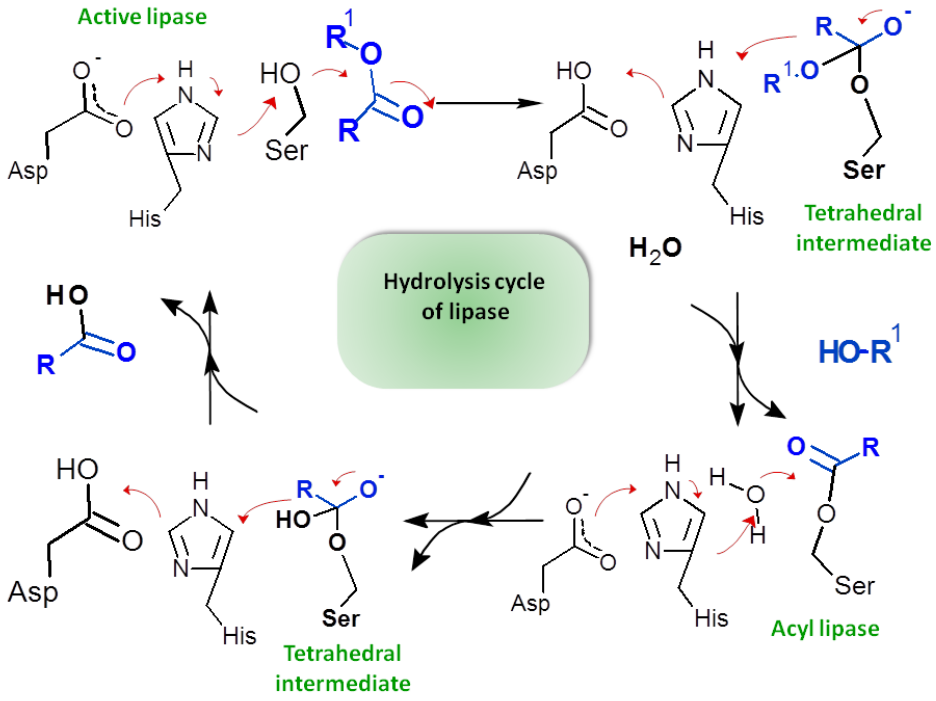


**Scheme 1.1** The mechanism of hydrolysis of lipase and the catalytic triad Ser, His, Asp. Adapted with permission from ref.[37] Copyright 2015 American Chemical Society."

The acyl-enzyme intermediate formed is stabilized by the residues of histidine of the catalytic triad, which accepts a proton from the serine residue. The aspartic/glutamic acid contributes to the stability of the activated complex by delocalizing the charge. This breaks the ester bond and allows the release of the alcohol. Secondly, the release of the acyl-group from the active site is catalyzed by a new nucleofilic attack by a water molecule, that promote the hydrolysis of the acyl group from the enzyme thus permitting its regeneration and the release of the acid.[38,39] This mechanism depicted in the scheme 1.1 is named ping-pong Bi-Bi mechanism.[38,39] The overall structure of lipase from *Rhizomucor miehei*, with the amino acid residues of the active site, is shown in Fig.1.2. The position of the catalytic triad in the lipase PM from *Pseudomonas sp.* MIS38[31] is shown in Fig. 1.3.

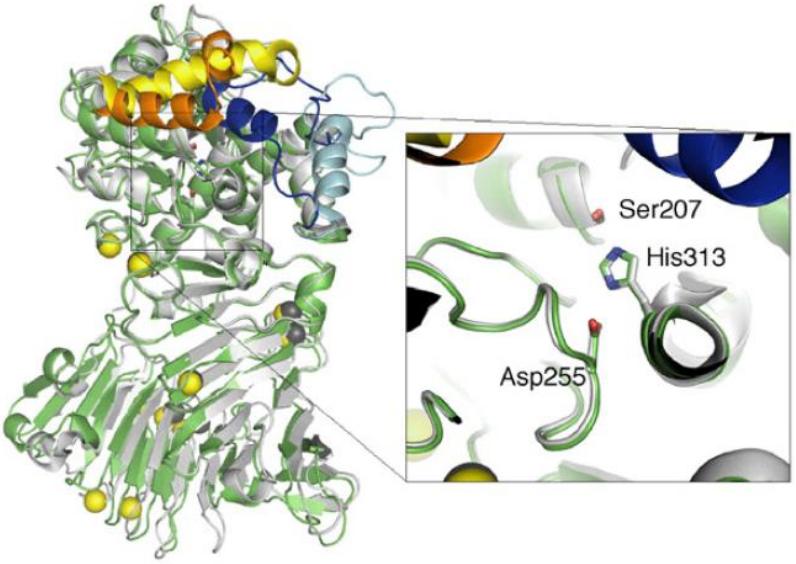


**Fig. 1.3** Lipase PM from *Pseudomonas sp. MIS38*, the Ser, His, Asp triad. Reproduced from ref.[31] Open access content.

The biological reaction catalyzed by lipases is the hydrolysis of triacylglycerols (TAGs) to fatty acids and glycerol, according to the mechanism shown in scheme 1.1 However, it has been found that lipases can also catalyze other unnatural reactions.[23] Indeed, under proper reaction conditions, namely in non aqueous media with a controlled water activity,[23,40,41] lipases catalyze esterification and transesterification reactions (see schemes 1.2b and 1.2c).

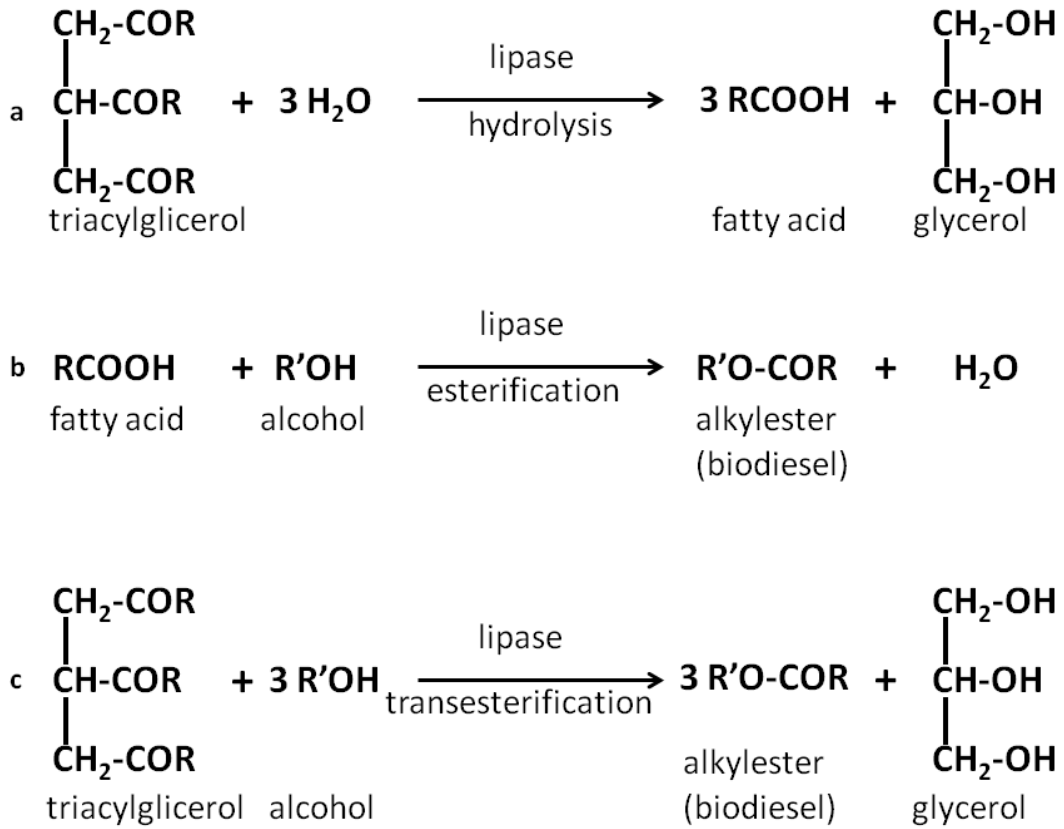


**Scheme 1.2**
All reaction catalyzed by lipases: a) hydrolysis; b) esterification; c) transesterification reaction, the transfer of an alcohol from an ester to another ester.

In this work, lipases from *Rhizomucor miehei* (RML) and lipase from *Pseudomonas species*. (i.e. lipase AK from *P. fluorescens*) (AKL) were immobilized *via* encapsulation on the Metal organic Framework ZIF-8, as discussed in the section dedicated to the accepted manuscript.

These two lipases are well characterized.[31,34,36,42], LRM is an enzyme of 32kDa, with isoelectric point (pI) at pH 3.8,[43] LAK is an enzyme of 33kDa with pI at pH 4,[44] it is specific for cleavage in 1,3 position of triacyl glycerols. Ser 144, Asp 203 and His 257 are the amino acids that constitute the catalytic triad.[26,45,46] These two enzymes are widely investigated for biodiesel production. For this application, they were immobilized by many authors in other supports, i.e. silica supports[43,47–49] but for the

best of our knowledge, in the literature, no data were available for these two lipases immobilized on ZIF-8.

### 1.3.2 Lysozyme

Hen egg white lysozyme (LYZ) or N-acetylmuramide glycanhydrolase (E.C. 3.2.1.17) is an hydrolytic enzyme constituted by 129 amino acids. LYZ has a molecular mass of 14.4 kDa, a size of 3 x 3 x 4.5 nm,[50] and an isoelectric point (p*I*) of 11.4. LYZ is a monomeric protein with two sub-domains, with the active site located in an inner cleft,[51,52] LYZ catalyzes the hydrolysis of the β-l,4 glycosidic bonds of oligosaccharides, including the polysaccharide N-acetyl glucosamine-N-acetyl muramic acid, that is a component of bacteria and fungi cell wall, hence with hydrolytic activity against numerous microorganisms.[52] LYZ is also able to catalyse transglycosylation reactions. Figure 1.4 shows the general structure[53] and catalytic cleavage of the β-1,4 bond of the polymer formed by 2-acetamido-2-deoxy-D-muramic acid (NAM) and 2-acetamido-2-deoxy-D-glucose (NAG), by means of two possible pathways. The path A (Phillips mechanism) proceeds via a oxocarbenium ion intermediate.[54,55] According to this mechanism the cleavage of the β-1,4 bond is allowed by a distortion of the NAM, that in the active site of lysozyme is forced to a half-chair conformation.[54,56] The path B, (Koshland mechanism) the cleavage of the proceeds via a covalent binding of aspartate residue. The residue of Glu35 gives a proton to the oxygen of the β-1,4 bond, while Asp52 provides a nucleophilic attack that completes the cleavage.[54,55]

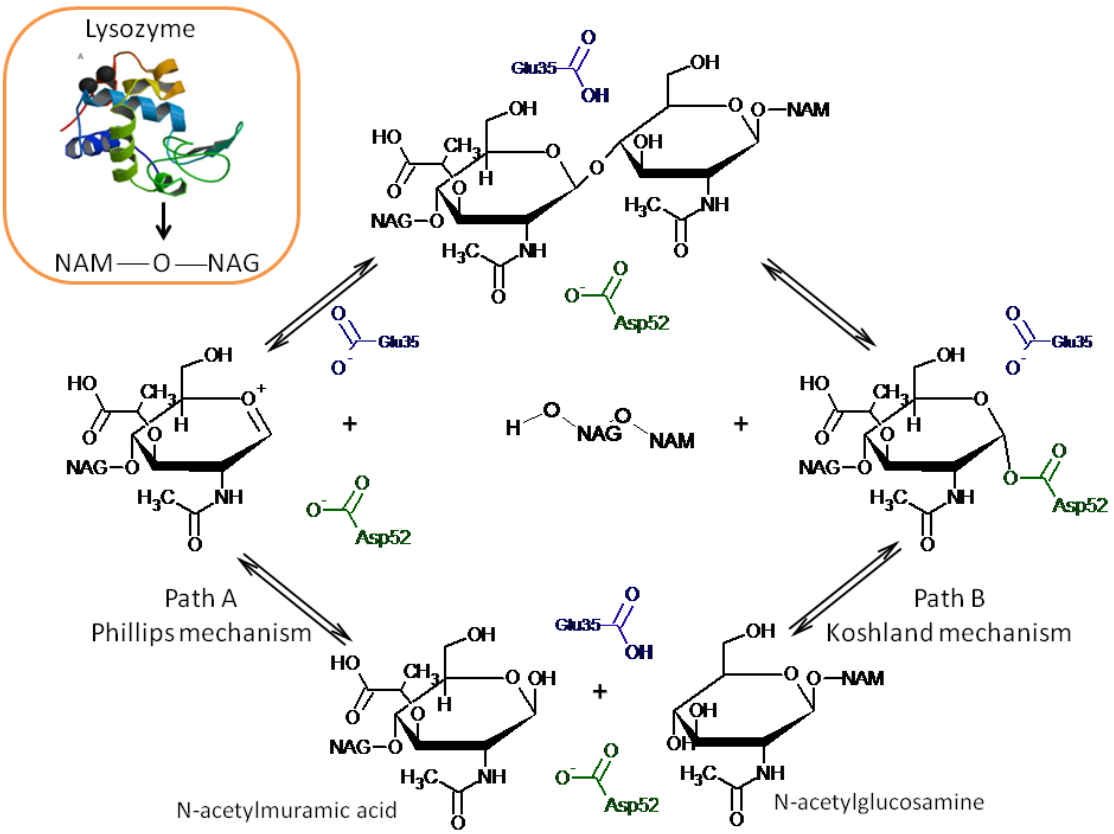


**Fig. 1.4** Lysozyme from hen egg white. The structure is reproduced from a deposited PDB file 1DPX from http://www.rcsb.org/pdb. The mechanism shows the two catalytic pathways of lysozyme. Adapted with permission from ref.[55] Copyright 2008 Royal Society of Chemistry.

Plants and animals, and the hen egg white are common sources of lysozyme. Due to its antimicrobial activity, lysozyme is an important enzyme for pharmaceutical applications,[11] for the food industry[57] as food preservative,[58,59] and very promising for biomedical[60] purposes. Due to its easy availability in pure form and well known structure and function, lysozyme is often used as a model enzyme/protein for many fundamental studies.[61] For this reason lysozyme has been immobilized in numerous supports such as polymers (cellulose acetate, nylon, chitosan and alginates),[62] and also in mesoporous silica,[63–65] ordered mesoporous carbon,[66] and MOFs.[67]

### 1.3.3 Glucose oxidase

Glucose oxidase (β-D-glucose-oxygen 1-oxidoreductase; E.C. 1.1.2.3.4) (GOx) is an ubiquitous enzyme of high biotechnological interest, for its large-scale applications.[68] The main source of GOx are fungi from genus *Aspergillus* and *Penicillium.*[68] Its three-dimensional structure, resolved by Hetch et al.,[69] consists of two identical monomers of ellipsoidal shape, with 28% of α-helix and 18% of β-sheets, that are covalently linked by disulfide bonds (Fig.1.5). The size of the unglycosilated dimer is 7.0x5.5x8.0 nm,[70] and its molecular mass can vary from 130 to 175 kDa depending on different amino acids and carbohydrates content.[68] Each monomer contains FAD (flavin-adenine dinucleotide) as a cofactor.[71] GOx has an isoelectric point (p*I*) of 4.2 [72] and an optimal activity pH at pH 5.5.

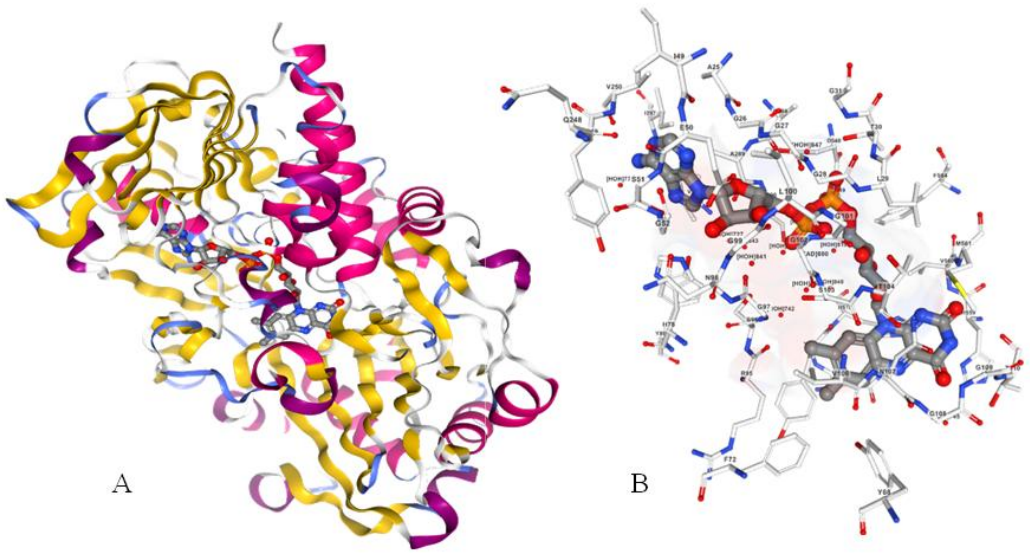


**Fig. 1.5** Glucose Oxidase from *Aspergillus niger*. A) The monomer is reported, with α-helix loops (red) and β-sheets (yellow). B) A detail, where the FAD cofactor is represented as a "ball and sticks" molecule. This picture is adapted from ref.[69] (PDB file 1GAL), using the NGL viewer from http://www.rcsb.org/pdb.[27,28]

Glucose oxidase catalyzes the oxidation of the β-anomer of D-glucose to gluconolactone according to the scheme 1.3. Due to its high specificity toward this

reaction, the most important application of GOx is the realization of biosensors for glucose detection.[68,73,74] Nonetheless, other applications as a food and beverage additive, toothpaste additive and in the textile industry have been investigated.[68,75] Its combined use with peroxidases to form a bienzymatic sequential (tandem) system[76,77] or in multienzymatic systems[78] is a promising application for biosensing[79–81] and bioremediation.[82]

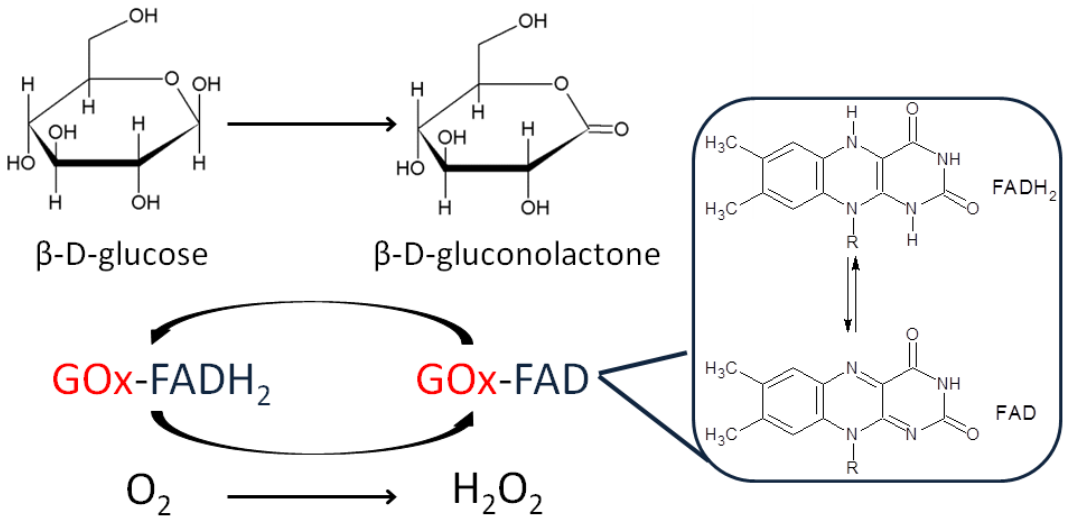


**Scheme 1.3** Oxidation of glucose to gluconolactone by GOX is associated to reduction of FAD to $FADH_2$ , the return to the oxidized form of the coenzyme occurs through the reduction of oxygen to hydrogen peroxide.

### 1.3.4 Horseradish Peroxidase

Peroxidases (E.C. 1.11.1.X) are a wide subclass of enzymes belonging to the oxidoreductase class. They are ubiquitous, either intracellular or extracellular enzymes. Peroxidases can be constituted by a number of amino acids in the range 153-753. This results in a variability of molecular mass from 17 to 84 kDa. Generally, their structure includes 10-11 α-helices, with a rare presence of β-sheets. Two main different domains can be distinguished, which host the prosthetic group Heme, ferriprotoporphyrin IX, at

their interface, in a hydrophobic pocket.[83] A typical reaction catalyzed by peroxidases is:

$$ROOR' + AH_2 \rightarrow A + ROH + R'OH$$

where $AH_2$ is an electron donor which is oxidized by the peroxidase, while hydrogen peroxide is the electron acceptor substrate which is reduced to water. The electron donors can be very specific for certain peroxidases, such as catalase or glutathione peroxidase, while other peroxidases, such as horseradish peroxidase, are able to oxidize a wide variety of organic compounds. The importance of peroxidases for living cells is related to their numerous protective functions. They are indeed involved in the removal of xenobiotics or in the protection from oxidative stress.[84]

Horseradish (*Armoracia rusticana*) is a vegetal whose roots are an important source of peroxidases. Numerous isoenzymes are known to be provided by this plant, and the most abundant and investigated is the isoenzyme C.[84] Horseradish peroxidase (HRP, E.C. number 1.11.1.7) type C is a single polypeptide chain of 308 amino acid, a molecular mass of 44 KDa, an isoelectric point p$I$ = 9, and an optimal activity around pH 6-8. Commonly, at least 8-9 potential glycosylated sites have been identified for this enzyme which are all linked to asparagine residues (Asn13, 57, 158, 186, 198, 214, 255, and 268). The total content of glycosides is generally between 18% and 22% along with different types of carbohydrates on the external surface.[84] Protoporphyrin IX is the prosthetic group, non-covalently bound to the apoenzyme, coordinating Fe (III) as metal ion in the center of the Heme ring.[84] HRP C binds two calcium ions in distal and proximal position with respect to the Heme plane, which are important for the stabilization and the integrity of the enzyme.[83] The overall structure and the catalytic site of HRP C are shown in Fig. 1.6.[85]

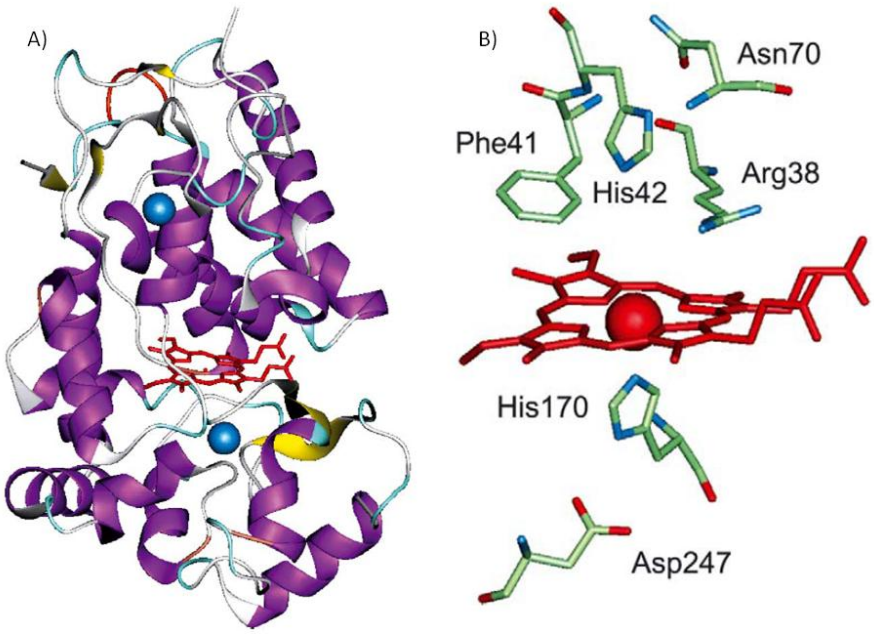


**Fig. 1.6** HRP overall structure. A)The whole enzyme, B) a detail showing the Heme prosthetic group and the amino acids involved in the catalytic site. Reproduced with permission from ref.[85] Copyright 2004 Elsevier.

*Mechanism of the active site of HRP*

HRP catalyzes hydrogen peroxide reduction through a radical mechanism:[85]

$$H_2O_2 + 2AH_2 \rightarrow 2H_2O + 2\ AH^{\bullet}$$

where $AH_2$ and $AH^{\bullet}$ represent a reducing substrate and its radical product, respectively. Aromatic phenols, phenolic acids, indoles, amines and sulfonates are typical HRP substrates. The oxidation of organic compounds is a complex multistep cycle that consists of various oxidative states of the Heme group. In the first step of the catalytic mechanism, HRP removes two electrons, one from the ferriprotoporphyrin IX and another from the iron atom. these two electrons are provided by the hydrogen peroxide. In this step the enzymatic cation radical intermediate, known as compound I, is formed. In the second step the reduction of the Heme proceeds with the transfer of one electron to one substrate molecule, with the formation of the intermediate compound II.

Successively, a second substrate molecule, provides another electron to reduce $Fe^{4+}$ back to $Fe^{3+}$, concluding the cycle and taking back the Heme to its initial state.[84,86,87] A complete description of the mechanism of peroxidases is reported in refs.[88,89] The Scheme 1.4 describes the multistep process of oxidation of ferulic acid showing the changes of the oxidation states of the Fe ion in the heme group.

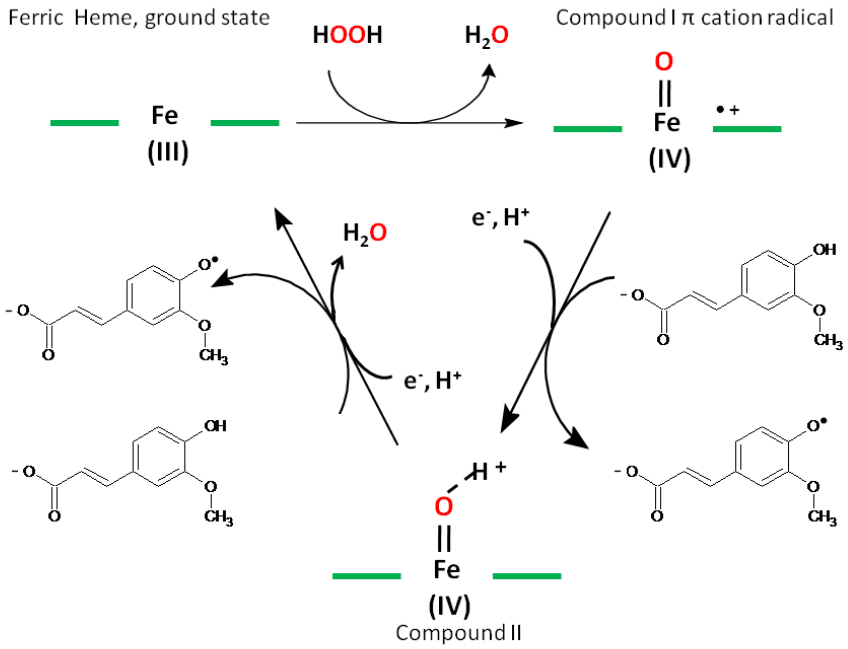


**Scheme 1.4** catalytic mechanism of HRP.

HRP is an important commercial enzyme which is used in diagnostic components of ELISA (enzyme-linked immunosorbent assay) kits. Moreover, HRP is a very important enzyme for research purposes, such as for biosensing,[74,90] the development of chemiluminescence-based immunoassays,[91] or for bioremediation of wastewaters.[12] Among the numerous substrates oxidized by HRP some chromogenic compounds, important for biosensing applications, are 2,2'-azino-bis-3-ethylbenzthiazoline-6-sulphonic acid (ABTS);[92] 3,3',5,5'-tetramethylbenzidine (TMB);[93]and 10-Acetyl-3,7-

dihydroxyphenoxazine (Amplex red).[94] Also the luminescent compound 5-Amino-2,3-dihydro-1,4-phthalazinedione (Luminol) is often used as a HRP substrate.[95]

### 1.3.5 Multienzymatic systems

In nature, cascade reactions are always performed in living cells, as occurs for Krebs cycle or in the chlorophyllian photosynthesis. The desire to reproduce the perfection of nature led scientists to try to reproduce natural mechanisms by pairing two or more enzymes, in order to mimic their natural multienzymatic cascade reactions for biotechnological applications.[96,97] Some advantages can be achieved by coupling enzymes, that catalyze different incompatible reactions,[98] or performing an *in situ* controlled production of reactants to avoid possible inactivations.[76] Among the infinite combinations of possible enzymatic couplings, a largely investigated couple of enzymes is constituted by oxidoreductases such as GOx, and peroxidases such as chloro peroxidases (CPO) or HRP. Their combined use has become a model system for the test of new supports,[99,100] mainly for biosensing.[79,101] Moreover, since high amounts of $H_2O_2$ can damage peroxidases, the combined use of GOx/CPO was also suggested for the *in situ* production of a controlled amount of substrate.[76] Moreover, also multienzymatic cascade reactions with more than two enzymes have been reported. Mallardi et al. realized a multi-enzyme immobilized system constituted by trehalase (TREH), GOx and HRP encapsulated in calcium alginate hydrogel beads.[78] The covalent immobilization of a bienzymatic system realized with the enzymatic couple GOx/HRP on SBA-15 mesoporous silica was investigated in this work. The combined reaction of this tandem system is summarized in the scheme 1.5 where the oxidation of a phenolic compound, ferulic acid, in the tandem reaction catalyzed by the two enzymes, is reported.

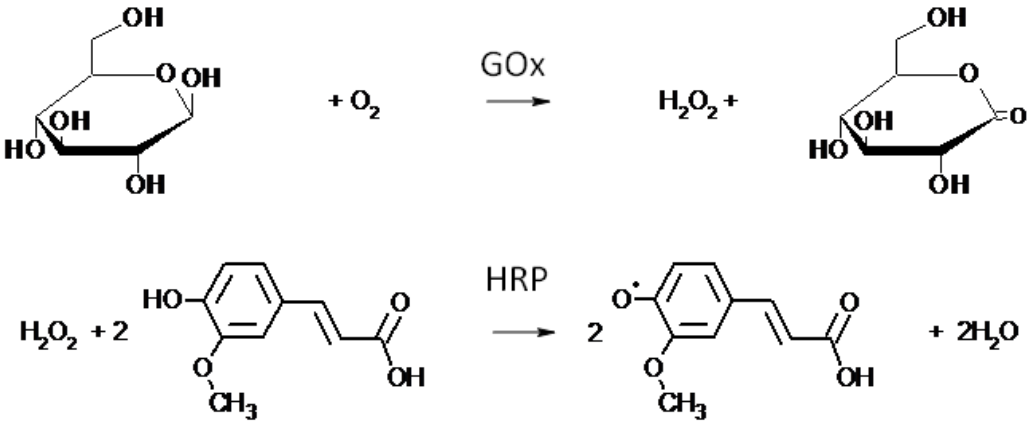


**Scheme 1.5** oxidation of ferulic acid by means of the bienzymatic (tandem) reactions of GOx and HRP.

# **Chapter 2:** *Immobilization of enzymes*

## 2.1 Enzyme immobilization: advantages and disadvantages

The main drawback in the use of free enzymes in industrial processes is due to their solubility in the aqueous reaction media which makes difficult their recovery at the end of the process. In addition, free enzymes are generally unstable and quite expensive, hence their high cost is a big limitation in the design of eco-friendly biocatalytic processes. With the immobilization of enzymes on solid supports heterogeneous biocatalysts are obtained. Immobilized enzymes are not soluble in the reaction mixture, can easily be separated, recovered and reused. Biocatalyst recycling makes a process less expensive than that using a free enzyme and it can provide purer products.[102] The immobilization of enzymes allows the following general advantages:[6]

- Retention of activity in the bioreactor, recovery and reuse of the biocatalyst, and possibility to run continuous processes.
- Improvement of enzyme stability, with protection from harsh denaturation conditions.
- High purity of products, due to less undesired reactions, and less contaminations with the reaction products that can be better separated from bulk reaction.
- High concentration of biocatalyst, with improvements in product yield.
- Control of reactions, allowing the design of multiple cascade enzymatic reactions (i.e. tandem systems).

Enzyme immobilization presents also the following disadvantages:[6]

- Support and immobilization costs. The use of enzyme supports as well as the immobilization process result in additional costs respect to the use of free enzymes.

- Loss of activity due to the immobilization. Immobilized enzymes can be affected by a strong loss of activity, that occurs since catalytic sites may be buried, damaged and inactivated by the immobilization procedure. For these reasons immobilization procedures need to be carefully designed.
- Diffusion of enzyme molecules in porous supports. If high surface area porous materials are used as enzyme supports, the pore size should be large enough to permit an easy enzyme diffusion. Macromolecules cannot easily diffuse in small pores or interstices.
- Instability of supports. High temperature, pH, microbial attack, can damage the support causing the loss of activity.[6]

The choice of a suitable support for immobilization of enzymes is a key issue for the development of an active biocatalyst.

### 2.1.1 Loading and loading efficiency

Regarding the immobilization, it is important to define some parameters such as loading (L) and Loading efficiency percent (LE%) that are widely used for the quantification of protein amount onto the support and the estimate of the effectiveness of the immobilization procedure.

Loading (L) is the amount (mg) of protein per mass unit (g) of support.

$$L = m_{protein}/m_{support}\ [mg_{protein}/g_{support}] \quad (2.1)$$

The loading can be calculated, subtracting from the initial amount of enzyme the remaining amount at the end of immobilization procedure:[65]

$$L = \frac{([P]_0 - [P]_f)V - [P]_w V_w}{m_{support}} \quad (2.2)$$

Where $[P]_0$, $[P]_f$, and $[P]_w$ are the protein concentrations of the initial final and washing solutions, respectively. V and $V_w$ are the volume of reaction solution and of washing solution. Alternatively, L can be obtained by using different kinetic models, such as the pseudo-second order, and the intra-particle diffusion models (Table 2.1).[65,103]

During an adsorption process, the fraction of an adsorbate adsorbed in a porous support, can be described as a three steps process. In the first step a quick diffusion of the adsorbate molecules in the exterior surface of the support occurs. In the second step, a slow diffusion inside the pores occurs. In the third step the adsorption of the adsorbate into the pores of the support is generally a slow process since the initial concentration in the bulk solution has decreased. Several kinetic models have been proposed and used to describe the process and estimate the loading. Among these there are the pseudo-second order, the intraparticle diffusion and Langmuir-type equations[104]. The Langmuir- type equation and the pseudo-second order, written in its linear form, can be used to quantify the amount of protein adsorbed at the equilibrium. The intra-particle diffusion model is characterized by a plot of $q_t$ versus $t^{0.5}$. A multi-linear plot is obtained, where each segment has a different slope, corresponding to a different rate of the steps involved in the process.[103,105] Although these models are most frequently adopted for physical adsorption,[65,103,106] in this PhD work, more precisely in the second paper, these models were used to predict the loading also in a covalent binding, resulting in a good agreement with the direct calculation. A detailed description of these kinetic models can be found in refs.[103–105,107]

**Tab. 2.1** Most used adsorption kinetic models for loading estimation.

| Models | Equations | Parameters | Ref. |
|---|---|---|---|
| Direct loading calculation | $q_t = \frac{([P]_0 - [P]_f)V - [P]_w V_w}{m_{support}}$ | $q_t$ = protein loading at time $t$ | [65] |
| Pseudo-second order | $\frac{t}{q_t} = \frac{1}{k_2 q_e^2} + \frac{1}{q_e} t$ | $k_{2=}$ pseudo-second order rate constant (h g mg$^{-1}$) | [103,105] |
| Intraparticle diffusion | $q_t = x_i + k_i t^{1/2}$ | $x_i$= intercept<br>$k_i$=intraparticle diffusion constant (mg g$^{-1}$ h$^{1/2}$) | [103,105] |
| Other fitting equations used | $q_t = \frac{q_e t}{a + t}$ | $q_t$ = protein loading at time $t$<br>$q_e$= protein loading at equilibrium<br>a= constant [104] | [65,104] |

Loading Efficiency % (LE%)[108] is the amount of immobilized protein relative to the total protein amount in the immobilizing solution, and it is calculated by means of the following equation:

$$LE\% = (1 - [P_f]/[P_0]) \times 100\% \quad (2.3)$$

where $[P_0]$ is the initial protein concentration in the immobilizing solution and $[P_f]$ is the residual protein concentration at the end of the immobilization process.[109] Commonly, this parameter is used for the immobilization procedure *via* encapsulation, and reported as Encapsulation Efficiency % (EE%).[110]

## 2.2 Strategies for enzyme immobilization.

The first important aspect to consider in the design of an immobilized enzyme is the choice of the support. A first difference among the different supports which can be used for enzyme immobilization is between porous or non porous materials. Another important feature is the use of nano-structured architectures, where at least one dimension of the particles is in the 'nano' range.[111–113] Current literature presents numerous examples of nanomaterials for enzyme immobilization. Among them non

porous nanoparticles, magnetic nanoparticles, nanofibers, nanocomposites, nanorods, and mesoporous particles (nanosized pores) are found.[90] Porous materials offer high surface area, tuning of pore dimensions and high effectiveness in loading. For these reasons, their use as enzyme carriers is promising and widely investigated.[48,65,114–117] Among porous materials, ordered mesoporous silica (OMSs) are one of the most investigated support for immobilization of enzymes.[96,118] Their high surface area, tunable porosity and the chemical stability, are suitable features for the immobilization procedure. Most recent trends deal with the immobilization on metal organic frameworks (MOFs).[102,119,120] OMS and MOF supports are described in the chapter 3. The strategies adopted for enzyme immobilization depend on the support. In general, it is possible to group immobilization methods in the following categories:

- physical adsorption
- covalent binding
- entrapment and encapsulation
- cross-linking

The choice of the best strategy of immobilization depends on the characteristics of both the support and the enzyme. The support should be characterized by determining its textural parameters - such as surface area, pore volume, pore size and shape of channels - presence of functional groups, surface charge, stability to temperature, pH, etc. Similarly, the enzyme should be characterized in terms of size, isoelectric point (p*I*), activity and stability. Magner and coworkers have proposed a general operational protocol for enzyme immobilization which is schematized in scheme 2.1.[121]

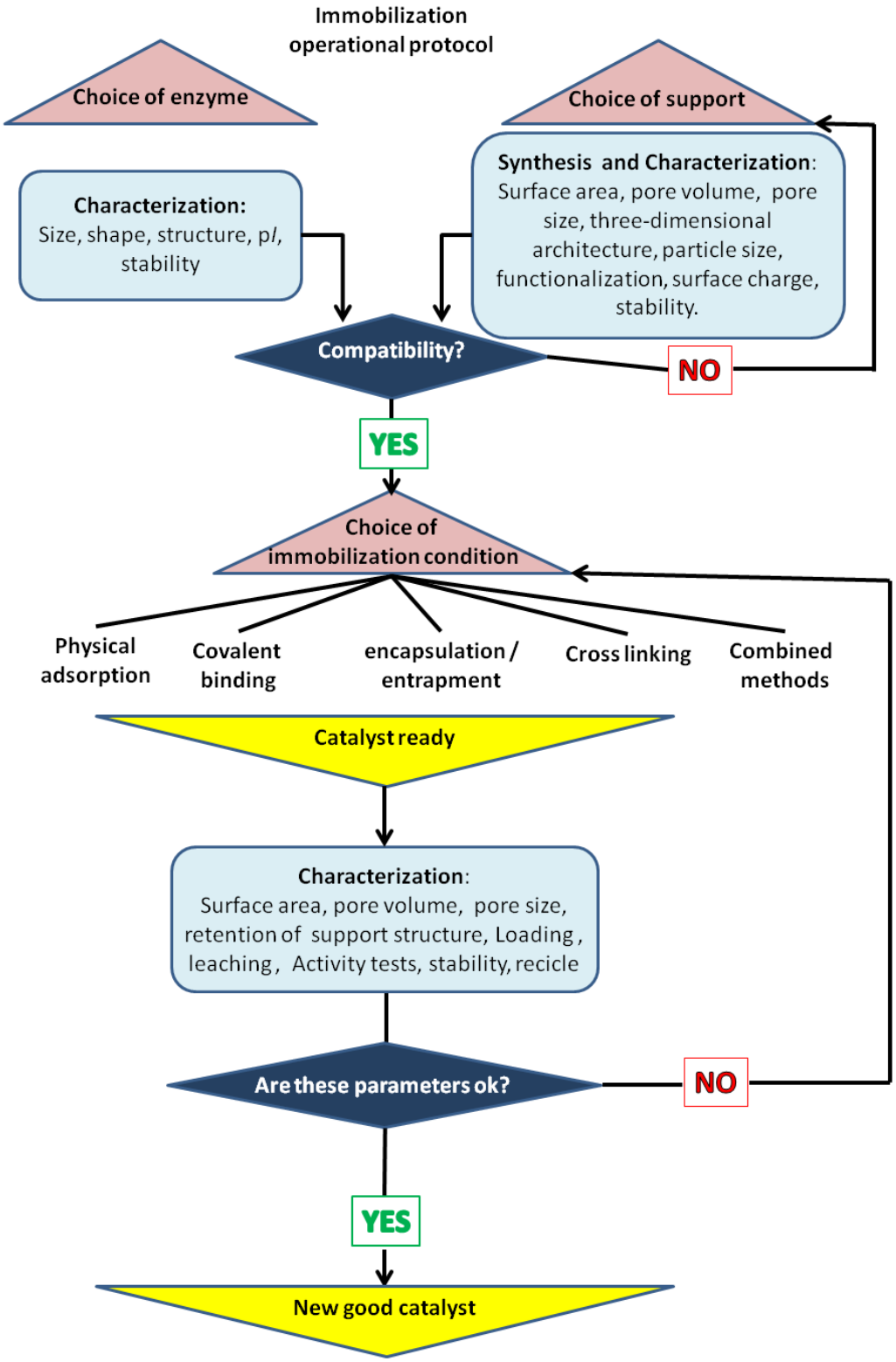


**Scheme 2.1** operational diagram of immobilization procedure. Adapted with permission from ref.[121] Copyright 2005 American Chemical Society

## 2.3 Physical adsorption

Physical adsorption is the easiest, cheapest, and hence widely investigated immobilization technique. It can be suitable for the recovery of expensive supports that do not undergo chemical modifications. The adsorption of the enzyme onto the support is generally driven by van der Waals forces, hydrophobic interactions, dipole-dipole interactions, hydrogen bonds, and electrostatic interactions. The first three interactions are often too weak to keep the enzyme anchored to the support, while hydrogen bonds as well as electrostatic interactions are generally stronger.[118]

For ion- ion interactions, the Coulomb potential energy V is

$$V = -\frac{1}{4\pi\varepsilon_0\varepsilon_r}\ \frac{q_1 q_2}{r} \quad (2.4)$$

$+q_1$ and $-q_2$ are the charged ions, r is the distance between the two ions, $\varepsilon_0\varepsilon_r$ is the permittivity of the medium.[122]

For Ion- dipole interaction

$$V = -\frac{1}{4\pi\varepsilon_0\varepsilon_r}\ \frac{q_1\,\mu}{r^2} \quad (2.5)$$

Where q is the charge of the ion and μ is the permanent dipole. The negative sign of the potential energy indicates attraction.[122]

The van der Waals force includes the effects of all non electrostatic intermolecular forces that depend on $r^{-6}$. They are: Keesom, Debye, and London forces.[123] Dipole-dipole interactions (Keesom forces) result by the electric field of a permanent dipole acting in the nearby of another permanent dipole and depends on the orientation of the two dipoles. For parallel dipoles that can freely rotate, the energy of this interaction, function of the distance $r^{-6}$, can be written as:

$$V_K = -\frac{1}{(4\pi\varepsilon_0\varepsilon_r)^2}\frac{2}{3kT}\frac{\mu_1^2\mu_2^2}{r^6} \quad (2.6)$$

Where $\mu_1$ and $\mu_2$ are the two permanent dipoles, k is the Boltzmann constant ($1.38 \times 10^{-23}$ J/K) and T is the absolute temperature (Kelvin).[122,123]

The interaction between a polar molecule and a polarizable molecule (permanent dipole $\mu_1$ -induced dipole $\mu_2$ or Debye forces) can be written as:

$$V_D = -\frac{1}{(4\pi\varepsilon_0\varepsilon_r)^2}\frac{\mu_1^2\alpha_2 + \mu_2^2\alpha_1}{r^6} \quad (2.7)$$

Where α is the polarizability of the induced dipole (namely the proportionality constant between an external electric field and an induced dipole $\mu=\alpha E$).[122,123]

The interactions between induced dipoles in non polar molecules, are caused by fluctuating electron cloud that move around nuclei, and are known as dispersion forces (London forces)

$$V_L = -\frac{1}{(4\pi\varepsilon_0\varepsilon_r)^2}\frac{3h\upsilon_1\upsilon_2}{2kT\,(\upsilon_1+\upsilon_2)}\frac{\alpha_1\alpha_2}{r^6} \quad (2.8)$$

Where h is the Plank constant ($6.63\times10^{-34}$ J/Hz); $\upsilon_1$ and $\upsilon_2$ are the frequencies.[123]

The overall effects of Keesom Debye and London are known as van der Waals forces

$$V_{VDW}(r) = V_K+V_D+V_L = -\frac{1}{(4\pi\varepsilon_0\varepsilon_r)^2 r^6}\left[\frac{2\mu_1^2\mu_2^2}{3kT} + (\mu_1^2\alpha_2 + \mu_2^2\alpha_1) + \frac{3h\upsilon_1\upsilon_2\alpha_1\alpha_2}{2kT\,(\upsilon_1+\upsilon_2)}\right] \quad (2.9)$$

The van der Waals interactions among molecules decay quickly as they depend on the inverse sixth power of the distance. However, for big molecules total dispersion interactions can become quite strong.[122,123]

Between the weak van der Waals forces (~1 kJ/mol) and the strong covalent or electrostatic interactions (~500 kJ/mol), there are the hydrogen bonds. These kind of interactions occur between hydrogen atoms and oxygen nitrogen or fluorine, that is

strong electronegative atoms, where hydrogen forms a bridge. The strength of this bond is around 10-40 kJ/mol. The potential energy of hydrogen bonds has has a $r^{-2}$ dependence from the distance[123]

$$V_{H^+} = -\frac{1}{4\pi\varepsilon_0\varepsilon_r}\frac{q_{H^+}\,\mu}{r^2} \quad (2.10)$$

Adsorption is often due to a combination of two or more of these forces. Suitable supports for physical adsorption must have high surface area and available pores with a diameter large enough to allow the easy diffusion of enzymes during the adsorption, and an easy diffusion of the reagents/products during the reaction. The main advantage of this method is the retention of a high level of enzymatic activity compared to that of the free enzyme. This because the physical interactions responsible of the adsorption do not distort the three-dimensional structure of the enzyme.[124] On the other hand weak physical interactions may give enzyme leaching. Leaching is the undesired release of the enzyme in the reaction medium and constitutes the main drawback of this immobilization method.[11] The physical adsorption of biomolecules on solid supports is a complex mechanism, clearly influenced by the physico-chemical features of the two interacting species (the biomolecule and the support). Moreover, the composition of the aqueous medium where the enzyme is dissolved plays a central role. The physical adsorption of enzymes on mesoporous silica involves two charged surfaces. At pH values different from the isoelectric point, enzymes carry a net (positive or negative) surface charge. Silica surface is generally negatively charged due to the dissociation of silanol groups at pH > 2.[125] As always occurs when electrostatics is involved beside pH also ionic strength affects enzyme adsorption. What is generally not considered is, instead the specific effect of salts (Hofmeister series) used to fix ionic strength and that of the buffer used to set pH.

### 2.3.1 Effect of pH

The pH of the medium where the immobilization is carried out, generally is chosen and set to foster maximum interaction. Many authors observed that the maximum interaction between protein and support occurs at pH close to the isoelectric point of the enzyme,[126] as the electrostatic repulsion among proteins is minimal, and van der Waals forces prevail over electrostatic lateral repulsions of the molecules having the same charge.[114] Salis et al. investigated different immobilization conditions of *M. javanicus* lipase (IEP in the range between 5.9-6.5) onto mesoporous silica supports, finding a maximum loading at pH 6.[126] Furthermore, silica surface is described by two values of p$K_a$ of the silanol groups (p$K_a \leq 2$ for 1/5 of silanol group and p$K_a \approx 8$ for the remaining 4/5).[127,128] Consequently, the pH of the microenvironment inside the pores can be different from the pH measured in the bulk solution, influencing the loading process. Indeed, a method to measure the pH inside the pores was reported by Yamaguchi et al. who found that pH measured on mesopores of trimethylaminopropyl silica remained weakly acid or neutral despite the different pH tested in the bulk solution.[129] However, the improvement of loading through pH changes is effective only when the pore size of the support is bigger than the diameter of the enzyme.

### 2.3.2 Effect of ionic strength

Ionic strength of the medium is another important parameter that influences the attractive or repulsive forces of the species involved in adsorption. Commonly, buffers (weak electrolytes) are used to set pH around their p$K_a$ value (pH set at values around p$K_a$ ±1), and the presence of strong electrolytes causes significant changes on measured pH in comparison to the theoretical expected value, according to the Hofmeister

series.[130] The surface charge of mesoporous silica at a fixed pH, is influenced by the presence of strong electrolytes,[131] in particular for high salt concentrations, the surface charge of mesoporous silica SBA-15 becomes more negative. Also the surface charge of enzymes is influenced by the presence of electrolytes, in particular strong electrolytes adsorb around the charged surface of an enzyme, and the Debye screening length decreases with increasing concentration of salts.[114] The high salt concentration depresses the effect of electrostatics, amplifying the effect of non-electrostatic interactions.[114] For instance, it was observed that strong electrolytes are able to shift the p*I* of BSA protein towards lower values. It was suggested that this effect is related to the adsorption of more anions than cations on the enzyme surface, due to their higher polarizability.[115] Similarly, the loading of lysozyme, was reported to be influenced by the ionic strength, becoming maximum at high concentration of salts.[65,132] The remarkable conclusion of these works was that at higher salt concentrations, the electrostatic interactions are reduced and van der Waals interactions become preponderant, thus easing the loading,[133] while at low concentration of salts, and low ionic strength electrostatic interactions predominate in the adsorption process.[114] Steri et al. immobilized lysozyme on SBA-15 mesoporous silica observing that the loading and the release of the enzyme were both influenced by ionic strength. Particularly, high ionic strength (NaCl 1M) increased the loading while low ionic strength (NaCl 0.1M) promoted the release of lysozyme more than either high or no ionic strength.[65]

### 2.3.3 Specific ion effects

The addition of electrolytes influences the solubility of proteins. This phenomenon is known since 1888, when Franz Hofmeister observed the effect of anions on

precipitating proteins.[130] Keeping fixed the cation, he ordered the anions in a series according to the increasing concentrations required to salt out the proteins:

$$SO_4^{2-}>HPO_4^{2-}>F^-> CH_3COO^->Cl^->Br^->NO_3^->I^->ClO_4^->SCN^-$$

Analogously, keeping fixed the anion, an ordered series of cations was observed

$$(CH_3)_4N^+>Rb^+>K^+>Na^+>Li^+>Mg^{2+}>Ca^{2+}$$

Moreover, at a fixed concentration, the effect of salts on precipitating proteins was observed to be ion specific for concentrations in the range 0.5-3M.[130] Specific ion effects, related to the Hofmeister series, were observed for physical adsorption of enzymes on mesoporous silica.[64] It was observed that the addition of salts (different sodium salts and different chloride salts) to a solution containing lysozyme (p$I$ ≈ 11) and amino modified mesoporous silica particles (PZC occurs at pH ≈ 11), promoted the loading at a pH=9 (i.e. below the p$I$ and the PZC) according to the inverse anion series:

$$SCN^- > ClO_4^- >Br^- > NO_3^- >Cl^- >SO_4^{2-}$$

more evident for low concentrations (0.2M) than at high concentrations (0.8M)

while the cation series:

$$Na^+>Li^+>K^+>Cs^+$$

showed a bell shape trend in loading, less pronounced at high concentrations of salts.

Recently, Medda et al. investigated specific ion (Hofmeister) effects on the surface charge of BSA (Bovine Serum Albumin). Below the IEP, the BSA surface charge changed as a function of solution pH, in presence of anions according to the series $Cl^-$ <$Br^-$ <$NO_3^-$ <$I^-$ < $SCN^-$. While, above the IEP the series displayed the same order of magnitude but with negative values. Also the Zeta potential of BSA as a function of pH displayed a clear dependence on the specific ions used to set the ionic strength.[115]

Moreover, more recently, specific influences of weak electrolytes upon lysozyme

loading on carboxyl-modified polystyrene nanoparticles[134] were investigated. The conventional mechanism of buffers to set the pH of solutions is based on the Henderson-Hasselbalch equation,[135] and no other effects are attributed to buffers in affecting chemical parameters of proteins such as electrophoretic mobility. Investigating the effect of buffers on electrophoretic mobility of proteins, it was observed that the type of weak electrolyte used for buffers influences the zeta potential of lysozyme,[116,134] thus suggesting an active action of buffers also (Fig. 2.1).

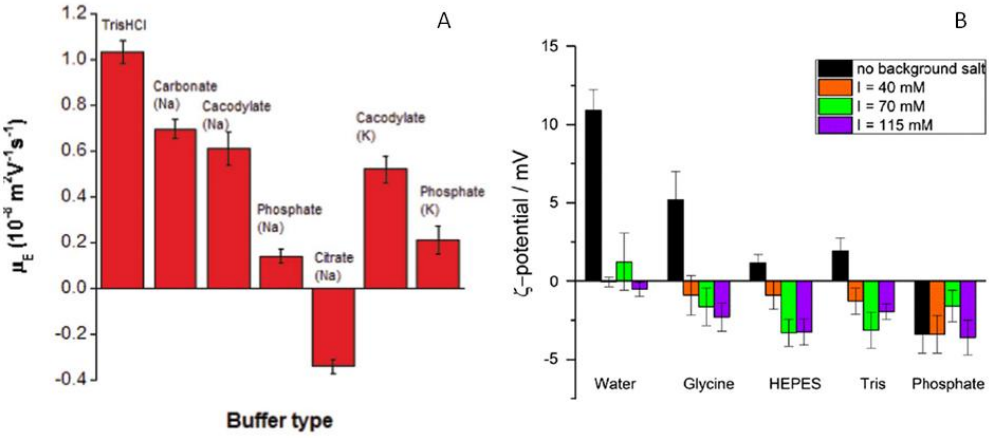


**Fig. 2.1** weak electrolytes affect the electrophoretic mobility of LYZ. In A) all buffers are set at pH 7.15. Reproduced with permission from ref.[116] Copyright 2013 Royal Society of Chemistry. In B) all buffers are set at pH 7.4 in absence or presence of NaCl at various concentrations. Reproduced with permission from ref.[134] Copyright 2017 Elsevier.

Likely, buffers ions are adsorbed on the surface of proteins (Fig.2.2), influencing surface charge until they can also partially or totally screen the net charge of the protein according to the concentration (or ionic strength) of solution.

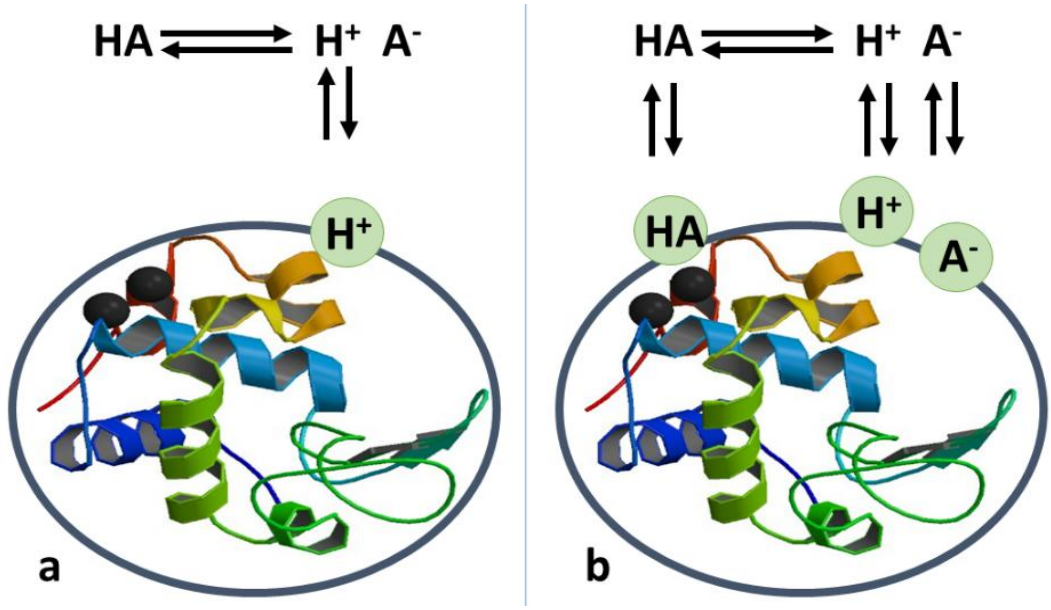


**Fig. 2.2** equilibrium at the surface of a protein in aqueous solution a) conventional model of buffers according to Henderson–Hasselbalch equilibrium, b) proposed mechanism for the effect of buffers at the protein surface. Adapted with permission from ref.[116] Copyright 2013 Royal Society of Chemistry.

Nearby the surface effects, the other parameter affecting physisorption of enzymes is the diffusion inside the pores of a porous support. Not only the pore diameter must be compatible with the size of enzyme but the microenvironment inside the pores (hydrophobicity, pH) should not be too different from the bulk conditions, otherwise the efficiency of the process can be compromised.[136]

## 2.4 Covalent binding

Covalent binding is an immobilization technique that allows to anchor the enzyme to the support thus avoiding the unwanted leaching. The high strength of the covalent bonds has the drawback of the possible distortion of the enzyme conformation. If the structure distortion involves the active site a significant loss of activity may occur.[6]

Among the suitable supports for covalent binding, surface functionalized ordered

mesoporous silica (OMS) materials are widely investigated. The free silanol groups occurring on the surface of the OMS can be functionalized with a wide range of organosilane molecules. With this strategy numerous functional groups - i.e. thiol, epoxide, alkyl chlorides, vinyl, amine, etc. - can be introduced on OMS surface. The main methods to introduce a modification on OMS surface are the post-synthesis modifications (or grafting), the co-condensation, and the preparation of ordered mesoporous organosilica.[137] The grafting is a modification of the surface after OMS synthesis with an organosilane molecule. According with Fig. 2.3 the free hydroxyl groups bind different organosilanes which permit to introduce a wide range of organic functional groups on OMS surface.[118] The post-synthesis modification of mesoporous materials usually results in the reduction of the pore size and surface area. [96,138,139]

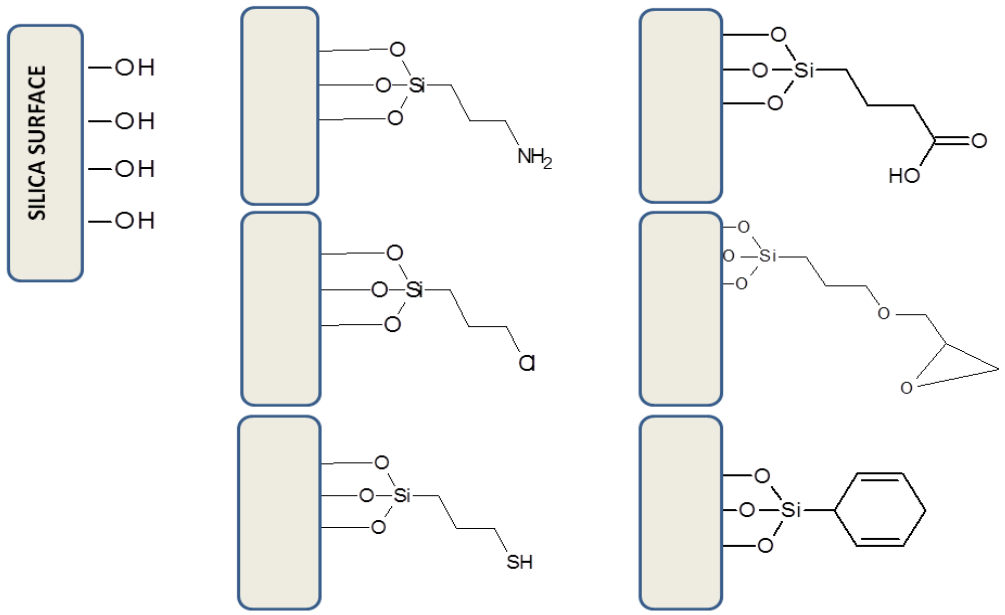


**Fig. 2.3** Chemical modifications at the surface of silica supports. Adapted with permission from ref.[118] Copyright 2013 Royal Society of Chemistry

An alternative to grafting is the co-condensation, where the trialchoxy-organosilane is added in added to the tetraalkoxysilane to obtain a *one-pot* synthesis and

functionalization. This procedure is quicker than grafting since performed only in one step instead of two. Moreover no reduction of the pore size and surface area of the support occurs. However, the amount of organic groups on the support surface that can be inserted through this method is generally low compared to the initial amount of functionalizing agent used.[96]

After functionalization the enzyme can finally be attached on the support surface. This can be directly or, more often, by mean of bi-functional linkers. They create a bridge between the enzyme and the functionalized support surface. Glutaraldehyde (GA) is a widely used linker. Its aldehyde groups react with ε-$NH_2$ groups of lysine residues which are then stabilized by a conjugation Schiff-base mechanism or a Michael-type addition mechanism.[140] The concentration of GA and the time of contact with the protein is an important parameter that can affect the enzyme activity as observed by Yang et al.[141] Other linkers such as glutaric anhydride or functionalizing agents which directly react with the enzyme, such as glycidyloxypropyl trimethoxysilane are shown in Fig. 2.4.

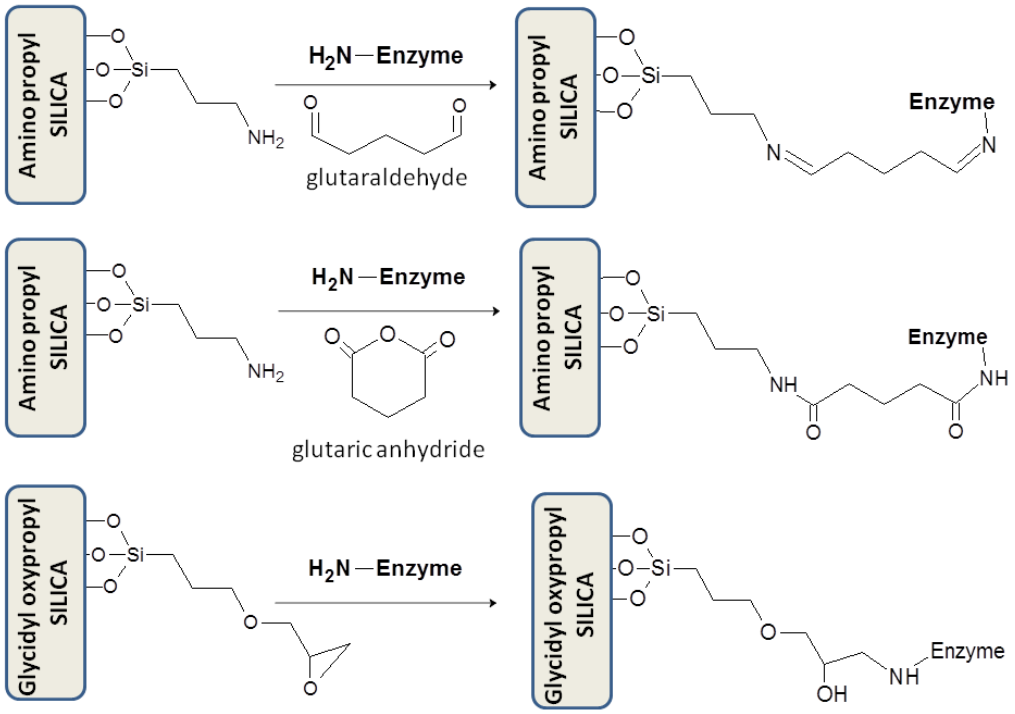


**Fig. 2.4** linkers for functionalized mesoporous silica. Adapted with permission from ref.[118] Copyright 2013 Royal Society of Chemistry

## 2.5 Entrapment and encapsulation

Entrapment and encapsulation are often used as synonyms to indicate a type of enzymatic immobilization that occurs simultaneously to the formation of the solid network constituting the support.[142] The main advantage of entrapment is due to the absence of covalent bonds between the biomolecule and the support matrix, so that the enzyme structure is not distorted and retains a high extent of its activity in the free form. If the matrix is porous, the diffusion process of reagent and product molecules can easily occur. Moreover, if the support pore size is lower than the size of the entrapped enzyme molecules the leaching, mainly observed for physically adsorbed enzymes, is kept at a very low level of even not observed at all. Among the matrices used for

enzyme entrapment silica sol-gels are likely the most investigated systems. The entrapment via silica sol-gels involves the dissolution of enzymes in a sol-gel precursors, generally tetraethoxysilane (TEOS). The following steps involve a hydrolytic polymerization and a drying process, which lead to the formation of xerogels (dried via evaporation, with shrinkage of pores),[142] ambigels (dried via evaporation, without shrinkage of pores),[142] or aerogels (dried via supercritical fluids, with complete retention of porosity).[143] The entrapment can also occur in natural or synthetic hydrogels[142] or cryogels[142,144] such as polyvinylalcohol (PVA) that are suitable not only for enzymes but also for whole cells. More recently, metal organic frameworks (MOFs) have emerged as a new class of supports for the encapsulation of enzymes.[145,146] Enzyme encapsulation into MOFs consists of a "*one-pot* synthesis" where the formation of the hybrid inorganic (metal)/organic (ligand) network occurs in the presence of the enzymes which remain entrapped within the MOF structure.[147] This is an useful procedure which leads to the immobilization of an enzyme into microporous supports. Such small pores would not allow neither physical nor covalent post-synthesis enzyme immobilization into MOFs. The pores are anyway enough large to permit the diffusion of small molecules such as substrates and products, but enough small to avoid enzyme leaching. Finally, MOF structure provides a protective coating against harsh environmental conditions, i.e. high temperature.[146] The in situ encapsulation can be carried out via two possible routes: the co-precipitation and the biomimetic mineralization.[145] This will be discussed in more detail in section 3.2.

## 2.6 Cross-linking

Cross-linking is a "support-free" immobilization that combines covalent bonding with entrapment.[11] Cross-linking may occur with intra-molecular inter-subunit or

intermolecular bonds, by means of cross-linked enzymes complexes (CLEs), namely: cross-linked enzyme crystals (CLECs), cross-linked enzyme aggregates (CLEAs), or cross-linked layers of previously immobilized enzymes.[142,148] Bi-functional chemical linkers such as bis-isodiacetamide, or glutaraldehyde can be used to form insoluble CLEs. The resulting biocatalyst is generally endowed of high productivity, namely in provides high mass of product per mass of biocatalyst.[142] Indeed the other immobilization methods require the presence of a support as a carrier for enzymes. This results in a kind of "activity dilution" because of the presence of a large percentage of non enzymatic (inactive) components in the catalytic preparation.[142] It should be noticed that this kind of immobilization improves the thermal stability of enzymes. However some factors such as pH, the amount of cross-linker, the ionic strength of the medium and the temperature can affect the final performance of the catalyst.[124] A careful design and set up of the experimental conditions is needed to optimize the whole cross linking process. Although, cross linking is generally a cheap immobilization method, some important drawbacks can be highlighted: low retention of activity (usually less than 50%), poor reproducibility and low mechanical stability.

CLECs are formed by cross-linking enzyme crystals by addition of glutaraldehyde to the crystallization solution carried out in an aqueous buffer at a suitable pH. A variation in the cross-linker ratio or in the cross-linking time leads to different size of the particles.[142] CLEAs are formed by precipitation, exploiting the salting-out effect of ammonium sulfate[142] or polymers as polyethylene glycol. They promote the precipitation of the enzymes without damaging their tertiary and quaternary structure. These physical aggregates are then cross-linked by means of glutaraldehyde which make them permanently insoluble. With this method high purity of enzymes is not

required, and CLEAs can be prepared from the enzyme fermentation broths.[142]

The activity of CLECs and CLEAs is about 10 to 1000 times higher than that of the corresponding biocatalysts immobilized on an inert support. This method is particularly suitable when a high loading (mg of protein/ g of biocatalyst) and activity (U/g of biocatalyst) is required, or enzymes cannot be immobilized covalently.[149] In all cases it was observed that the dimensions of CLEs particles is very important.[124] Small particles exhibit high activity, but can hardly be recovered by filtration or centrifugation. Large particles can easily be recovered but display low activities due to diffusion problems.[124] Some modifications of CLEAs were developed by coupling CLEAs to co-polymers or nanoparticles (i.e. magnetic nanoparticles) obtaining more stable biocatalysts, or biocatalysts suitable for magnetically stabilized bed reactors.[142]

# **Chapter 3:** *Supports for enzyme immobilization*

## 3.1 Mesoporous silica

A porous material is a solid with internal voids that can be filled with gas or liquids. Pores can be closed, that is without connections with other pores or open, with connections among the internal voids and with the external surface. According to IUPAC (International Union Pure and Applied Chemistry), porous materials are classified on the basis of the pore diameter:

- macroporous material: diameter > 50 nm;
- mesoporous material: diameter 2-50 nm;
- microporous materials: diameter < 2 nm.

Moreover, on the basis of the chemical structure, they can be classified as purely inorganic (silica, metal oxides, combined metal-silica based materials), purely organic (hollow carbon particles, organic polymers) or hybrid organic-inorganic materials (organosilica, metal organic frameworks).

Mesoporous silica is a synthetic amorphous silicon dioxide-based material, widely used in current development of modern nanotechnologies, with a wide range of applications, such as nanomedicine,[150,151] adsorption,[152] catalysis and biocatalysis,[118,153] and biosensors[154] etc.. Among the various silica-based mesostructures, MCM-41 (Mobile composite of matter)[155] and SBA-15 (Santa Barbara Amorphous)[156] have attracted great interest in the international scientific literature.[96,114,117,157,158]

The first procedure for the preparation of a low density silica, by means of the self-assembly of a soluble silicate over a the micellar template, was described in a patent of 1969.[159] But it was in 1992 that the researchers of Mobile Corporation Laboratories synthesized and characterized a new family of silica based mesoporous materials named M41S, including cubic phases, lamellar phases, and hexagonal phases which were

called MCM-48, MCM-50, and MCM-41, respectively.[155] Then in 1998, Zhao et al. reported the synthesis of the hexagonal mesoporous silica particles named SBA-15.[156] The success of mesoporous silica is related to some important physical parameters, that can easily be controlled during the synthesis, namely the size of particles (from nanometers to centimeters), the pore dimensions (2-4 nm for MCM-41, 6-10 nm for SBA-15, larger than 20 nm for MCF), the surface area (around 700-1000 $m^2/g$), the pore volume (around 0.5 $cm^3/g$), the wall thickness (around 4-5 nm for SBA materials) and the morphology.[150,158,160,161] The amorphous solid state of mesoporous silica allows low rigidity/stiffness and good control of the above parameters.[161] In addition, important properties such as exceptional stability towards high temperatures, extreme pH conditions, microbial attack[96], biocompatibility[133], etc., make these materials suitable for many applications.

Despite the different structural parameters that can be designed in the synthesis of different mesoporous silica, there are some common points. The general approach starts from the molecular self-assembly of surfactants, that act as structure-directing agents.[137] When surfactants are dissolved in solution above their *critical micelle concentration* (CMC), the non covalent intermolecular interactions (such as hydrophobic interaction, Van der Waals forces, including London forces, Keesom and Debye interaction, hydrogen bonds) and the electrostatic charge of polar segments promote the formation of micelles. One of the hypothesis proposed to explain the mechanism of formation of mesoporous materials is the cooperative self-assembly.[137,155,162–165] The surfactant self-assembles into micelles, which constitutes the basis for the subsequent polymerization of the silica precursor. This occurs at lower concentration than the surfactant CMC. The addition of the silica precursor, i.e.

(Tetraethylorthosilicate TEOS, Tetramethylorthosilicate TMOS, Glycidoxypropyltrimethoxysilane GPTMS), directly influences the formation of rod shape micelles because the tetraalkoxysilane preferentially distributes on the external surface of micelles, acting as a structure directing agent, reducing the micelles mobility and stabilizing the dispersion.[164]

The formation of liquid-crystal phase is necessary and temperature is a critical parameter that influences the surfactant CMC.[117] Different surfactants allow different arrays, lamellar, hexagonal, cubic and bicontinuous according to their physico-chemical properties[166] determining the final morphology of the mesoporous silica particles. For instance, MCM-41 mesoporous silica with hexagonal array of pores having a size around 2-4 nm, is formed by mean of the cationic surfactant cetyltrimethylammonium bromide ($C_{16}H_{33}N(CH_3)_3$- Br, CTAB.[155] Amphiphilic triblock copolymers, such as poly(ethylene oxide)–poly(propylene oxide)–poly(ethylene oxide) ($PEO_{20}$-$PPO_{70}$-$PEO_{20}$, Pluronic 123), with long hydrophobic tails is used as template for the synthesis of the SBA-15 mesoporous silica, that has an hexagonal array of pores with a size distribution ranging from 7.5 to 32.0 nm.[156]

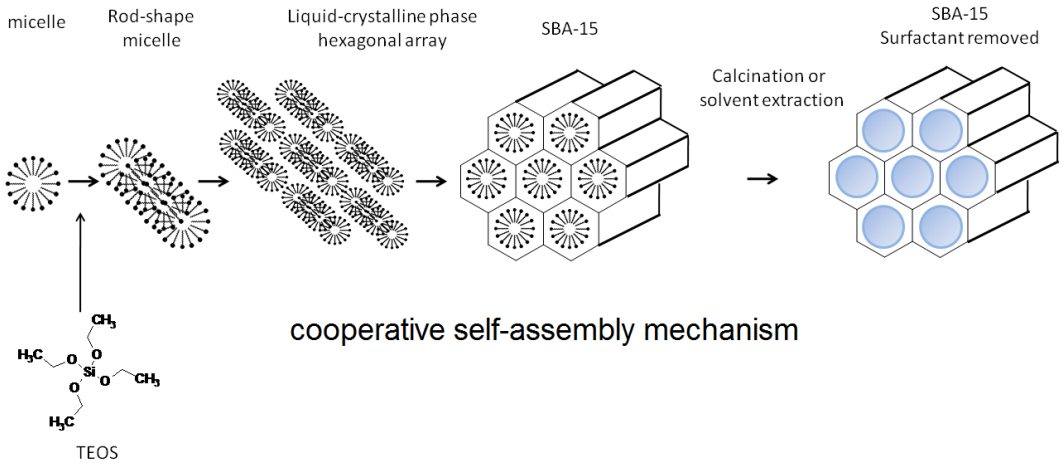


**Fig. 3.1** Self-assembly of surfactant, addition of silica precursor and formation of mesoporous particles via a cooperative self-assembly liquid-crystal template

mechanism; the silica precursor acts as a structure directing agent. Adapted with permission from ref.[137] Copyright 2006 John Wiley and Sons

Mesoporous silica can be prepared either in the form of particles or deposited thin films. The latter are commonly prepared by using Pluronic F127 ($PEO_{106}$-$PPO_{70}$- $PEO_{106}$) as a templating agent. The self-assembly and the cooperative templating mechanism occur after the liquid-crystal phase deposition on a proper solid, generally a silicon strip or a quartz slide. The evaporation of the solvent is the driving force to promote the self-assembly and the polymerization of the silica film. This procedure is known as evaporation induced self-assembly (EISA).[167] Mesoporous silica films can be prepared through deposition by immersion (dip-coating) or by rotation (spin-coating), and can show a hexagonal pattern or a wormlike structure.[168,169]

Up to now, these kinds of mesophases, disordered, worm-like, hexagonal, cubic, and lamellar, have been reported and different morphologies (e.g. spheres, radial porous spheres, rods, films, and various hierarchical structures), and dimensions (microparticles or nanoparticles) were obtained by changing the block copolymer, the silica precursor or the reaction conditions (temperature, pH)[161,170] Moreover, the final array and the porosity of mesoporous silica can be influenced by inorganic mineralizing agents, such as $NH_4F$ which is used to improve the formation of highly ordered hexagonal arrays. The addition of specific linear alkanes or aromatic compounds to the liquid crystalline phase may result instead in changes of the porosity and of the final array.[171] For instance, the transition from the hexagonal array to a disordered structure, typical of mesoporous silica foams particles (MSF), is achieved by adding increasing amounts of oils, that act as swelling agents, such as 1,3,5-Trimethylbenzene (TMB or mesitylene), in the liquid-crystal phase. The mechanism of pore enlargement is related to the high partition coefficient of swelling agents, that tend to distribute in the core of hydrophobic

chains of surfactants, causing a change in the packed structure.[172] This variation in the synthesis protocol causes the enlargement of pore diameter, and the increase of pore volume but with loss of the narrow size distribution and of the ordered hexagonal array, thus leading to the formation of particles known as mesocellular foam (MCF), as shown in Fig. 3.2.[173,174] The oil/ surfactant molar ratio, the type of chain, the temperature, and the pH can be controlled to obtain different structural textures.[171] Tab.3.1 shows the typical structural parameters of SBA-15, MCM-41, and MCF mesoporous silicas.

**Tab. 3.1** typical structural parameters of SBA-15 MCM-41 and MCF

| MPS | Surfactant | Surface area ($m^2/g$) | Pore volume ($cm^3/g$) | Pore diameter (nm) | Wall thickness (nm) | Lattice spacing (nm) | Ref. |
|---|---|---|---|---|---|---|---|
| SBA-15 | $EO_{20}PO_{70}EO_{20}$ | 820-920 | 1.0-1.2 | 7.7-8.5 | 3.1-3.8 | 10.3-10.8 | [156] |
| MCM-41 | $C_nH_{2n+1}(CH_3)N^+$ n= 8-16 | 1040 | 1.0-3.0 | 1.5/10 | 0.7-1.6 | 2.7-3.9 | [155,175] |
| MCF | P123/TMB | 550-900 | 1.0-2.4 | 22-36 | Not given | Not resolved | [173] |

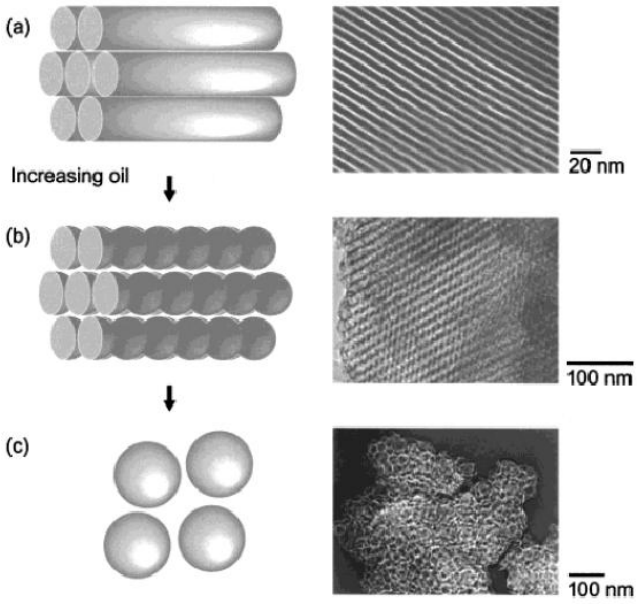


**Fig. 3.2** Transition from hexagonal SBA-15 to mesocellular foam MCF caused by TMB. Reproduced with permission from ref.[174] Copyright 2000 American Chemical Society

## 3.2 Metal organic frameworks

Metal Organic Frameworks (MOFs) are constituted by metal ions coordinated by organic ligands to form a crystalline porous solid. The term MOF was used by Yaghi et al. for the first time in 1995 for a material constituted by a copper 4,4′-bipyridyl complex.[176] MOFs are microporous materials which exhibit a high degree of crystallinity due to a three-dimensional network of metal-organic ligand bonds.[176] Presently a huge number of new MOFs have been synthesized by using different metal ions and ligands. The obtained materials have peculiar and special characteristics, such as magnetic and electrochemical properties, and can be used for catalysis, for molecular capture or as molecular sieve properties.[119] In the last decade these compounds have also been suggested as new, but still few explored, supports for the immobilization of enzymes.[102] Due to their nature of inorganic/organic compounds, the possible interactions between MOFs and enzyme biomacromolecules range from covalent and coordinative bonds to weak van der Waals forces or hydrogen bonds. Moreover, also electrostatic interactions can occur due to the large presence of metal ions in the MOFs structure and the charges on enzyme surfaces. [145]

As described in chapter 2, the immobilization of enzymes into MOFs can be done post-synthesis or during the synthesis (one-pot synthesis immobilization). The choice of the best procedure depends on the type of enzyme, the type of MOF, and the application. However, the most investigated immobilization strategies are the physical and the in situ encapsulation of the free or modified enzymes. Fig. 3.3 shows the different strategies for enzyme immobilization in MOFs

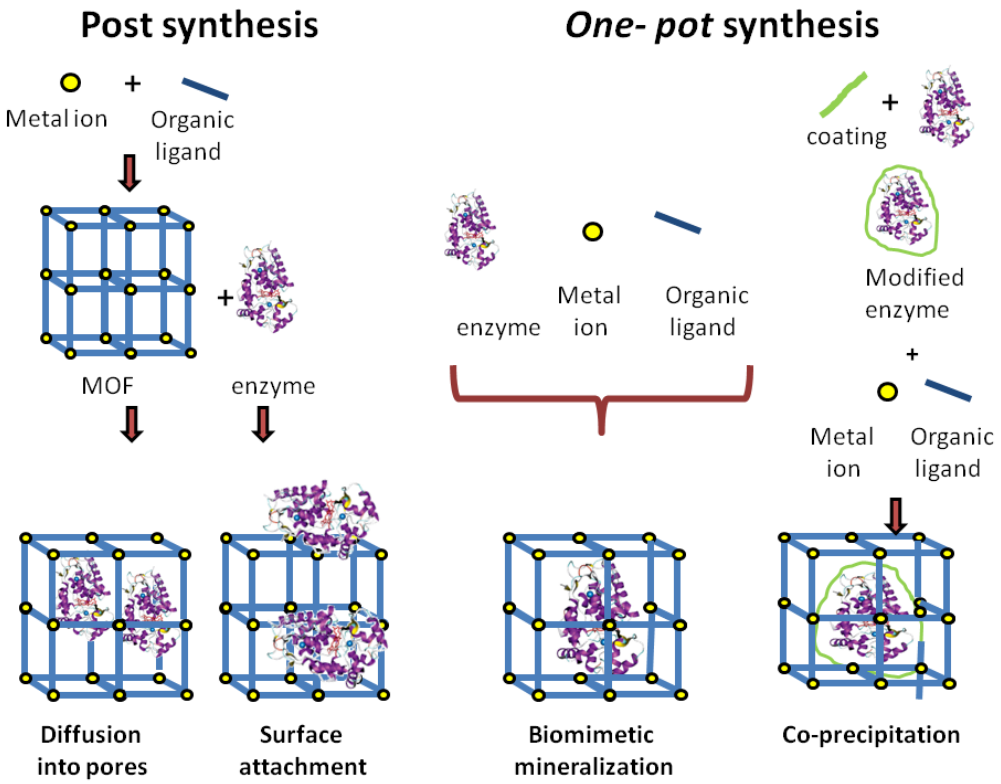


**Fig. 3.3** scheme of immobilization of enzymes in MOFs. In the post-synthesis methods, the enzyme is immobilized by physical adsorption into pores, or alternatively by means of a superficial attachment, on a preformed MOF. In the "*one-pot*" synthesis the framework is built around the pure or coated enzyme.

The procedure of MOFs synthesis can be carried out by means of several synthetic protocols. The in situ encapsulation, with the simultaneous formation of the framework in presence of the pure or modified enzymes, has been investigated by many authors by means of mechanosynthesis[177], solvothermal[106] and hydrothermal[178] protocols. The in situ encapsulation by means of hydrothermal protocols, consists in the dissolution of the enzyme in an aqueous solution containing the organic ligand. Then the ligand/enzyme solution is mixed with that containing a metal precursor, thus forming an enzyme@MOF biocomposite.[67,99] If the synthesis is carried out in water or via mechanochemical,[177,179] the enzyme can be added in its native form, and the procedure is named biomineralization.[67,177,180–183] A similar mechanism occurring in nature

corresponds to the deposition of minerals to form an exoscheletal coating that protect living tissues. If the synthesis is carried out in organic media, like methanol or DMF, a polymeric coating (i.e. polyvinylpyrrolidone -PVP, polyacrylammide, polyvinyl acetate) is often used to protect the enzyme from denaturation. This procedure is named co-precipitation.[184] However, co-precipitation can also be used in aqueous media.[180]

The post-synthetic immobilization is carried out by means of physical adsorption[185] or covalent bonding[186] from aqueous buffer solutions. In order to optimize the immobilization process several experimental parameters have to be considered, namely: the immobilization temperature, the time of contact between the MOF and the enzyme, and the stability of both MOFs and enzymes to the pH of the immobilizing solution.[102] As written in the chapter 2, the post synthesis immobilization requires that enzyme diffuse into the MOF pores. This can occur only if MOF supports have a pore diameter bigger than the enzyme size.[145] In addition also the three-dimensional architecture of MOFs plays an important role. In channel-type MOFs the diameter is uniform along the whole pore, so the diffusion is permitted if MOF and enzyme diameters are compatible. In cage-type MOFs the diameter of the pores in the cage is larger than the diameter of pores at the entrance, thus determining a bottle-neck effect, that produces limitations to the diffusion of the enzymes.[145]

### 3.2.1 ZIF

Zeolite Imidazolate Frameworks (ZIFs) are a subclass of MOFs that were firstly synthesized by Huang et al.[187] and by Park et al.[188] in 2006. The aim was the synthesis of a new class of microporous crystalline solids for petrochemical cracking, water purification, gas separation. ZIFs are obtained by copolymerization of either Zn(II) or Co(II) with imidazole, alkyl-imidazole or phenyl-imidazole ligands and have a high

level of crystallinity and an exceptional thermal stability. The porosity of ZIF materials is similar to that natural zeolites.[188–190] By changing the ligand or the metal ion different structures i.e. SOD (sodalite), MER (merlinoite), GIS (gismondine), RHO (rho)[191] can be obtained (Fig. 3.4).

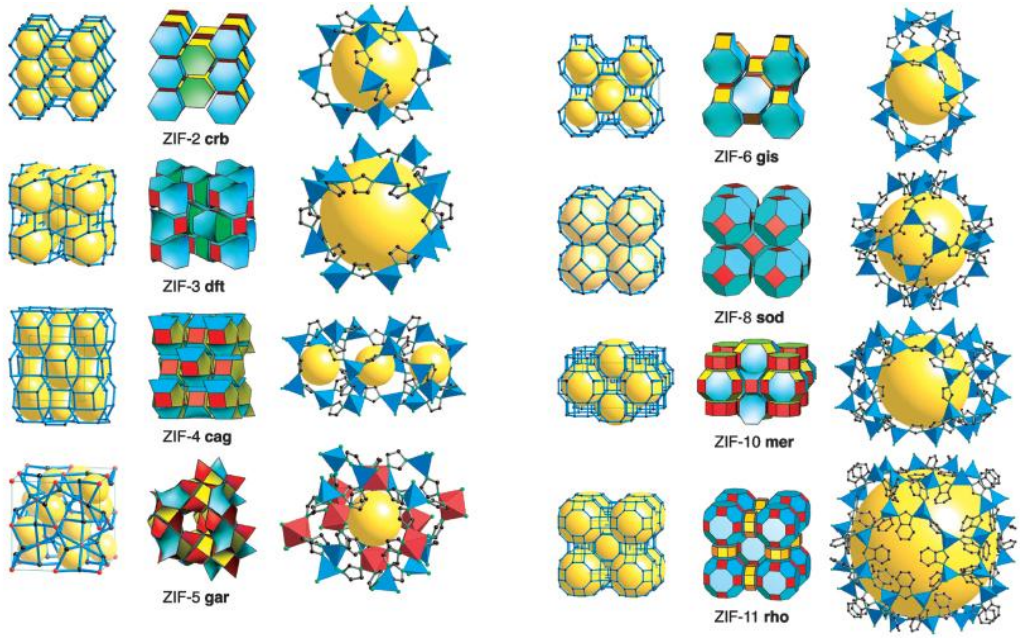


**Fig. 3.4** different 3D structures of ZIFs grouped by topology. Reproduced with permission from ref.[188] Copyright 2006 National Academy of Sciences.

The corresponding parameters for different ZIFs are reported in Tab. 3.1. For all ZIFs the similarity with zeolites derives from the tetrahedral bond of metal ion with the nitrogen atoms in the imidazole ring. The bridges between metal ions and imidazole nitrogen atoms form an angle close to 145°, similar to the Si-O-Si bond which occurs in natural zeolites,[188,192] as shown in Fig. 3.5

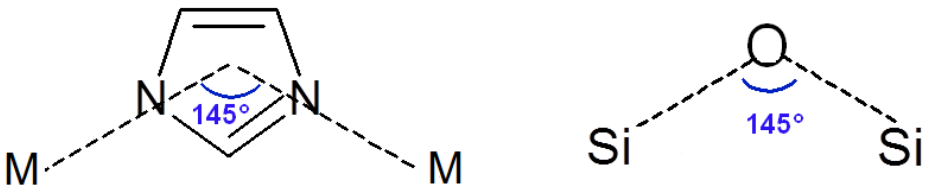

**Fig. 3.5** the angle between metal (M) and ligand (imidazole) in ZIFs is similar to the angle between silicon and oxygen in natural zeolites. Adapted with permission from ref.[188] Copyright 2006 National Academy of Sciences.

ZIF-8 ($Zn(MIM)_2$) is a crystalline microporous MOF obtained by a tetrahedral coordination bond between $Zn^{2+}$ ions and 2-methylimidazole (MIM) ligand, geometrically arranged according to the structure of the sodalite (SOD topology). The SOD cage presents pores of 11.6 Å accessible through a window of 3.4 Å.[189] This microporosity results in large values of the surface area (up 1800$m^2$/g for conventional synthesis in methanol). Moreover the exceptional thermal stability (up to 350°C), and the tunable porosity[193] are suitable parameters to produce a good solid support for enzyme immobilization. On the other hand the versatility of synthesis methods of the pure ZIF-8, including those previously mentioned, such as mechanosynthesis,[177] solvothermal,[106] and hydrothermal[178] methods, and also microwave assisted,[194] steam assisted,[189] do not always lead to the SOD topology. Particularly the hydrothermal synthesis is strongly influenced by the Zn:Ligand (Zn:L) molar ratio. Shi et al. reported that the synthesis of the ZIF-8 (SOD) was achieved with Zn:L ratios higher than 10. The Zn:L ratio 1:2 instead resulted in an unknown phase, whereas the Zn:L ratio 1:4 resulted in a mixed phase of both ZIF-8 and an unknown phase.[189] Similar results were obtained by Kida et al. who obtained SOD and mixed phases at high and low Zn:L ratios, respectively.[195] Katsenis et al. observed the amorphization of ZIF-8, namely a transition from crystalline to amorphous phase, and then a recrystallization on a non porous material, by changing the mechanochemical synthesis conditions, resulting in different three-dimensional structures.[179]

Similarly to ZIFs obtained from Zn and 2-Methyl imidazole, also for the ZIFs obtained by polymerization of Zn and imidazole, ($Zn(IM)_2$) different topologies were reported,

i.e. MER (merlinoite) of ZIF-10, GIS (gismondine) of ZIF-6, body centered tetragonal tectosilicate or BCT of ZIF-1 and 2, but also the zni dense structure[190,196] (Table 3.1). This suggests that complex mechanisms are involved during nucleation and growth of ZIFs crystals. For zeolite topologies refer to the paper[191] and to the web site: www.iza-structure.org/databases/.

**Tab. 3.1** composition, structure and net parameters of some ZIFs. IM = imidazole, MIM = 2-methylimidazole, PhIM = phenylimidazole This table is adapted with permission from ref. [188] Copyright 2006 National Academy of Sciences.

| ZIF-X | Composition | Periodic net [197,198] | Zeolite topology | Pore diameter (Å) | Surface area $m^2/g$ | Ref. [188] |
|---|---|---|---|---|---|---|
| ZIF-1 | $Zn(IM)_2$ | Crb | BCT | 6.94 | | |
| ZIF-2 | $Zn(IM)_2$ | Crb | BCT | 6.00 | | |
| ZIF-3 | $Zn(IM)_2$ | Dft | DFT | 8.02 | | |
| ZIF-4 | $Zn(IM)_2$ | Cag | - | 2.04 | 300 | [199] |
| ZIF-5 | $In_2Zn_3(IM)_{12}$ | Gar | - | 3.03 | | |
| ZIF-6 | $Zn(IM)_2$ | Gls | GIS | 8.8 | | |
| ZIF-7 | $Zn(PhIM)_2$ | Sod | SOD | 4.31 | | |
| ZIF-8 | $Zn(MIM)_2$ | Sod | SOD | 11.6 | 1.724 | [199] |
| ZIF-9 | $Co(PhIM)_2$ | Sod | SOD | 4.31 | 1.144 | [200] |
| ZIF-10 | $Zn(IM)_2$ | Mer | MER | 12.12 | | |
| ZIF-11 | $Zn(PhIM)_2$ | Rho | RHO | 14.64 | Non porous to $N_2$ | [188] |
| ZIF-12 | $Co(PhIM)_2$ | Rho | RHO | 14.64 | | |

The strategies for immobilization of enzymes on ZIFs are the same described for the general synthetic protocols of MOFs. They include the *in situ* encapsulation of native enzymes (biomimetic mineralization) or polymer-entrapped enzymes (co-polymerization),[180] but also the post-synthesis incorporation on unmodified[201] or modified[202] ZIF-8 surface. An overview of recent trends concerning the applications of immobilized enzymes on ZIFs is discussed in the following paragraph.

## 3.3 An overview of immobilized enzymes on mesoporous silica and ZIFs

The importance of studying immobilized biocatalysts is demonstrated by a wide scientific literature and increasing industrial applications of enzymes.[203] In order to improve the performance of an immobilized biocatalyst it is important a deep comprehension of the molecular mechanisms involved in the immobilization process. This means that the efforts to immobilize model proteins, such as lysozyme or BSA, play a crucial role in the development of new strategies for the design of new efficient biocatalysts.[12,204]

Although it is always challenging to give an exhaustive overview of the wide field of the enzyme immobilization, some recent significant examples of immobilized enzymes on ZIFs and mesoporous silica, are worth to be described. In the following paragraphs the recent papers about the immobilization of lipases, glucose oxidase, peroxidases, and lysozyme on ZIFs (published from 2015 to 2017) and mesoporous silica, (published from 2016 to 2017), are reported. A synthetic list of the reviewed literature is reported in Table 3.2 (ZIF) and 3.3 (mesoporous silica). The possible applications proposed for these new biocatalysts, mainly concern the pharmaceutical field, the design of new biosensors, the wastewater treatment and the production of biodiesel.

### 3.3.1. Immobilized enzymes on ZIFs

Recently, several enzymes were immobilized on MOFs, mainly in ZIF-8 by means of both post-synthesis immobilization or in situ encapsulation. Liu et al. investigated the catalytic performance of porcine pancreatic lipase (PPL) immobilized in several microporous MOFs in comparison with SBA-15. The PPL was physically adsorbed into

the supports and the catalyst was tested for pharmaceutical applications: the synthesis of warfarin, an important thrombolytic drug.[205] Nadar and Rathod immobilized a lipase from *Aspergillus niger* on ZIF-8 by a biomimetic mineralization approach, and found an enhanced activity of the catalyst induced by exposure to ultrasounds.[206] He et al. immobilized a thermophilic lipase from *Alcaligenes sp*. on ZIF-8, through a mechanochemical synthetic method, and investigated the long-term stability and recycling of the biocatalyst after a 5 days storage at two different temperatures (37°C and 60°C). They obtained an activity retention of 20.3% and 6.0% with respect to the initial biocatalyst activity. Moreover, their biocatalyst was recycled 10 times with an activity retention of 75.7% at the $10^{th}$ reaction cycle.[177] Cheong et al. immobilized *Burkholderia cepacia* lipase on amino-functionalized ZIF-8 through physical adsorption, and investigated the activity at the aqueous/organic interface. The biocatalyst could be recycled obtaining a retention of 60% of the initial activity after 10 reaction cycles.[207] Shi et al. immobilized the lipase from *Candida rugosa* on ZIF-8 synthesized via a solvothermal method using methanol as the solvent.[202]

Oxidoreductase enzymes such as glucose oxidase and peroxidase are widely investigated immobilized enzymes for biosensing. Glucose oxidase was encapsulated on ZIF-8 by Zhang et al., and the biocatalyst surface was modified with streptavidine. The obtained complex reacted with the biotinilated antibodies specific for galectin-4, that is a marker expressed in cancer cells. The authors combined the enzyme/MOF immunoassay composites with a gold nanoclusters (AuNCs-iron(II)) system to construct a fluorescence immunoassay.[208] Wang et al. prepared a new amperometric biosensor based on glucose oxidase@ZIF-8 conjugated to graphene nanosheets for glucose detection, using the intrinsic peroxidase-like property of ZIF-8 to reduce the hydrogen

peroxide produced by the glucose oxidase.[209] Wu et al. investigated the catalytic efficiency of the enzymatic tandem system constituted by glucose oxidase and horseradish peroxidase immobilized on ZIF-8 for glucose detection via a colorimetric assay.[99]

The immobilization of peroxidases was also investigated, among them, the catalase, an enzyme that specifically decomposes hydrogen peroxide, with several applications such as wastewater treatment, and biosensing.[89] For example, Shieh et al. immobilized the peroxidase catalase in ZIF-90 (a MOF obtained by the combination of $Zn^{2+}$ ions and imidazole-2-carboxaldehyde).They investigated the activity of the catalyst in presence of protease, an enzyme that cuts the peptide bond, observing a high stability of the biocatalyst in presence of the protease.[210] Du et al. immobilized a catalase in ZIF-8 via a *in situ* encapsulation, in presence or absence of a protective coating of polyvinylpyrrolidone, and compared the activity of the different biocatalysts obtained. Both biocatalyst were 10 times recyclable, with a retention of activity around 70% and 90% for the uncoated and coated biocatalyst, respectively.[211]

**Table 3.2.** enzymes immobilizes onto ZIFs (ZIF-8[1] and ZIF-90[2]) and their biocatalytic applications.

| ZIF | Enzyme | Immobilization conditions | application | Remarks | Ref. |
|---|---|---|---|---|---|
| ZIF-8 | Lipase from *Burkholderia cepacia* | Post synthesis physical adsorption | hydrolysis and trans-esterification | Immobilization on external surface | [207] |
| ZIF-8 | Lipase from *Alicagenes sp.* | Biomimetic mineralization | hydrolysis | mechanosynthesis | [177] |
| ZIF-8 | Lipase from *Candida antarctica B* | Co- precipitation<br>Core-shell structure | transesterification | Encapsulation of enzyme in hydrogel coated by ZIF-8 | [212] |
| ZIF-8 | Lipase from *Candida rugosa* | Post-synthesis physical adsorption | Hydrolysis and stabilizing solid for emulsions | Solvothermal synthesis of ZIF-8 and post modification with polydopamine before physical adsorption of lipase | [202] |
| ZIF-8 | Lipase from *Aspergillus niger* | Biomimetic mineralization | catalysis | Hydrothermal synthesis<br>Enhanced activity after ultrasound treatment | [206] |
| ZIF-8 | β –galactosidase | Biomimetic mineralization | Coating shell for survival of cells in harsh environment | hydrothermal | [146] |
| ZIF-8 | Glucose Oxidase | Biomimetic mineralization | Biosensor | hydrothermal | [208] |
| ZIF-8 | Catalase | Co-precipitation of coated enzyme | catalysis | hydrothermal | [211] |
| ZIF-8 | Lysozyme, BSA, BHb | Post synthesis physical adsorption | Antimicrobial activity of LYZ | Hydrothermal synthesis of hierarchical micro/meso ZIF-8 | [201] |
| ZIF-8 | peptide harboring iron porphyrin DhHP-6 | Biomimetic mineralization | Catalyst for polymerization | Precursors incubated with traces of methanol | [181] |
| ZIF-8 | Catalase (+ HRP, GOx, Lipase from bovine pancreas) | Biomimetic mineralization | Catalysis/ crystal growth mechanism | Different morphology of crystals associated to Zn/2-MIM ratio | [213] |
| ZIF-8 | Trypsin | Post synthesis physical adsorption in column with continuous flow | catalysis | on metal-organic framework–polymer monolith hybrids | [214] |
| ZIF-8 | bovine hemoglobin vs synthetic Heme protein | Post synthesis physical adsorption | $H_2O_2$ and phenol detection | Hydrothermal synthesis | [215] |
| ZIF-8 | Glucose Oxidase | Co-precipitation of coated enzyme | Glucose biosensor | Hydrothermal synthesis | [209] |
| ZIF-8 | Urease | Co-precipitation vs Biomimetic mineralization | catalysis | PVP-modified urease in co-precipitation, hydrothermal synthesis | [180] |
| ZIF-8 | Urease, HRP Lipase, BSA | Biomimetic mineralization | Crystal growth | Hydrothermal synthesis. Shape of crystals affected by type of enzymes | [67] |

| | | | | | |
|---|---|---|---|---|---|
| ZIF-8 | GOx/hemin | Biomimetic mineralization | Glucose sensor<br>For in-vivo applications in living rats brain | Hydrothermal synthesis | [216] |
| ZIF-8 | GOX/HRP | Biomimetic mineralization | Glucose biosensor | Hydrothermal synthesis<br>Tandem system | [99] |
| ZIF-8 | HRP | Co-precipitation from reverse micelles | catalysis | Reverse micelles of water in cyclohexane | [217] |
| ZIF-8 | Cytochrome-c | Co-precipitation | Biosensor for organic peroxides | PVP-modified cyt-c | [184] |
| ZIF-90 | Catalase | *In situ* encapsulation | Catalysis_ $H_2O_2$ degradation | | [210] |

[1]ZIF-8 = ...Zn/ 2-methyl imidazole.
[2]ZIF-90 = Zn/imidazolate-2-carboxaldehyde

### 3.3.2 Immobilized enzymes on silica

Although MOF materials are having an increasing interest as supports for enzyme immobilization, mesoporous silica is still one of the most investigated materials to this purpose. This because this carrier has a high versatility. Indeed, mesoporous silica can easily be functionalized and eventually coupled to magnetic matrixes or entrapped in gels for new hybrid supports. Recent works investigated the use of functionalized mesoporous silica as carriers for drug delivery[151,218,219] and for the internalization of biomolecules in cells and tissues.[150,220] However the use of mesoporous silica for enzymatic immobilization is very appealing as demonstrated by the huge number of scientific papers published in the past two year (2016-2017) summarized in Table 3.3.

As far as concerns the immobilization of lipase on silica matrix, it is worth mentioning the work of Gao et al. who immobilized *Candida antarctica* B lipase in dendritic silica based colloidosome nanospheres (a silica support with center-radial porosity). They obtained a biocatalyst of enhanced stability in comparison with free and commercial immobilized enzymes. Moreover, in that work the retention of activity with respect to the as synthesized catalyst was investigated towards temperature and solvents, obtaining a retention of 49 %, after exposure to 50°C for 6h, and over 100% after exposure to t-butanol for 96 h.[221] Ali et al. covalently immobilized *Candida rugosa* lipase on core-shell magnetic silica and fibrous silica nanoparticles to test the activity on different supports.[222,223] Kalantari et al. reported the synthesis of octadecylalkyl-modified mesoporous silica nanoparticles for physical immobilization of lipase from *Candida rugosa.* The observed enhanced activity of the immobilized biocatalyst respect to the free enzyme was attributed to the high hydrophobicity and to the large pore size of the support. Karimi immobilized *Burkholderia cepacia* lipase in super paramagnetic iron

oxide nanoparticles covered by silica and amino functionalized silica. The obtained biocatalyst was used for the transesterification of triacylglycerols.[224] Sadighi et. al physically immobilized *Thermomyces lanuginosa* lipase on metal chelated MCM-41 for the esterification of valeric acid with ethanol to obtain ethyl valerate (an apple flavor).[225] Metal ions $Co^{2+}$, $Cu^{2+}$, and $Pd^{2+}$ were chelated on the surface of the silica support to investigate the effect on lipase adsorption capacity. These metal ions facilitate a multipoint enzyme attachment through cysteine thiol groups. A good catalytic activity (over 70%) was retained after a 14 days storage.

Maroneze et al. developed a new hybrid platform for biosensing, constituted by a ionic liquid-alkoxysilane modified silica, bound to Pt nanoparticles, thus obtaining a peroxidase-like activity. The glucose oxidase, adsorbed on the surface of this hybrid platform allowed the oxidation of glucose and the formation of $H_2O_2$. The hydrogen peroxide was then detected by a colorimetric assay through the peroxidase-like activity of Pt.[226] Balistreri et al. investigated the kinetics and the catalytic efficiency of GOx covalently immobilized on SBA-15 and MCF with similar pore volume and surface areas but different pore diameters. They observed a higher loading and activity on the supports with large pores. Moreover the MCF-based biocatalyst showed a high resistance to solvents at high temperature[227] compared to the free enzyme. Paulami et al. investigated the activity of GOx physically adsorbed on mesoporous silica to obtain a glucose biosensor.[228] The covalent immobilization of the bienzymatic system constituted by GOx and HRP on mesoporous SBA-15 was one of the tasks of this work. The performance of the biocatalyst towards the biodegradation of aromatic model molecules such as ferulic and caffeic acid was investigated. Paper II deals with this topic.

**Table 3.3** enzymes immobilizes onto mesoporous silica and their applications

| Silica support | Enzyme | Immobilization conditions | Application | remarks | Ref. |
|---|---|---|---|---|---|
| Dendritic silica based Colloidosome nanospheres | Lipase from *Candida antarctica B* | Physical adsorption | Biodiesel | Enhanced stability respect free and commercial immobilized enzyme | [221] |
| Core-shell mesoporous silica and fibrous mesoporous silica | Lipase from *Candida rugosa* | Covalent binding with glutaraldehyde | Not given | Different supports tested | [222,223] |
| Modified MCM-41 | Lipase from *Thermomyces lanuginosa* | Physical adsorption on external surface | Chemical synthesis | Apple flavor | [225] |
| C18-MSN | Lipase from *Candida rugosa* | Physical adsorption | Kinetic study | octadecylalkyl- modified mesoporous-silica nanoparticles | [229] |
| Amino grafted $Fe_3O_4$@$SiO_2$ | Lipase from *Burkholderia cepacia* | Covalent binding with glutaraldehyde | Biodiesel | | [224] |
| Epoxy SBA-15 | Lipases from *Candida antarctica Thermomyces lanuginose*, and *Rhizomucor miehei* | Covalent binding with the epoxy-functionalized support | Biodiesel | operational stability up to 20, 14 and 7 runs for the TLL CAL and RML respectively | [230] |
| Wrinkled silica NP | Lipase from *Candida rugosa* | Physical adsorption | Esterification reaction | highly ordered, radially oriented porous improve the activity of enzyme | [231] |
| SBA-15 with various porosity | lipase B from *Candida antarctica* | Physical adsorption | glycerolysis reaction | Diacylglycerol synthesis | [41] |
| Core–shell $Fe_3O_4$@MCM-41 | Lipase from *Candida rugosa* | Covalent binding with glutaraldehyde | Transesterification reaction | | [232] |
| SBA-15 with two silanizing agents | lipase from *Rhizomucor miehei* | Physical adsorption+ Covalent binding with epoxy | Kinetic study | GPTMS/OTES both in the silica surface | [47] |
| SBA-15, MCF, KIT-6 with various porosity | feruloylesterases from *Myceliophthora thermophila* | physical adsorption | Transesterification reaction | | [233] |
| Magnetic silica microbeads | Laccase from *T. Versicolor* | CLEAs on magnetic silica | Bioremediation | | [234] |
| Mesoporous silica | Laccase from *Aspergillus sp.* | covalent bond via GA | Bioremediation, degradation of | | [235] |

| | | | | | |
|---|---|---|---|---|---|
| | | | chlorophenol | | |
| Silica/Imi/PtNP/ | Glucose Oxidase | Physical adsorption | Glucose biosensor | | [226] |
| Amino-propyl silica | β-galactosidase/ lysozyme | Entrapment/ covalent | Catalyst and antimicrobial for milk treatment | | [236] |
| SBA-15; SBA-3; MCM-48 | Poliphenol oxidase | Physical adsorption | Kinetic study | | [237] |
| macro/mesoporous silica sphere (HMMS) | catalase | adsorption | Catalytic application | | [238] |
| Mesoporous silica/carbon paste electrode | Glucose oxidase | adsorption | Glucose biosensor | Ferrocene as mediator | [239] |
| SBA-15 conjugated to CMC and PVA | Papaine | Post synthesis adsorption/cross-linking | Proteolysis | enhanced pH, thermal and storage stability than free enzyme | [240] |
| Magnetic MPS using tannic acid as a templating agent | nitrile hydratase from *Rhodococcus rhodochrous* | Covalent binding with GA | Catalysis: biotransformation of 3-cyanopyridine to nicotinamide | New method for magnetic MSP, improved thermal, pH, mechanical and storage stability of the catalyst compared to free enzyme | [241] |
| Hierarchical micro/meso silica particles | Catalase | Covalent binging with GA | Degradation of $H_2O_2$ | Fast mass transfer due to hierarchical micro/meso | [242] |

# **Chapter 4:** *Characterization techniques*

The characterization of the free enzymes, the supports, and the immobilized biocatalysts were carried out to study their physico-chemical properties by means of different techniques. The structure of the supports and of the immobilized biocatalysts was investigated by X-rays scattering/diffraction and electron microscopy techniques. In particular, SBA-15 mesoporous silica, and enzyme@SBA-15 biocatalysts were characterized by small angle X-ray scattering and Transmission Electron Microscopy (TEM) ZIFs support and enzyme@ZIF biocatalysts were characterized by X-ray diffraction (XRD) and scanning electron microscopy (SEM). $N_2$ adsorption/desorption isotherms (BET) were used to estimate surface area and pore size of the porous materials. Thermo gravimetric Analysis (TGA) and FT-IR spectroscopy were used to confirm the chemical functionalization of the supports and the effective immobilization of the enzymes. Electrophoretic light scattering were used to determine the zeta potential of enzymes and particles.

## 4.1 Small Angle X-ray Scattering (SAXS)

When the atoms of a sample are hit by X-rays, the energy associated to the photons of the radiation can be absorbed or scattered by the sample. If the radiation is scattered elastically, that is without energy transfer (Rayleigh and Thomson scattering), the electrons oscillate with the same frequency of the incident radiation, coherent waves are produced. The radiations scattered by sample regions of different electronic densities give rise to interference phenomena that can be revealed by a detector. This constructive, destructive or partial interferences produces the SAXS pattern. The observed interference pattern depends on the source and the wavelength $\lambda$ of the

primary beam, the 2θ angle between the incident ray and the scattered ray, and the distance, *d*, between the atom layers, according to the Bragg's law:

$$n\lambda = 2d\sin\theta \quad (4.1)$$

where, n is a positive number that indicates the order of the diffraction.

A crystalline phase or an amorphous phase with ordered array of pores (i.e. mesoporous silica) have characteristic patterns that can be characterized with XRD or SAXS, respectively. Amorphous ordered mesoporous silica (OMS) materials (MCM-41 and SBA-15) have long range ordered channels, large d-spacing and large wall thickness, so the scattering appears at small angles included in the typical region of a SAXS (0.1-10°). Fig. 4.1 shows a schematic representation of a typical SAXS experiment.

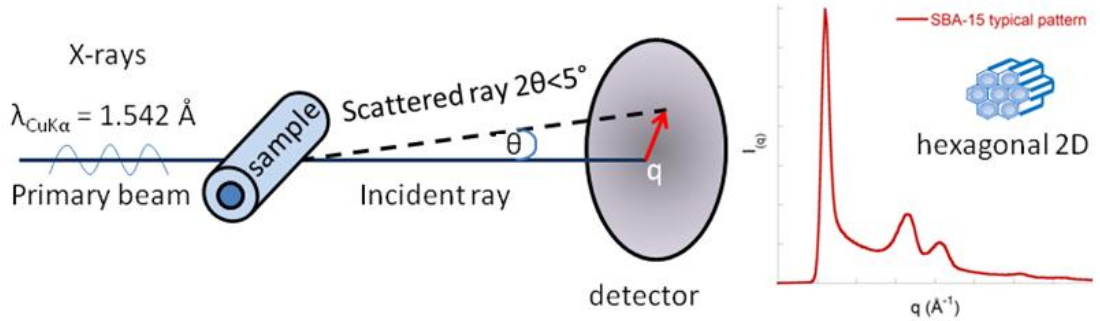


**Fig. 4.1** a scheme of the SAXS measurement. The primary beam hits the sample, the intensity of the scattered ray is revealed by the detector and measured as a function of the vector q. Each sample produces a typical pattern, with peaks in typical position. In this image the pattern of SBA-15 is reported.

In a SAXS experiment the angular dependence of the scattered intensity is usually reported as a function of the scattering vector, *q* ($nm^{-1}$):[243]

$$q = (4\pi/\lambda)\sin\theta \quad (4.2),$$

which can also be written as:

$$q = \frac{2\pi}{d} \quad (4.3)$$

A SAXS plot is a complex curve of the scattered intensity *I*, as a function of *q*:

$$I(q) = K \times P(q) \times S(q) \qquad (4.4)$$

where K is a constant that depends on the surface/volume ratio; P(q) is the form factor, that gives information about shape and density distribution of particles; S(q) is the structure factor that gives information about particle-particle interactions, inter-particle distance and degree of order. In the SAXS plot three distinct regions can be identified and used to obtain different information about the sample under investigation. In the Guinier region, where q values tend to zero, information about the size (gyration radius) of the particles can be obtained. In the Fourier region and in the Porod regions (high q values) information about the shape of particles and the surface per volume can be obtained, respectively.[243,244] If a sample has a long range order, SAXS analysis allows the characterization of its phases (lamellar, hexagonal, cubic), and the determination of the lattice parameter *a*. For a hexagonal phase (i.e. SBA-15) *a* is calculated by the formula:

$$a = d\frac{2}{\sqrt{3}}\sqrt{(h^2 + k^2 + hk} \qquad (4.5)$$

Where *d* is the distance between the plans, while *h* and *k* are the Miller indexes (h, k, l).

## 4.2 Powder X-rays Diffraction (XRD)

When a crystalline powder undergoes an X-ray beam, all possible interatomic planes can be hit by the rays. X-ray diffraction (XRD) occurs when X-ray wavelength λ and the distance between atom layers in the sample have a comparable size. This means that, according with the Bragg's law (eq. 4.1) and differently by SAXS, the explored angular region ranges from 5° to 50°. The geometrical 3D topology of atoms produces peaks of characteristic position and intensity. This allows to determine the unit cell

lattice parameters, the crystal structure, the crystallites dimensions, the d-spacing and to carry out quantitative analysis of the crystal phases. A scheme of XRD measurement and a typical patter are reported in Figure 4.2

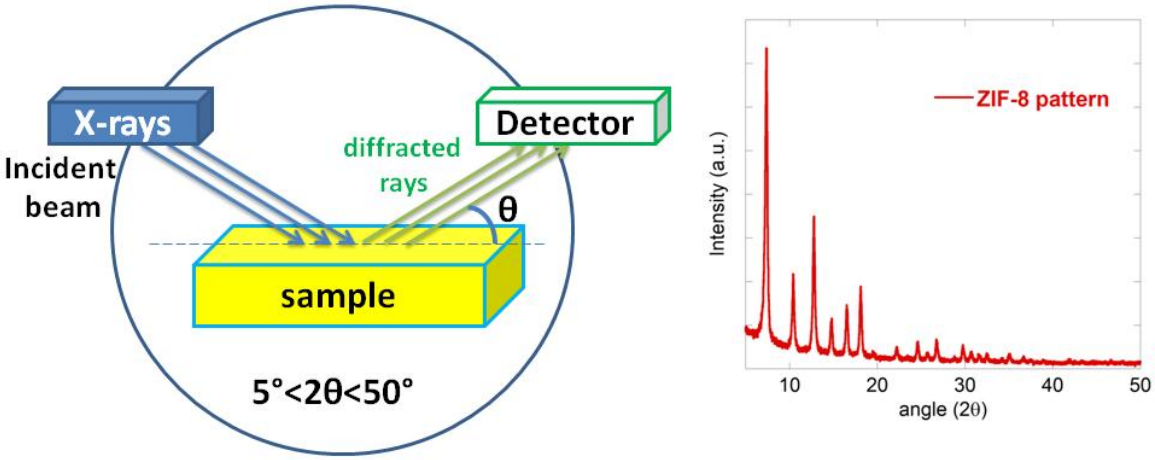


**Fig. 4.2** a scheme of the XRD measurement. The incident beam hits the sample, the diffracted rays are revealed by the detector. Variation of the angle produce a series of peaks. The XRD pattern of a ZIF-8 sample is reported.

## 4.3 Transmission electron microscopy (TEM) and scanning electron microscopy (SEM)

In the transmission electron microscopy (TEM) technique, a beam of electrons, generated from a cathode filament of an electron gun, is accelerated towards a sample, by a high voltage electric field. The beam is collected to condenser lens and hits the sample determining a scattered diffraction pattern. The beam interacts with the sample resulting in an image that can be impressed into a photographic layer or revealed by a CCD-camera.[245] If the direct beam is chosen to form the TEM image, this produces a bright- field image, while the scattered electrons from the sample produce a dark-field image. TEM is a powerful technique for the structural characterization of mesoporous

silica. Fig.4.3 shows an image of a typical hexagonal phase of ordered mesoporous silica (i.e. SBA-15)

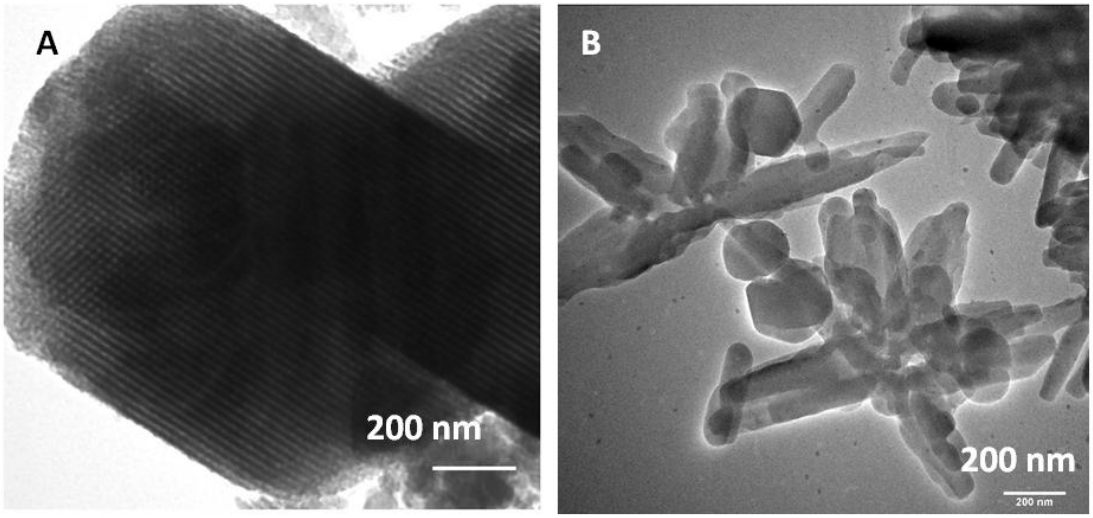


**Fig. 4.3** Transmission electron microscopy images. A) an SBA-15 sample, showing projections of the hexagonal cylindrical pores, B) a ZIF-8 sample.

In scanning electron microscopy (SEM), electrons are emitted from a cathode made of tungsten or lanthanum hexaboride. The primary beam of electrons is focused in a fine spot, and collides with the sample passing through scanning coils, determining the scan of a rectangular area. The sample emits a secondary beam that can be revealed resulting in a 3D image of the sample that shows the surface structure.[245,246] SEM can be used to characterize particle shape/morphology of enzyme supports. Fig. 4.4 shows the SEM image of ZIF-8 and a lipase immobilized on ZIF-8 samples.

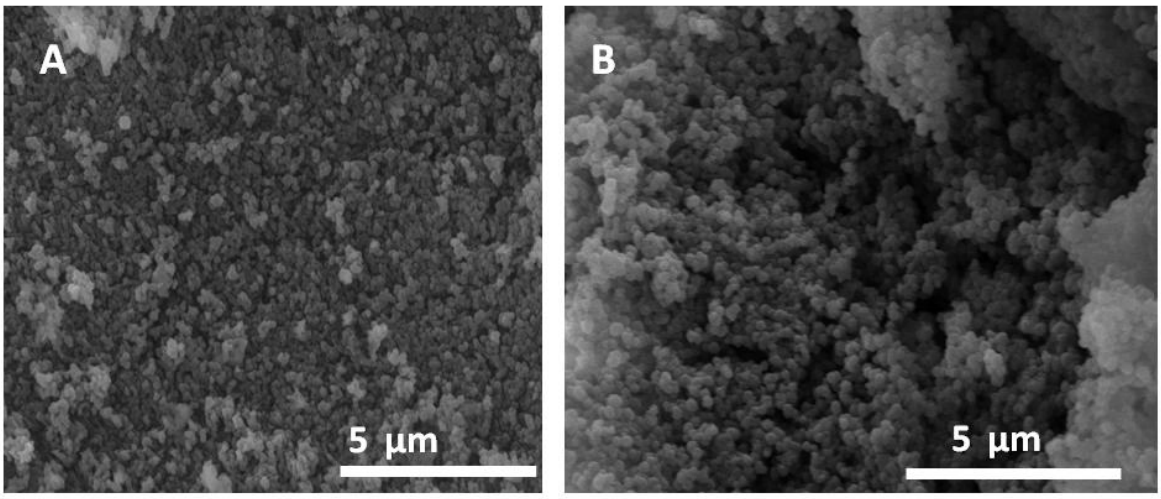


**Fig. 4.4** Scanning electron microscopy images. A) a ZIF-8 sample, B) an immobilized lipase on ZIF-8.

## 4.4 $N_2$ adsorption desorption isotherms

Surface area and pore size distribution are textural parameters commonly determined by means of $N_2$ adsorption/desorption isotherms. According to the Brunauer Emmett and Teller theory,[247] the multilayer physical adsorption of an inert gas on a surface of a material can be interpreted as an extension of the monolayer Langmuir theory which can be applied to each layer, with the assumption that gas molecules interact with adjacent layers without influencing the interaction with the deeper layers. The equation is:

$$\frac{1}{V(\frac{P}{P_0}-1)} = \frac{1}{cV_m} + \frac{c-1}{cV_m}\frac{P}{P_0} \qquad (4.6)$$

where, P and $P_0$ are the equilibrium pressure and the saturated vapor pressure of the adsorbate at the temperature of adsorption, respectively; V and $V_m$ are the volume occupied by all molecules adsorbed at equilibrium pressure and the volume occupied by of the monolayer adsorbate, respectively; *c* is the BET constant related to the

temperature of adsorption. From eq. 5.1, by plotting $\frac{1}{V(P_0/P-1)}$ as a function of $\frac{P}{P_0}$ a slope of $\frac{c-1}{cV_m}$ and an intercept of $\frac{1}{cV_m}$ can be determined, and used to calculate the surface area of the sample with the following formula;

$$\text{Surface area } (m^2/g) = \frac{(V_m * N_0 * a_m)}{22.414 * weight\ of\ sample} \quad (4.7)$$

Where $N_0$ is the Avogadro number and $a_m$ is the surface area of $N_2$ at 77 K.

The measurement of pore diameter and pore volume of microporous and mesoporous materials is obtained by means of this technique. These parameters are usually calculated by the desorption branch of the isotherm. In mesoporous materials, during the adsorption of an adsorbate capillary condensation can occur. Firstly the pores are partially occupied by the adsorbate, the capillary condensation occurs in the small pores before than in big pores, then the pressure increases until all pores are fully occupied. The capillary condensation occurs at a vapor pressure that is lower than the saturation vapor pressure of the pure adsorbate. This happens since the smaller the radius of the capillary is, the more van der Waals forces increase inside the space of the capillary. In the desorption step, the pressure decreases and the gas evaporates from the system with a the desorption isotherm a slight different from the adsorption one. Hence, the capillary condensation phenomenon is associated to the presence of an hysteresis cycle.

The porosity in mesoporous materials is analyzed by means of the BJH (Barrett, Joyner, Halenda) model, that provides information about pore distribution and diameter. According to this model, the pore size distribution is calculated as a variation of the

ratio *Volume adsorbed / pore Width* as a function of the pore width. The pore diameter distribution is calculated by the Kelvin-Wheler equation (6.3):

$$\ln \frac{P}{P_0} = -\frac{2\gamma V_m cos\theta}{RTr_p} \quad (4.8)$$

Where P is the equilibrium vapor pressure and $P_0$ is the saturation vapor pressure of the adsorbate, $P/P_0$ is the relative condensation pressure, R is the gas constant, T is the absolute temperature, $r_p$ is the porous radius, γ is the surface tension of the condensed adsorbate, $V_m$ is the molar Volume of the adsorbate and θ is the contact angle between the solid surface and the liquid (condensed) adsorbate.

From the Kelvin equation it is possible to determine the radius of the pores

$$r_p = -\frac{2\gamma V_m cos\theta}{RTln\, {}^{P}/_{P_0}} \quad (4.9)$$

The IUPAC classifications of physisorption isotherms and hysteresis loops[248] are reported in Fig. 4.5. The type I isotherms are characteristic of microporous materials. At low values of $p/p_0$ a rapid increase of adsorbate is observed, corresponding to the filling of micropores. A plateau, where no further adsorption occurs, is quickly reached. Finally at high values of $p/p_0$ the rapid increase of the adsorbate corresponds to the liquefaction. The type II isotherms occur on macroporous or not porous solids. The thickness of the adsorbed layer increases progressively with the relative pressure. The knee of this type of isotherm (the arrow in Fig.4.5A), indicates the formation of molecular multilayers. The ordinate of this point is the monolayer capacity, namely the mass of adsorbate that fully covers a mass of solid with a monomolecular layer. The type III isotherm is typically observed in non porous materials with weak adsorbent-adsorbate interactions, it shows a convex shape. The type IV isotherm is typical of

mesoporous materials. In the first part of the isotherm the trend is similar to that observed in the type II. Above the point indicated by the arrow (Fig. 4.5A-IV), the multilayer filling starts. However, in the mesopores the capillary condensation occurs, leading to a second knee. During the desorption branch, the partial pressure $p/p_0$ required to reach the equilibrium results in a different amount of adsorbate subtracted to the system. This leads to an hysteresis cycle. The type V isotherm presents a hysteresis loop and it is observed in porous materials with weak interactions adsorbate-adsorbent. Type VI isotherm occurs in materials characterized by morphological and energetic uniformity and no porosity. Each step indicates a filling stages of an individual layers. the plateau sections between the steps, indicate that, in that specific pressure intervals, the amount of adsorbed gas is very low. The hysteresis loops (Fig.4.5B) are ascribable at four types: H1 hysteresis loop, with parallel and vertical branches, is typical of pores with parallel channels and narrow size distribution. H2 hysteresis loop is typical of interconnections among pores of different size and shapes. H3 hysteresis loop is associated to the porosity of aggregates of plate-like particles. H4 hysteresis loop is ascribable to narrow slit-shaped pores[248].

The type IV isotherm with H1 hysteresis is typical of mesoporous silica SBA-15 with monomodal distribution of pores, while the Type I isotherm is typical of microporous materials such as the zeolite imidazolate framework ZIF-8.

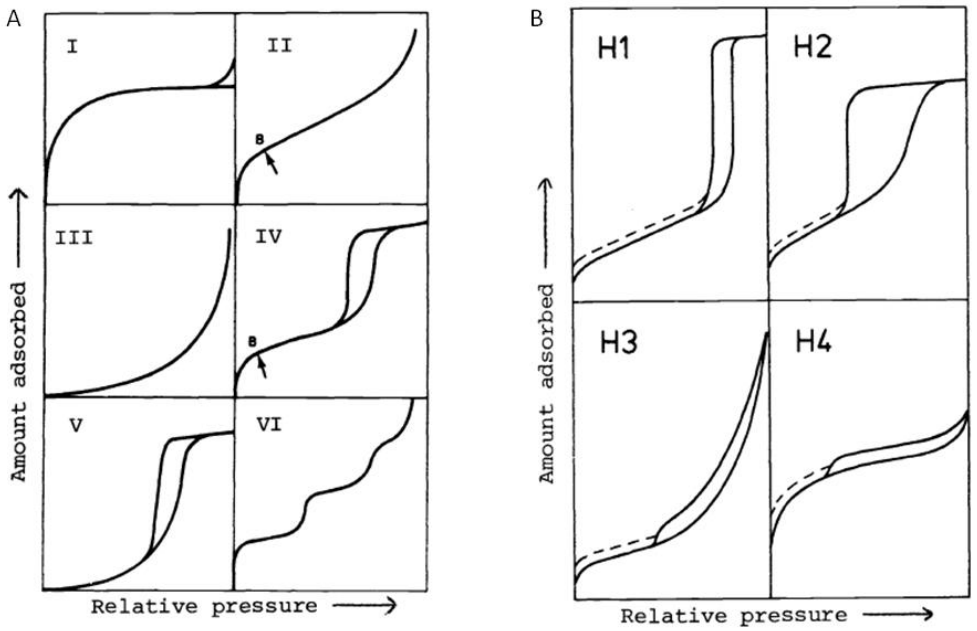


**Fig. 4.5** A) physisorption isotherms; B) hysteresis loops according to the IUPAC classification. Reproduced from ref.[248].Open access content.

## 4.5 Thermogravimetric Analysis

Thermogravimetric analysis (TGA) is the measurement of the mass loss of a sample during a ramp of controlled heating. The resulting plot is reported as a mass loss % as a function of temperature, generally in Celsius degrees. Typical mass losses occur at characteristic temperatures such as around the evaporation temperature of water or the structural decomposition of organic components of a sample. In some cases it is also possible to observe the increase of mass %, that occurs when the decomposition of the sample causes reactions with molecules of the atmosphere. The horizontal ranges of the curve are the regions of stability of the sample. The obtained curves are characteristics for each type of materials. The first derivative of the curve (DTG) is often used to better visualize the temperatures where the slope of the TGA changes.[249]

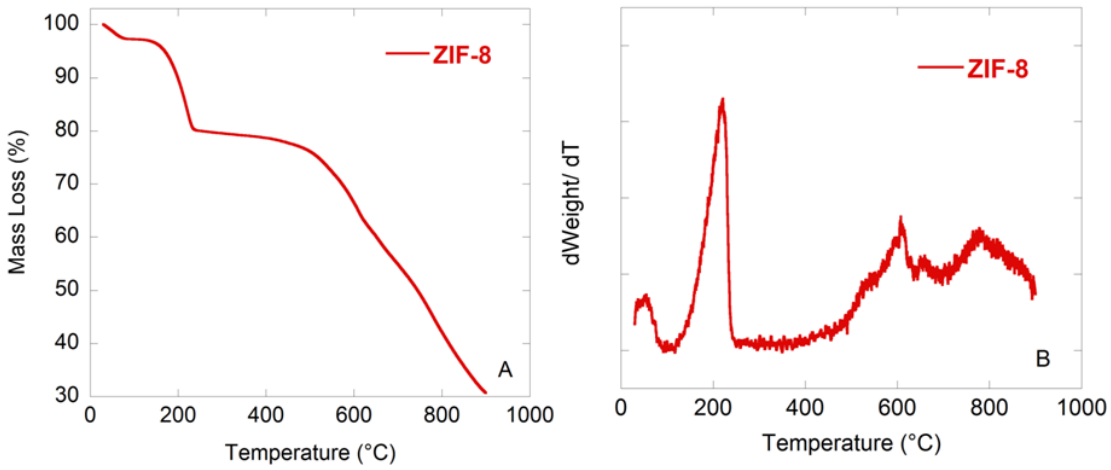


**Fig. 4.6** examples of TGA plots. A) ZIF-8 TGA and B) derivative

## 4.6 Attenuated total reflection (ATR) accessory for FTIR spectroscopy

The Attenuated Total Reflection (ATR) is an accessory of modern infrared (FTIR) spectrometers which allows the non destructive direct analysis of a liquid or solid sample without necessity of the KBr pellet. The infrared light passes through the ATR crystal with a high refractive index, directed according to a certain angle. Therefore, using the property of total internal reflection of the crystal, the light undergoes multiple reflections causing an evanescent wave that hits the sample in contact with the crystal. The evanescent wave goes through the crystal surface and penetrate the sample only for some microns (0.5 µ - 2 µ), but deeply enough to be absorbed by the sample. The typical vibration modes of common functional groups and those investigated in this PhD thesis are reported in Tab.4.1.

**Tab. 4.1** vibration modes of typical bonds that can be identified by means of IR spectroscopy.

| Typical vibration modes | Wavenumbers ($cm^{-1}$) | Ref.s |
|---|---|---|
| C-H stretching | 2850-2960 | [122] |
| C-H bending | 1340-1465 | [122] |
| C-C stretching | 700-1250 | [122] |
| C=C stretching | 2100-2260 | [122] |
| HC≡CH stretching | 2100-2260 | [122] |
| O-H stretching | 3590-3650 | [122] |
| Hydrogen bonds | 3200-3570 | [122] |
| C=O stretching | 1654-1780 | [122] |
| N-H stretching | 3200-3500 | [122] |
| N-H bending | 1546 | [219] |
| Amide I and amide II | 1650 and 1550 | [64] |
| Si-O-Si symmetric stretching | 800 | [219] |
| Si-O-Si asymmetric stretching | 1067-1070 | [219] |
| C=N stretching | 1584 | [250] |
| Aromatic rings bending | 900-1350 | [250] |
| Zn-N stretching | 421 | [250] |

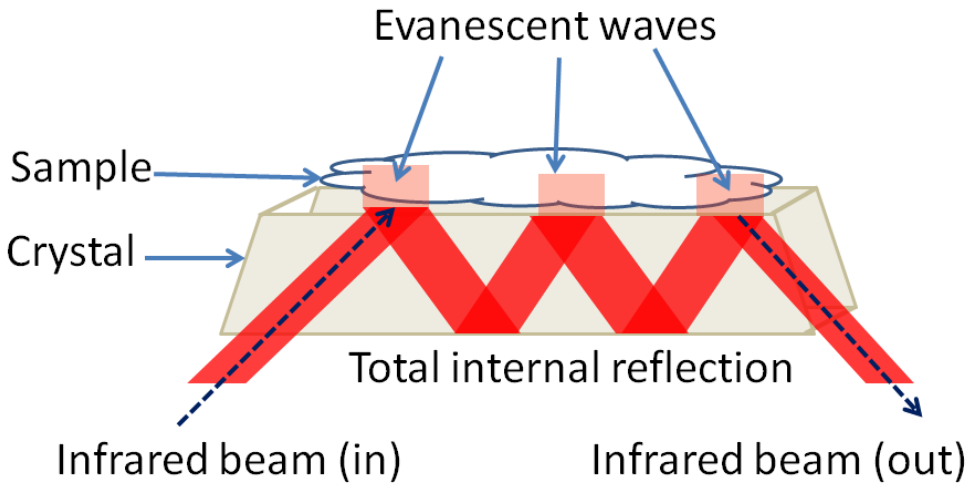


**Fig. 4.7** A scheme of the total reflection of crystal and the evanescent wave that penetrates the sample. The picture is an adaptation from an image available in the website https://www.chromacademy.com/infrared-training.html

## 4.7 Zeta potential from Electrophoretic Light Scattering

The application of an electric field to a solution containing charged colloidal particles, causes their movement towards the electrode carrying the opposite charge. The

viscosity of the medium hinders the movement, and at equilibrium the velocity of particles becomes constant and depends on the applied voltage, the dielectric constant and the viscosity of the medium, and the electrical potential of the moving particles. The zeta potential, ζ, is the electric potential of charged colloidal particles in solution, measured at the slipping plane, that is an unknown region within the double layer which includes, besides the particles itself, also solvent molecules and adsorbed ions.

Electrophoretic light scattering (Doppler shift spectroscopy) is a technique which permits the measurements of zeta potentials. the light scattered from the moving particles undergoes a Doppler shift of frequency (Δν), that can be monitored and measured. The electrophoretic mobility ($\mu_e$) is related to the Doppler frequency shift by the relationship:

$$\Delta\nu = 2\mu_e \frac{\sin(\frac{\theta}{2})}{\lambda} \qquad (4.10)$$

where $\mu_e$ is the electrophoretic mobility, θ is the scattering angle and λ the wavelength of incident light. From $\mu_e$ value the zeta (ζ) potential can then be calculated:

$$\mu_e = \frac{2\varepsilon\zeta f(\kappa a)}{3\eta} \qquad (4.11)$$

where ε ($\varepsilon_r\varepsilon_0$) and η are the dielectric constant and the viscosity of the medium, respectively; κ is the reciprocal of the Debye length and *f*(κa) is the Henry function, a scalar number ranging from 1 to 1.5 (Hückel and Smoluchowsky limits) that indicates the mobility delay caused by the ionic medium.

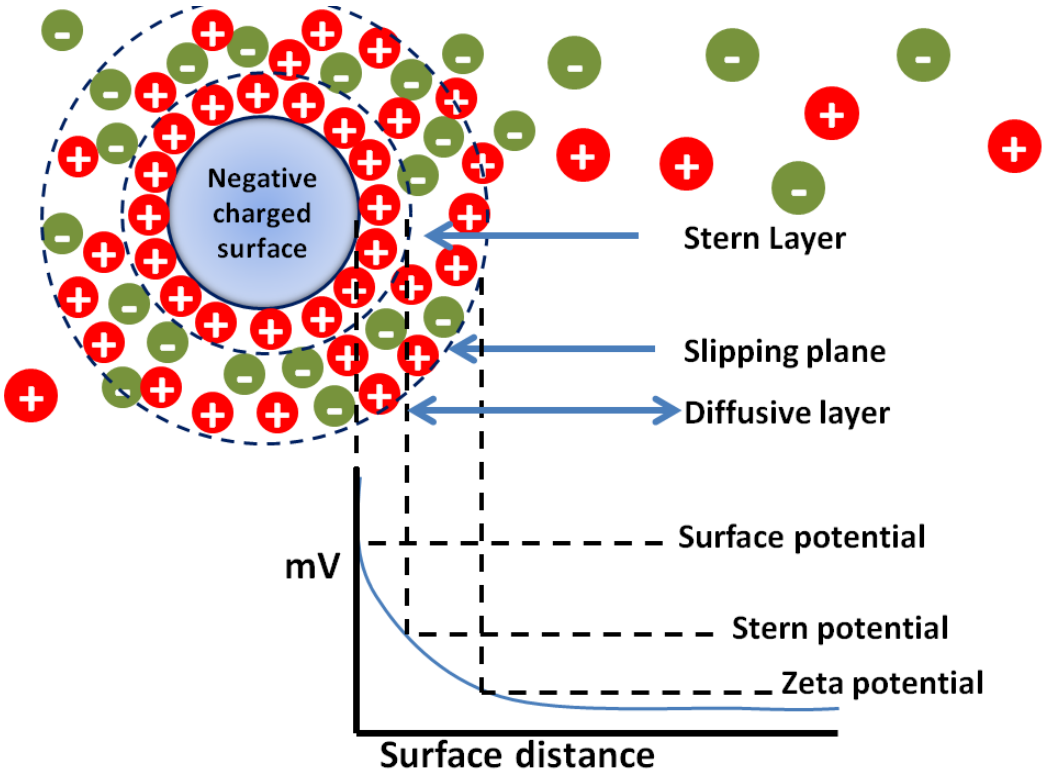


**Fig. 4.8** A representation of a charged particle in a electrolyte solution. A large value of zeta potential means that the solution is stable, particles have no tendency to aggregation. A low value of zeta potential, particles aggregate or flocculate. This picture is adapted from a PDF file available in the website https://www.malvern.com/en

## 4.8 Enzymatic concentration and activity measurements

The measure of the concentration of an enzyme in a solution, in terms of protein content is an important parameter, used for calculation of loading, according to the following equation.[65]

$$q = \frac{([P]_0 - [P]_f)V - [P]_w V_w}{m_{support}} \quad (4.12)$$

where $[P]_0$ is the protein concentration at time 0, $[P]_f$ is the protein concentration at the final time, $[P]_w$ is the protein content in the washing solution, V is the volume of the reaction solution, $V_w$ is the volume of the washing solution.

Commonly, spectrophotometric assays are used for this purpose. As aromatic residues of tyrosine and tryptophan absorb at λ = 280 nm, using the Lambert-Beer's law (A = εbc, where b is the path length of the cuvette and ε is the extinction coefficient of the absorbing specie, c is the concentration of the protein), the absorbance can be measured and the concentration of proteins calculated. Another common test is the Bradford assay[251], very useful for diluted protein solutions as it is a very sensitive test. Bradford assay is a colorimetric test based on the interaction between the Coomassie brilliant blue and aromatic amino acids and arginine. The detection occurs at the wavelength of 595nm. The absorbance is calculated by comparison with a calibration curve of a standard protein, generally Bovine Serum Albumin (BSA).

The activity tests used un this PhD work are two well known spectrophotometric assays: the ABTS and the p-nitrophenyl butyrate assays[92,252,253]. A complete description of the procedure is reported in the published papers (Paper II for ABTS assay and Paper III for p-nitrophenyl butyrate assay). The figure 4.9 shows the typical equipment and procedure adopted for measurements, and the scheme 4.1 shows the reactions involved.

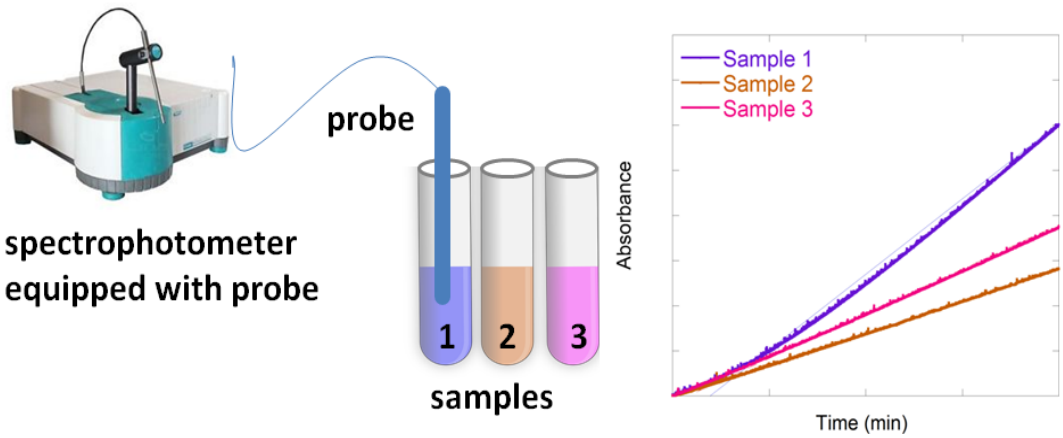


**Fig. 4.9** An example of activity measurements. A spectrophotometer equipped with a probe was used to determine the increase of absorbance of the product of reaction. The reactions require constant temperature (i.e. 25°C).

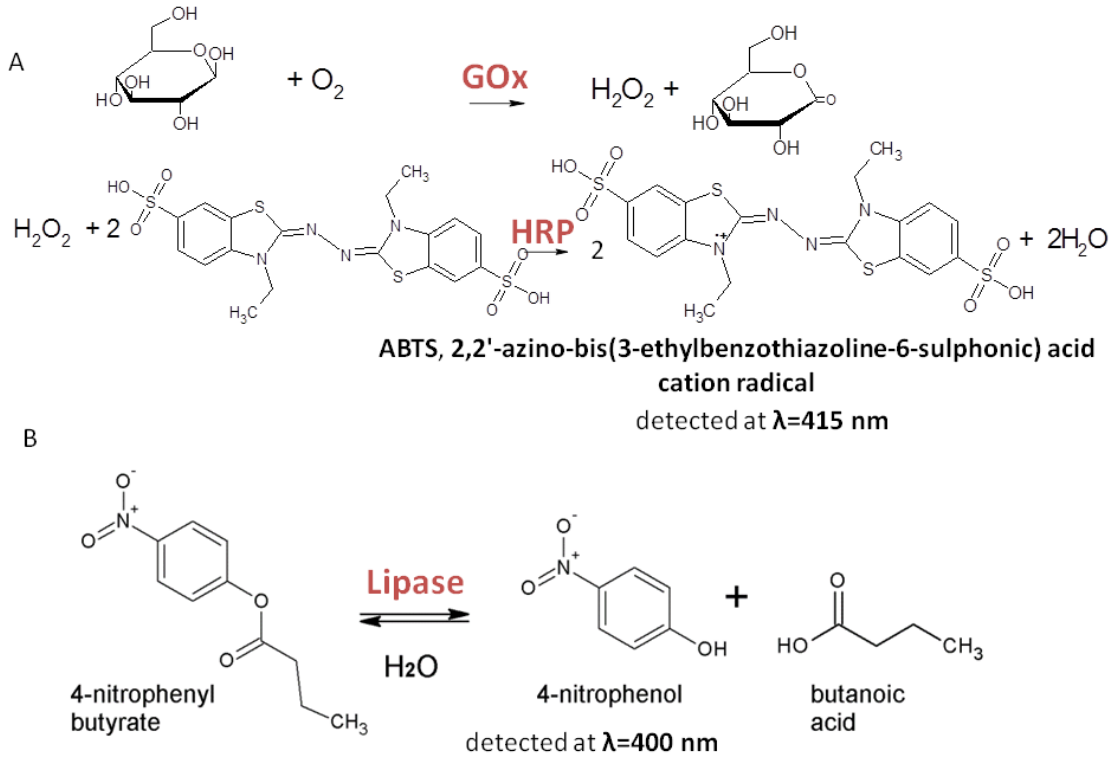


**Scheme 4.1** The reactions involved in activity measurements in this PhD work. A) The activity of the bienzymatic sequential system GOx-HRP was detected with the ABTS assay (papers II). B) The lipase activity was detected with the p-nitrophenyl butyrate assay (paper III).

# Aim of the thesis

The aim of this thesis work was the study of different enzyme immobilization techniques on SBA-15 mesoporous silica and zeolite imidazolate frameworks (ZIF-8) supports. Different enzymes were chosen for different immobilization strategies.

Firstly, the synthesis and functionalization of ordered mesoporous silica (SBA-15 particles was carried out. The samples were characterized by means of small angle X-rays scattering, $N_2$ physisorption, thermo gravimetric analysis and FTIR spectroscopy. The first investigated immobilization method was physical adsorption, SBA-15 and amino functionalized SBA-15-$NH_2$ were the adsorbents and lysozyme the adsorbate. In these systems the intermolecular interactions responsible of enzyme adsorption are electrostatic forces, hydrogen bonds and van der Waals interactions. A change of pH or of ionic strength are generally considered to modulate the loading of the adsorbed enzyme. The effects of the change of the weak electrolyte (buffer) used to fix pH, or of the salt used to regulate ionic strength are not generally considered. The loading of the physically adsorbed on on SBA-15 and amino functionalized support, SBA-15-$NH_2$, was in fact modulated by the different buffers and salts used to fix pH and ionic strength respectively (**PAPER I**).

The covalent immobilization of the bienzymatic system constituted by glucose oxidase and horseradish peroxidase in amino functionalized SBA-15, was then investigated. The loading and the activity of the various immobilization conditions were evaluated, showing that the catalyst was strongly affected by the drying process. An application in bioremediation was tested, by investigating the degradation of the model phenolic molecules, ferulic acid and caffeic acid (**PAPER II**).

Metal Organic Frameworks are new promising host materials for immobilization of enzymes. Thus, the encapsulation of Lipase AK from *Pseudomonas fluorescens* and Lipase RM from *Rhizomucor miehei* was carried out into ZIF-8. The obtained biocatalysts were characterized by means of $N_2$ physisorption, SEM, and XRD, TGA, and FTIR spectroscopy. The loading and the catalytic activities of lipase@ZIF-8 biocatalysts were then measured via spectrophotometric methods. The effect of the molar Zn: Ligand ratio and of the pH on the synthesis process was investigated. The stability and recycling of the best catalyst obtained was finally studied (**PAPER III**).

All these studies are described in detail in the following attached papers. The main findings of this studies are finally summarized in the conclusions chapter at the end of the thesis.

# Paper I

*Cugia, F., Sedda,S.,* ***Pitzalis, F.****, Parsons, D.F. , Monduzzi M., Salis A. "Are specific buffer effects the new frontier of Hofmeister phenomena? Insights from lysozyme adsorption on ordered mesoporous silica" RSC Advances, 6 (2016) 94617-94621.*
***DOI:*** *10.1039/C6RA17356J*

http://pubs.rsc.org/en/content/articlelanding/2016/ra/c6ra17356j#!divAbstract

RSC Advances

COMMUNICATION

View Article Online
View Journal | View Issue



Cite this: *RSC Adv.*, 2016, **6**, 94617

Received 6th July 2016
Accepted 27th September 2016

DOI: 10.1039/c6ra17356j

www.rsc.org/advances

# Are specific buffer effects the new frontier of Hofmeister phenomena? Insights from lysozyme adsorption on ordered mesoporous silica†‡

Francesca Cugia,[a] Silvia Sedda,[a] Federica Pitzalis,[a] Drew F. Parsons,[b] Maura Monduzzi*[a] and Andrea Salis*[a]

Lysozyme adsorption on mesoporous silica at pH 7.15 is buffer specific. The synergistic action of buffers and salts induces relevant effects on the charged interfaces, and thus on lysozyme loading. These findings, rising doubts on the validity of the Henderson–Hasselbalch equation, suggest the occurrence of Hofmeister phenomena also for buffers.

Hofmeister (ion specific) effects are phenomena related to the chemical nature of electrolytes. Although they are ubiquitous in all chemical, colloidal, and biological systems,[1–5] they cannot be quantified in terms of the conventional physico-chemical theories (*i.e.* Debye–Hückel, DLVO, *etc.*). These are limit theories, based on electrostatics, and valid at infinite dilution only. The gap between theories and Hofmeister related experiments is usually very large since the ion specific effects are generally observed at high concentrations in the presence of strong electrolytes 0.3–3 M.[6] This is very far from the validity's domain of both limit laws, and their extensions (valid up to $10^{-3}$ to $10^{-2}$ M).[3] Nevertheless, it has been demonstrated that high concentrations of strong electrolytes are not strictly necessary to observe ion dependent phenomena. Several experiments showed that ion specificity occurs at physiological salt concentrations (0.1–0.15 M), and even below.[7,8] Very recently, the occurrence of ion specificity at low salt concentrations (Hofmeister charging) has found a theoretical basis.[9] The finding that Hofmeister effects occur at low salt concentrations poses new questions. Can the weak electrolytes used for buffers give Hofmeister effects? According to the Henderson–Hasselbalch equation,[10] they should not. In biochemistry, it is necessary to use a buffer to fix the pH of the experiment. This procedure has been used in many 'Hofmeister related' studies, in particular on protein aggregation, electrophoretic mobility and enzyme activity.[11–15] Typical buffer concentrations are in the range 10–100 mM. The implicit assumption is that, due to their low concentration, the buffer ions should not display any specific effect. This is not so. Indeed we recently observed that, even at the same nominal pH, lysozyme electrophoretic mobility was buffer dependent.[16] The conventional wisdom says that protein charges – and hence electrophoretic mobilities – depend on pH only, regardless of the buffer used to fix it. As shown below, here we confirmed and extended that work.[16] It should be acknowledged that the original idea to investigate specific buffer effects is due to B. W. Ninham. Following his pioneering work on restriction enzymes,[17] we then observed specific buffer effects on pH measurements,[18] and lipase activities.[19] Moreover, by looking at the literature more in detail,[20] we found that similar specific buffer effects were discerned for DNA mobility,[21] protein stability,[22–24] antibody aggregation,[25,26] swelling kinetics of polyelectrolyte gels[27] *etc.* Hence, buffers, besides setting pH, may specifically interact with surfaces to modulate their effective charges.[20] This is not considered in the Henderson–Hasselbalch model for buffer action.[28]

Ordered mesoporous silica (OMS) materials have shown a very high propensity towards the adsorption of proteins and enzymes.[29–31] The most common OMS materials (*i.e.* MCM-41, SBA-15), besides a very high surface area, have pore sizes in the range 2–10 nm. These features allow for the penetration of proteins inside the inner architecture of the OMS particles.[32,33] When an enzyme is adsorbed on OMS an immobilised biocatalyst is obtained.[34] In nanomedicine applications, OMS can be used to adsorb antibodies or other proteins which either act as targeting agents (molecular recognition), or as therapeutics which require a sustained release.[35] The potentiality of OMS–proteins composites has promoted a growing interest in different applied fields.[35] In these systems protein/silica interfacial interactions play a fundamental role. It is widely acknowledged that the pH and the ionic strength of the

[a]*Department of Chemical and Geological Sciences, University of Cagliari-CSGI and CNBS, Cittadella Universitaria, S.S. 554 Bivio Sestu, 09042-Monserrato, CA, Italy. E-mail: asalis@unica.it; monduzzi@unica.it*

[b]*School of Engineering and Information Technology, Murdoch University, 90 South St, Murdoch, WA 6150, Australia*

† Dedicated to Prof. Barry W. Ninham for his 80th birthday.

‡ Electronic supplementary information (ESI) available: Experimental details and additional experimental data. See DOI: 10.1039/c6ra17356j

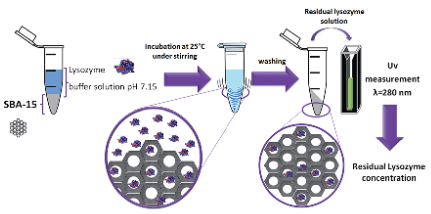


Scheme 1 Schematic representation of the experimental procedure.

adsorbing solution affect the interactions.[36–38] Less investigated, but not really surprising, is that ions affect specifically protein adsorption on silica.[39] Generally 'ion-specific' works are carried out by fixing pH by means of a buffer and then varying the salt type and/or concentration.[11–13] Here, our purpose is to demonstrate that, besides strong electrolytes, also weak electrolytes, used to fix pH, play a specific role. This has not yet been investigated systematically. The system chosen to this purpose was the physical immobilisation of lysozyme (LYZ) on SBA-15 and amino functionalised SBA-15 (SBA-$NH_2$), which we studied in the presence of different buffers (pH 7.15) and different 0.1 M salts. The performed experiments are described in the ESI file‡ and schematised in Scheme 1.

Briefly, LYZ adsorption on SBA-15 (or SBA-$NH_2$) mesoporous silica was carried out at 298 K and pH 7.15 in the presence of different buffers (Tris, BES, phosphate, and citrate), and quantified through spectrophotometry at $\lambda = 280$ nm. Buffers dissociation equilibria and p$K_a$ values are listed in Table 1. Phosphate and citrate are typical buffers occurring in living systems. Tris and BES are commonly used in biochemistry labs. The p$K_a$s values listed in Table 1, confirm that all buffers would have a good 'buffering action' at a physiological pH = 7–7.4. LYZ adsorption was carried out also in the presence of different 100 mM sodium salts, namely: NaCl, $NaNO_3$ and NaSCN (and for some experiments also NaBr and NaI). Firstly, the SBA-15 and SBA-$NH_2$ adsorbent materials were synthesised and characterised according to the procedures reported in the ESI file.‡ Textural characterisation of SBA-15 (Fig. S1 in ESI‡) provided a surface area (BET) of 777 $m^2\ g^{-1}$, and a maximum of the pore size distribution (BJH) at 6.4 nm (Table S1 in ESI‡). The functionalisation with aminopropyl group to obtain SBA-$NH_2$ resulted in a decrease of both surface area to 398 $m^2\ g^{-1}$, and pore size to 5.9 nm. The structural characterisation, carried out through SAXS, showed that both SBA-15 and SBA-$NH_2$ have an ordered hexagonal structure with a lattice parameter of 11.7 nm and 11.6 nm, respectively (Fig. S1C and D, ESI‡). The functionalisation with the aminopropyl group produced a change of the sign of the silica surface charge, as demonstrated through potentiometric titrations. The curves of surface charge density ($\sigma$) as a function of pH (Fig. S1F, ESI‡) (obtained in the absence of buffers or other electrolytes) showed that, at pH 7.15, $\sigma$ of SBA-15 is negative ($-0.04$ C $m^{-2}$), while that of SBA-$NH_2$ is positive (+0.23 C $m^{-2}$). This means that, in the absence of any added electrolyte, the two materials have opposite surface charges. Therefore we can expect that the adsorption of LYZ (isoelectric point: pI = 11) is much more favoured on SBA-15 than on SBA-$NH_2$.

This is demonstrated in Fig. 1 where LYZ adsorption is reported for the two silica matrices in the presence of different 10 mM buffers, at the same pH 7.15. In the case of SBA-15 (Fig. 1A) LYZ loading is always higher than 250 mg $g^{-1}$, and increases along the series Tris < BES < phosphate < citrate. Interestingly, the use of citrate instead of Tris buffer, resulted in a loading increase of 44%. A very low loading (in the range 0–10 mg $g^{-1}$) was instead obtained for LYZ adsorption on SBA-$NH_2$. This was expected on the basis of electrostatic considerations. For comparison, we also measured LYZ loading by adjusting pH at about 7.15 with addition of strong acid/base. We obtained a loading of $159 \pm 58$ mg $g^{-1}$ for SBA-15 and about zero for SBA-$NH_2$. We assign the high uncertainties to the difficulty to control pH without using a buffer. From the results in Fig. 1 we can argue that the chemical nature of both silica surfaces and buffers is relevant in addressing the observed phenomena. Recent experiments suggested that buffer ions adsorb

Table 1 Buffers used in this work and their p$K_a$ values at 25 °C. Extracted from ref. 40

| Buffer name | Dissociation equilibrium | p$K_a$ |
|---|---|---|
| Tris [tris(hydroxymethyl) aminomethane] | 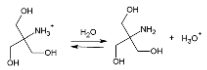 | 8.06 |
| Bes [*N*,*N*-bis-(2-hydroxyethyl)-2-aminoethanesulfonic acid] | 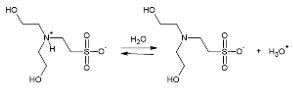 | 7.09 |
| Phosphate | 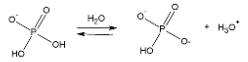 | 7.22 |
| Citrate | 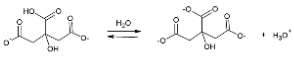 | 6.40 |

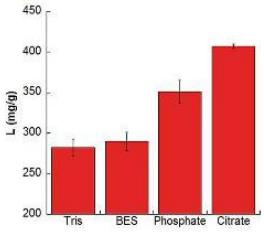


Fig. 1 Effect of 10 mM buffers (pH 7.15; $T = 298$ K) on LYZ adsorption on SBA-15 mesoporous silica.

specifically at LYZ surface, thus modifying its effective electric charge, thus affecting its electrophoretic mobility.[16] Zeta potential ($\zeta$) measurements shown in Fig. 2 confirm those previous results. Indeed, at pH 7.15, LYZ carries a positive net charge thus a positive $\zeta$ value would be expected, independently of the buffer used to fix pH. But Fig. 2A shows that the $\zeta$ values depend significantly on the buffer, and decrease along the series Tris > BES > phosphate > citrate. The effect of buffers on $\zeta$ measurements was here investigated also for the silica matrices. In the case of SBA-15 (Fig. 2B) $\zeta$ values are always negative and do not depend on the different type of buffer significantly. On the contrary, in the case of SBA-$NH_2$ (Fig. 2C), $\zeta$ values display a clear specific buffer dependence exactly as observed for LYZ (Tris > BES > phosphate > citrate). Remarkably, confirming what previously observed for LYZ,[16] citrate gives a reversal of zeta potential from positive to negative values also for SBA-$NH_2$. These results demonstrate that the specific effect of buffers is important for LYZ and SBA-$NH_2$, but not for SBA-15. Hence, the effect of the buffer (at pH 7.15) can be related to the presence of the positively charged amino groups at the SBA-$NH_2$ surface, and amino, imidazole and guanidino groups at LYZ surface.

Differently, the negatively charged silanol ($SiO^-$) groups of SBA-15 are negligibly affected by the different buffers. It is evident that buffers' anions, particularly citrate buffer (constituted by the divalent hydrogen citrate and the trivalent citrate anions, see Table 1) displays a very high affinity and selectivity towards binding at the positively charged interfaces. Hence, a combination of electrostatic, and van der Waals interactions could be suggested to justify the observed trends.[36] In fact, a more detailed approach has recently been proposed.[9,41] The effects of increasing the buffers' concentration (from 10 mM to 100 mM) on LYZ loading on SBA-15 was also studied, as shown in Fig. S2 (ESI‡). The increase of the buffers' concentration also affected the absolute value of zeta potentials of SBA-15 (see

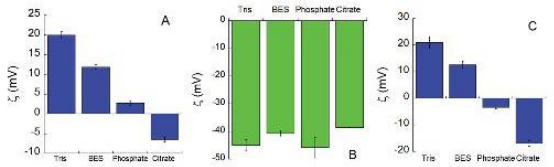


Fig. 2 Specific buffer effects on zeta potential of (A) LYZ (B) SBA-15 (C) SBA-$NH_2$ ($T = 298$ K; pH = 7.15; buffer concentration 10 mM).

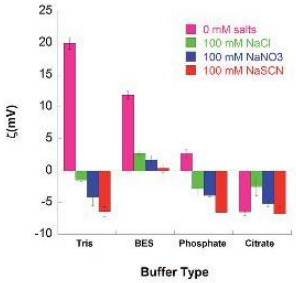


Fig. 3 Effect of strong electrolytes on LYZ zeta potential in different 10 mM buffers (pH = 7.15).

Fig. S3 ESI‡). However, the increase of buffer concentration did not provide any significant advantage to loading, therefore we used a 10 mM buffer concentration to evaluate the effect of adding strong electrolytes.

Different 100 mM sodium salts were added during the LYZ loading experiments on SBA-15 and SBA-$NH_2$. The investigated anions were $Cl^-$ and $SCN^-$, that are located respectively in the middle and at the 'chaotropic end' of the Hofmeister series, and $NO_3^-$ which is in between these two. Fig. 3 shows the effect of the salt addition on $\zeta$-potentials of LYZ in different buffer solutions. The salt addition produces negative $\zeta$ values on LYZ in the presence of all buffers except BES, probably due to the zwitterionic nature of this buffer. Fig. 4A and B show the effect of salt addition on $\zeta$-potential of the two silica matrices in the presence of Tris (cationic) and citrate (anionic) buffers. These buffers were selected since, in the absence of added salt, they gave the lowest and the highest LYZ loading on SBA-15, respectively (Fig. 1). In the case of SBA-15, the addition of salt just decreases the absolute value of $\zeta$-potentials as a result of cations' binding to the negatively charged silica surface.

For SBA-$NH_2$ besides the effect of NaCl, $NaNO_3$, and NaSCN, we also investigated the effect of NaBr and NaI, as shown in Fig. 4B. Also in this case the addition of 100 mM sodium salts decreases $\zeta$-potentials, but a 'bell shaped' Hofmeister series is observed (when anions are ordered by the conventional series) in the presence of both buffers. Interestingly, SBA-$NH_2$ sample is more sensitive than SBA-15 to both buffer and salt type as shown by the corresponding $\zeta$-potentials. Definitely, the addition of salts reduces significantly the surface charge in all cases,

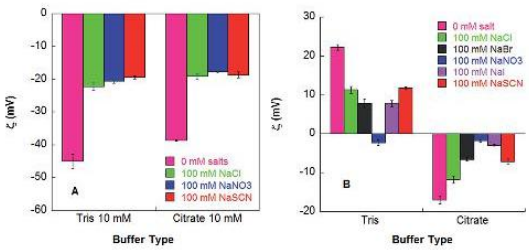


Fig. 4 Effect of salt and buffers on $\zeta$ potentials of (A) SBA-15; (B) SBA-$NH_2$.

but does not cancel the effect of buffers in the cases of the two positively charged surfaces of LYZ and SBA-$NH_2$.

Finally, let us focus on LYZ loading in the presence of buffers and salts. Fig. 5 shows the results for the two silica matrices in Tris and citrate buffers: for SBA-$NH_2$ the effects of NaBr and NaI are also enclosed. In the case of SBA-15 (Fig. 5A) in Tris buffer a LYZ loading increase along the series 'No Salt' < NaCl < NaBr << NaSCN was observed. In citrate buffer, instead, ions specificity was lost. Evidently, the background buffer, used to set the pH, triggers a further dependence on the anion type of the added strong electrolytes. In the case of SBA-$NH_2$, LYZ loading data, in the presence of NaCl, NaBr, and $NaNO_3$, are very low (<20 mg $g^{-1}$). Strikingly, the addition of either NaI or NaSCN induced a huge increase of loading. This high loading is achieved for both buffers (and also for BES and phosphate buffers: see Fig. S4 in ESI‡). Fig. 5 shows another noteworthy result: in the presence of 100 mM NaSCN (or NaI), LYZ loading obtained for SBA-15 (Tris buffer) and SBA-$NH_2$ (all buffers) is very similar. In a recent interesting work Meissner *et al.* proposed a model for the calculation of the maximum uptake capacity of SBA-15.[42] A rough comparison between the adsorption data of the present and that work would lead to the conclusion that the very high loading obtained here for SBA-15 and SBA-$NH_2$ in the presence of 0.1 M NaSCN (or NaI) exceed the maximum loading capacity. In fact, although the Meissner model is highly reasonable, this is based on geometric considerations of pore size and pore volume of the sorbent material as well as LYZ size. There might be several explanations for that apparent inconsistency. In particular, we argue that the different method used to calculate the pore size might be the main cause.[43] Indeed we used the BJH method (ESI‡), whereas the KJS method was used by Meissner *et al.*[42] It has been shown that different methods can result in different pore sizes.[44] Moreover, we cannot exclude that, in addition to adsorption, an unwanted LYZ co-precipitation phenomenon may occur. A systematic investigation of the reasons of the high loading observed in the presence of 0.1 M NaI and NaSCN is, although of extreme interest, beyond the scopes of this work which was mainly devoted to investigate the specific effect of buffers.

The high LYZ loading observed for SBA-$NH_2$ found in the presence of the most polarisable anions $I^-$ and $SCN^-$, might be due to their ability to counteract, and exceed both the electrostatic repulsion between the positively charged LYZ and SBA-$NH_2$ surfaces. Definitely, the effect of NaSCN (and NaI) is so strong to overcome all other types of interactions or buffer specific effects involved in LYZ loading. This striking result cannot be justified in terms of electrostatic interactions only, since salt addition reduces significantly all surface charges, as demonstrated by ζ-potential data shown in Fig. 3 and 4. Indeed, the LYZ loading around 600–700 mg $g^{-1}$ obtained for both positively and negatively charged silica matrices, is likely promoted by non-electrostatic interactions mainly. A recent work investigating the effect of ionic strength on the adsorption and release of lysozyme from SBA-15 at pH 7 (10 mM phosphate buffer),[38] showed that a high ionic strength (1 M NaCl) favours the LYZ adsorption but not its release. Here we fixed pH (7.15) and ionic strength (100 mM) but varied the nature of the buffer used to set pH, the salt used to set ionic strength, and the sorbent surface. The fact that buffers and salt ions give rise to different loadings suggests that they interact specifically with LYZ and silica surface sites, thus affecting their actual dissociation constants and effective surface charges.[9,41,45] The main outcome is that protein loading on OMS is the result of the complicated interplay among the specific effects of the buffers, the salts, and the charged interfaces. Sometimes the dominant effect is due to the buffer, sometimes to the salt, sometimes both matter. In this work the buffer effect is more important for LYZ loading on SBA-15 (Fig. 1), whereas the specific anion effect is strong also for SBA-$NH_2$ sorbent (Fig. 5B).

Finally, we remark that the consequences of this work go beyond the specific case described here. The Henderson–Hasselbalch equation, known to be one of the pillars of chemistry, considers buffers action only in terms of the p$K_a$ of the weak electrolyte. But in the presence of charged interfaces the buffer species tend to adsorb thus modifying the effective surface charges and the physico-chemical behaviour of the system. Here, a competition between buffer and salt ions for adsorption on LYZ and OMS surfaces can clearly be inferred. Hence, specific buffer effects would require to be included in the plethora of phenomena that we classify as 'Hofmeister effects'.

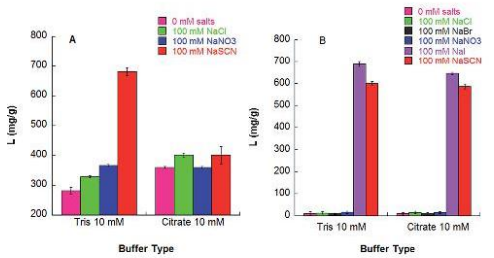


Fig. 5 Effect of buffers (10 mM) and added salts (100 mM) on LYZ loading at 298 K and pH 7.15 on (A) SBA-15; (B) SBA15-$NH_2$.

## Acknowledgements

Fondazione Banco di Sardegna (PRID 2015) is acknowledged for financial support. F. P. Thanks Agenzia delle Dogane e dei Monopoli for financing her PhD scholarship.

## References

1 P. Lo Nostro and B. W. Ninham, *Chem. Rev.*, 2012, **112**, 2286–2322.
2 F. Tadini-Buoninsegni, M. R. Moncelli, N. Peruzzi, B. W. Ninham, L. Dei and P. Lo Nostro, *Sci. Rep.*, 2015, **5**, 14282.
3 A. Salis and B. W. Ninham, *Chem. Soc. Rev.*, 2014, **43**, 7358–7377.
4 C. Carucci, P. Haltenort, M. Salazar, A. Salis and E. Magner, *ChemElectroChem*, 2015, **2**, 659–663.

5 B. W. Ninham and P. Lo Nostro, *Molecular Forces and Self Assembly In Colloid, Nano Sciences and Biology*, Cambridge University Press, Cambridge, 2010.
6 A. A. Green, *J. Biol. Chem.*, 1932, **95**, 47–66.
7 L. Medda, C. Carucci, D. F. Parsons, B. W. Ninham, M. Monduzzi and A. Salis, *Langmuir*, 2013, **29**, 15350–15358.
8 L. Medda, M. Monduzzi and A. Salis, *Chem. Commun.*, 2015, **51**, 6663–6666.
9 D. F. Parsons and A. Salis, *Curr. Opin. Colloid Interface Sci.*, 2016, **23**, 41–49.
10 R. de Levie, *J. Chem. Educ.*, 2003, **80**, 146.
11 Y. Zhang and P. S. Cremer, *Proc. Natl. Acad. Sci. U. S. A.*, 2009, **106**, 15249–15253.
12 A. Salis, F. Cugia, D. F. Parsons, B. W. Ninham and M. Monduzzi, *Phys. Chem. Chem. Phys.*, 2012, **14**, 4343–4346.
13 L. Medda, A. Salis and E. Magner, *Phys. Chem. Chem. Phys.*, 2012, **14**, 2875–2883.
14 P. Lo Nostro, N. Peruzzi, M. Severi, B. W. Ninham and P. Baglioni, *J. Am. Chem. Soc.*, 2010, **132**, 6571–6577.
15 Y. R. Gokarn, R. M. Fesinmeyer, A. Saluja, V. Razinkov, S. F. Chase, T. M. Laue and D. N. Brems, *Protein Sci.*, 2011, **20**, 580–587.
16 F. Cugia, M. Monduzzi, B. W. Ninham and A. Salis, *RSC Adv.*, 2013, **3**, 5882–5888.
17 H. Kim, E. Tuite, B. Norden and B. W. Ninham, *Eur. Phys. J. E*, 2001, **4**, 411–417.
18 A. Salis, M. C. Pinna, D. Bilanicová, M. Monduzzi, P. Lo Nostro and B. W. Ninham, *J. Phys. Chem. B*, 2006, **110**, 2949–2956.
19 A. Salis, D. Bilanicová, B. W. Ninham and M. Monduzzi, *J. Phys. Chem. B*, 2007, **111**, 1149–1156.
20 A. Salis and M. Monduzzi, *Curr. Opin. Colloid Interface Sci.*, 2016, **23**, 1–9.
21 N. C. Stellwagen, A. Bossi, C. Gelfi and P. G. Righetti, *Anal. Biochem.*, 2000, **287**, 167–175.
22 M. A. Metrick, J. E. Temple and G. Macdonald, *Biophys. Chem.*, 2013, **184**, 29–36.
23 S. O. Ugwu and S. P. Apte, *Pharm. Technol.*, 2004, 86–113.
24 D. S. Katayama, R. Nayar, D. K. Chou, J. J. Valente, J. Cooper, C. S. Henry, D. G. Vander Velde, L. Villarete, C. P. Liu and M. C. Manning, *J. Pharm. Sci.*, 2006, **95**, 1212–1226.
25 D. Roberts, R. Keeling, M. Tracka, C. F. van der Walle, S. Uddin, J. Warwicker and R. Curtis, *Mol. Pharm.*, 2015, **12**, 179–193.
26 D. Kameoka, E. Masuzaki, T. Ueda and T. Imoto, *J. Biochem.*, 2007, **142**, 383–391.
27 L. Y. Chou, H. W. Blanch, J. M. Prausnitz and R. A. Siegel, *J. Appl. Polym. Sci.*, 1992, **45**, 1411–1423.
28 H. N. Po and N. M. Senozan, *J. Chem. Educ.*, 2001, **78**, 1499–1503.
29 N. Carlsson, H. Gustafsson, C. Thörn, L. Olsson, K. Holmberg and B. Åkerman, *Adv. Colloid Interface Sci.*, 2014, **205**, 339–360.
30 M. Hartmann and X. Kostrov, *Chem. Soc. Rev.*, 2013, **42**, 6277–6289.
31 E. Magner, *Chem. Soc. Rev.*, 2013, **42**, 6213–6222.
32 M. Piludu, L. Medda, F. Cugia, M. Monduzzi and A. Salis, *Langmuir*, 2015, **31**, 9458–9463.
33 M. Piras, A. Salis, M. Piludu, D. Steri and M. Monduzzi, *Chem. Commun.*, 2011, **47**, 7338–7340.
34 J. M. Bolivar, I. Eisl and B. Nidetzky, *Catal. Today*, 2015, **259**, 66–80.
35 A. Baeza, M. Colilla and M. Vallet-Regí, *Expert Opin. Drug Delivery*, 2015, **12**, 319–337.
36 A. Salis, L. Medda, F. Cugia and M. Monduzzi, *Colloids Surf., B*, 2016, **137**, 77–90.
37 H. Essa, E. Magner, J. Cooney and B. K. Hodnett, *J. Mol. Catal. B: Enzym.*, 2007, **49**, 61–68.
38 D. Steri, M. Monduzzi and A. Salis, *Microporous Mesoporous Mater.*, 2013, **170**, 164–172.
39 A. Salis, M. S. Bhattacharyya and M. Monduzzi, *J. Phys. Chem. B*, 2010, **114**, 7996–8001.
40 V. S. Stoll and J. S. Blanchard, in *Methods in Enzymology*, 2009, vol. 463, pp. 43–56.
41 D. F. Parsons and A. Salis, *J. Chem. Phys.*, 2015, **142**, 134707.
42 J. Meissner, A. Prause, C. Di Tommaso, B. Bharti and G. H. Findenegg, *J. Phys. Chem. C*, 2015, **119**, 2438–2446.
43 M. A. Smith, M. G. Ilasi and A. Zoelle, *J. Phys. Chem. C*, 2013, **117**, 17493–17502.
44 M. Jaroniec and L. A. Solovyov, *Langmuir*, 2006, **22**, 6757–6760.
45 C. Bunton, F. Nome, F. H. Quina and L. S. Romsted, *Acc. Chem. Res.*, 1991, **24**, 357–364.

# Supporting information of paper I

Electronic Supplementary Material (ESI) for RSC Advances.


# ESI file

## Are specific buffer effects the new frontier of Hofmeister phenomena? Insights from lysozyme adsorption on ordered mesoporous silica

*Francesca Cugia,[a] Silvia Sedda,[a] Federica Pitzalis,[a] Drew F. Parsons,[b] Maura Monduzzi,[a,]* and Andrea Salis[a,]**

Department of Chemical and Geological Sciences, University of Cagliari-CSGI and CNBS, Cittadella Universitaria, S.S. 554 bivioSestu, 09042- Monserrato (CA), Italy;

School of Engineering and Information Technology, Murdoch University, 90 South St, Murdoch, WA 6150, Australia

### Material and methods

**Chemicals.** Pluronic P123 ($PEO_{20}PPO_{70}PEO_{20}$), tethraethylorthosilicate (TEOS 98%), hydrochloric acid (37%), 3-aminopropyltriethoxysilane (APTES; 97%), lysozyme (E.C.3.1.1.17) from hen egg white (70,000 units/mg; 62971), $NaH_2PO_4$ (99%); sodium chloride (≥ 99%; S3014), sodium thiocyanate (≥ 98%; 251410) and sodium phosphate dibasic (≥ 99.5%; S0876), sodium hydroxide (≥ 97%; 221465), and N,N-Bis-(2-hydroxyethyl)-2-aminoethanesulfonic acid (BES ≥ 99%; B9879) were purchased from Sigma-Aldrich. Sodium nitrate (≥ 99%; 205960010), sodium bromide (99%), and sodium iodide (99%) were purchased from Acros Organics. Tris

(hydroxymethyl)aminomethane (≥ 99.8%; 1610719) was from Biorad. Citric acid (≥ 99.5%; 27490) was purchased from Fluka.

**Synthesis of SBA-15 and SBA-$NH_2$.** SBA-15 mesoporous silica was prepared according to the method previously reported by Zhao et al [1]. In a typical synthesis, triblock copolymer Pluronic P123, as a structure-directing agent, was dissolved in a mixture of millipore water and hydrochloric acid under magnetic stirring at 35 °C. Once the surfactant was completely dissolved, tetraethyl orthosilicate (TEOS) was added as the silica source. After aging at 100 °C for 24 h in a sealed teflon autoclave, gels were filtered, washed with deionized water, and dried in air at 40°C for 24 h. Finally, dried powders were thermally treated to remove the surfactant at 550°C for 5h. SBA-$NH_2$ was prepared by adding 1 mL of APTES to a suspension of 1 g SBA-15 in 30 mL of dry toluene under refluxing condition for 18 h. Resulted amino-functionalized material was collected by filtration, washed properly with acetone to remove the unreacted reagent, and was dried overnight under vacuum at room temperature

**Characterization of SBA-15 and SBA-$NH_2$.** A S3-MICRO SWAXS camera system (HECUS X-ray Systems, Graz, Austria) was used to recorder SAXS patterns (1200 s). Cu Kα radiation of wavelength 1.542 Å was provided by a GeniX X-ray generator, operating at 50 kV and 1 mA. A 1D-PSD-50 M system (HECUS X-ray Systems, Graz, Austria) containing 1024 channels of width 54.0 $\mu$m was used for the detection of scattered X-rays in the small-angle region. Transmission electron microscopy (TEM) images were obtained on a JEOL 100S microscope. Finely ground samples were placed directly onto formvar-coated electron microscopy nichel grids. A Thermoquest-Sorptomatic 1990 was used for the nitrogen physisorption isotherms at 77 K. Before analysis, pure silica samples were heated up to 240 °C at a rate of 1°C $min^{-1}$ under vacuum. The BET [2] and BJH [3] (calculated from the desorption branch) methods were used to calculate the specific surface area, the total pore volume and the pore size distribution. Fourier Transform

Infrared (FTIR) spectra were determined through a Bruker Tensor 27 spectrophotometer equipped with a diamond-ATR accessory and a DTGS detector. A number of 64 scans at a resolution of 2 $cm^{-1}$ were acquired in the range 4000-400 $cm^{-1}$. Surface charge densities of SBA-15 and SBA-$NH_2$ were determined through potentiometric titrations according to the procedure reported in ref. [4].

**Electrophoretic mobility measurements.** Zeta potential ($\zeta$) measurements of either mesoporous silica or lysozyme in buffer and buffer-salt solutions were carried out through electrophoretic light scattering (laser Doppler velocimetry) technique by means of a Zetasizer nano series (Malvern Instruments). A weighed amount of lysozyme powder was dissolved in a 10 mM sodium phosphate buffer (pH 7) solution to obtain a final concentration of 1 mg/mL. NaCl was dried overnight at 110°C and cooled at room temperature in a desiccator. Different amounts of NaCl were then added to 100 mL of the lysozyme solution obtaining a concentration range 1 mM - 200 mM. A small volume of the resulting solution was introduced in a scattering cell for the measurement of the electrophoretic mobility. Experiments were repeated 3-5 times. Each value of mobility is the average of 5-7 measurements obtained by mediating 20 simple readings per each salt concentration. Standard deviations were calculated and displayed as error bars in Fig.s 2-4.

**Lysozyme adsorption on mesoporous silica.** Different samples of SBA-15 (or SBA-$NH_2$) having the same mass (12.5 mg) were suspended in different tubes each containing 1 mL of a 10 mg/mL lysozyme solution in 10 mM (Tris, BES, phosphate, citrate) buffer at pH 7.15. The suspensions were kept at constant temperature of 25°C under orbital shaking in an incubator for 24h. The suspension was centrifuged for 5 min at 4000 rpm and washed twice with 0.5 mL of fresh buffer solution. The concentration of lysozyme in the supernatant was analyzed by an UV-Vis spectrophotometer at a $\lambda$ = 280 nm. The loading of lysozyme adsorbed onto SBA-15 ($L_{Lyz}$ = mg/g), was calculated according the following formula:

$$L_{Lyz} = \frac{([Lyz_i] - [Lyz_r]) \times V - [Liz_w]V_w}{m_s} \quad (1)$$

Where, $[Lyz]_i$ is the lysozyme concentration ($mg_{Lyz}/mL_{solution}$) at t=0; $[Lyz]_r$ is the residual concentration of lysozyme in the solution ($mg_{Lyz}/mL_{solution}$) at time t= 24h; $[Lyz]_w$ is the concentration of lysozyme in the washing solution ($mg_{Lyz}/mL_{solution}$); $V$ is the volume of the lysozyme solution (mL), $V_w$ is the volume of the washing solution, and $m_s$ is the mass (g) of either SBA-15 or SBA-$NH_2$. The same experiment was also carried out in the presence of different 100 mM salts (NaCl, $NaNO_3$, NaBr, NaI, NaSCN).

## Results

### Characterisation of SBA-15 and SBA-$NH_2$.

**Table 1.** Characterization of SBA-15 and SBA-$NH_2$ obtained through $N_2$- adsorption/desorption isotherms, SAXS, and zeta potential.

| Sample | $S_{BET}$ ($m^2/g$)[a] | $V_p$ ($cm^3/g$)[b] | $d_p$ (nm)[c] | $a$ (nm)[d] |
|---|---|---|---|---|
| SBA-15 | 777 | 1.1 | 6.4 | 11.7 |
| SBA-$NH_2$ | 398 | 0.8 | 5.9 | 11.6 |

[a] Surface area calculated with the BET method
[b] Pore volume
[c] Pore diameter calculated through the BJH method applied to the desorption branch
[d] Lattice parameter calculated from the equation $a=2d_{100}/\sqrt{3}$, where $d_{100}$ is the spacing of the (1 0 0) plane of the hexagonal array (p6mm) of the pores.

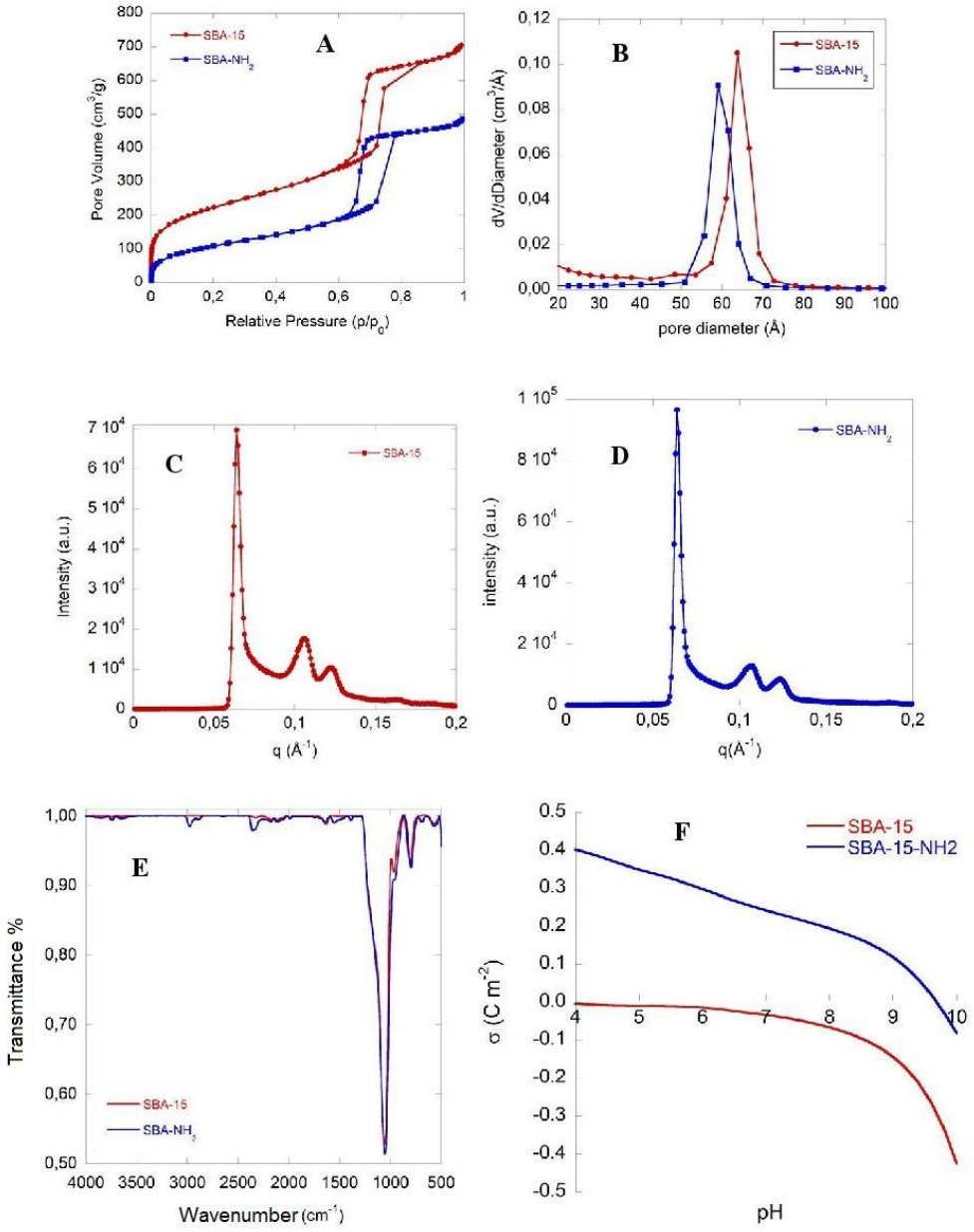


**Figure S1.** Characterisation of SBA-15 and SBA-$NH_2$ samples. A) $N_2$ adsorption/desorption isotherms; B) Pore size distribution; C) SAXS pattern of SBA-15; D) SAXS pattern of SBA-$NH_2$; E) FTIR spectroscopy; F) surface charge density (σ) as a function of pH.

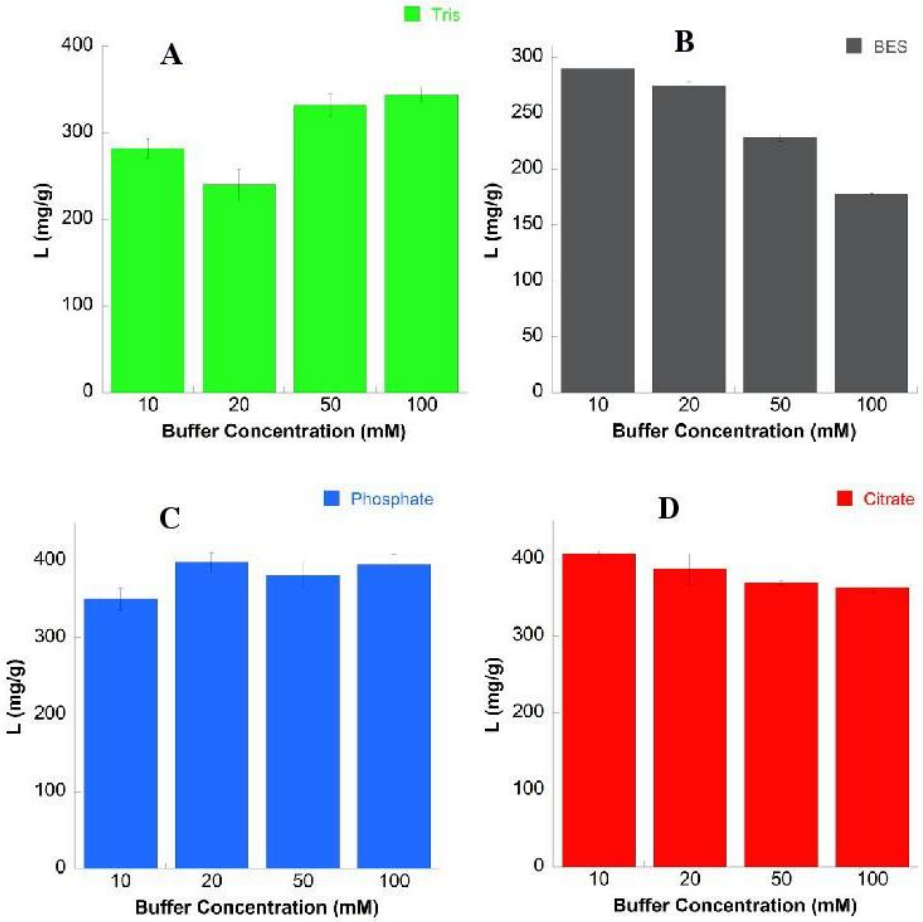


**Fig. S2** Effect of buffer concentration (pH 7.15) on lysozyme adsorption on SBA-15 (T= 298 K; pH = 7.15). A) Tris; B) Bes; C) Phosphate; D) Citrate.

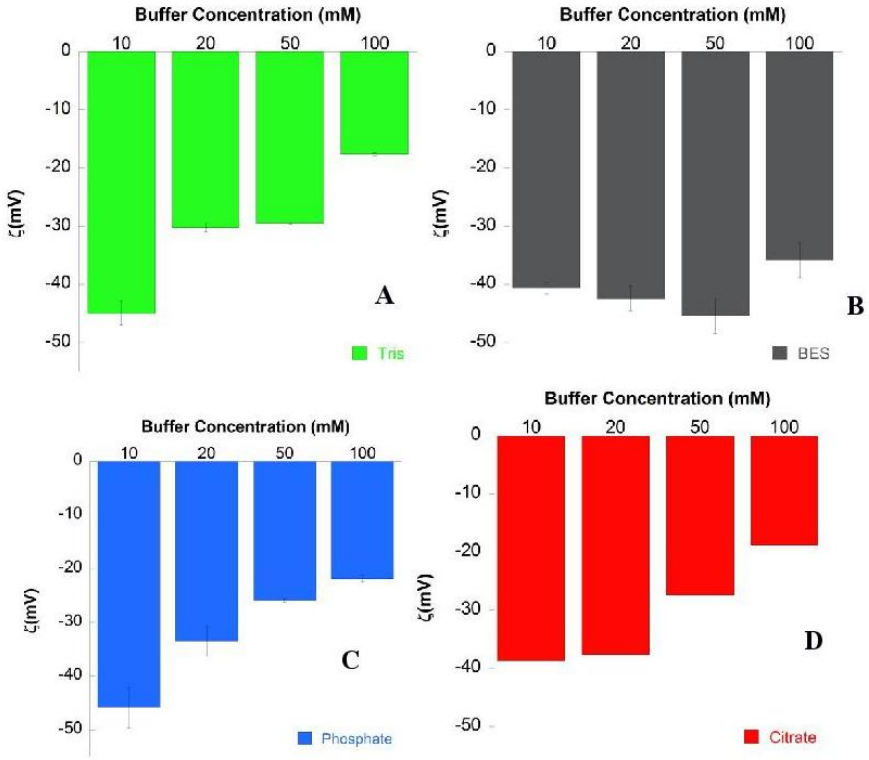


**Fig. S3** Effect of buffer concentration (pH 7.15) on zeta potential of SBA-15 suspensions (T= 298 K; pH = 7.15). A) Tris; B) Bes; C) Phosphate; D) Citrate.

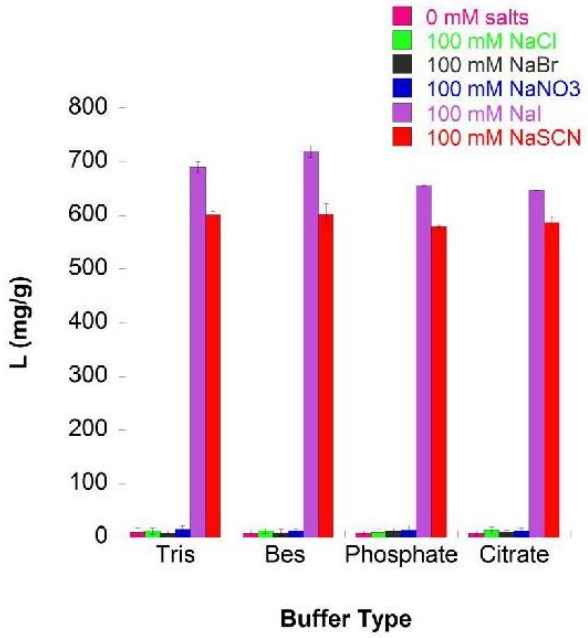


**Fig. S4** Effect of 10 mM buffers 100 mM salts on LYZ loading (T = 298 K; pH 7.15) on SBA-$NH_2$.

## References

[1] D. Zhao, J. Feng, Q. Huo, N. Melosh, G. Fredrickson, B. Chmelka, et al., Triblock copolymer syntheses of mesoporous silica with periodic 50 to 300 angstrom pores, Science. 279 (1998) 548–552. doi:10.1126/science.279.5350.548.

[2] S. Brunauer, P. Emmett, E. Teller, Adsorption of gases in multimolecular layers, J. Am. Chem. Soc. 407 (1938) 309–319.

[3] E.P. Barrett, L.G. Joyner, P.P. Halenda, The Determination of Pore Volume and Area Distributions in Porous Substances. I. Computations from Nitrogen Isotherms, J. Am. Chem. Soc. 73 (1951) 373–380. doi:10.1021/ja01145a126.

[4] A. Salis, D.F. Parsons, M. Bostrom, L. Medda, B. Barse, B.W. Ninham, et al., Ion specific surface charge density of SBA-15 mesoporous silica, Langmuir. 26 (2010) 2484–2490. doi:10.1021/la902721a.

# Paper II

***Pitzalis,F.**, Monduzzi,M., Salis, A. "A bienzymatic biocatalyst constituted by glucose oxidase and Horseradish peroxidase immobilized on ordered mesoporous silica" Microporous and Mesoporous Materials 241 (2017) 145-154, **DOI:** 10.1016/j.micromeso.2016.12.023*

http://dx.doi.org/10.1016/j.micromeso.2016.12.023

Microporous and Mesoporous Materials 241 (2017) 145–154

Contents lists available at ScienceDirect

Microporous and Mesoporous Materials

journal homepage: www.elsevier.com/locate/micromeso

# A bienzymatic biocatalyst constituted by glucose oxidase and Horseradish peroxidase immobilized on ordered mesoporous silica

Federica Pitzalis, Maura Monduzzi, Andrea Salis*

*Department of Chemical and Geological Sciences, University of Cagliari-CSGI and CNBS, Cittadella Universitaria, S.S. 554 bivio Sestu, 09042, Monserrato, CA, Italy*

ARTICLE INFO

*Article history:*
Received 19 September 2016
Received in revised form
28 November 2016
Accepted 21 December 2016
Available online 23 December 2016

*Keywords:*
Bienzymatic biocatalyst
Glucose oxidase
Horseradish peroxidase
SBA-15 mesoporous silica
Phenolic compounds

ABSTRACT

It is presently extremely challenging to realize an active immobilized multi-enzyme biocatalyst which allows to run *in vitro* multi-step cascade reactions. This work deals with the obtainment of a bienzymatic immobilized biocatalyst constituted by Glucose Oxidase (GOx) and Horseradish Peroxidase (HRP) immobilized onto SBA-15 mesoporous silica. The effect of co-immobilization (GOx/HRP@SBA-15) versus the separated immobilization (GOx@SBA-15/HRP@SBA-15), and the effect of covalent versus physical immobilization, on protein loading and enzymatic activity were investigated. Regardless the different immobilization strategy used, it was found that the catalytic activity could be retained only if the immobilized bienzymatic biocatalyst was kept wet. The obtained wet GOx/HRP@SBA-15 biocatalyst could be recycled 14 times keeping a good activity. Finally, the bienzymatic biocatalyst was tested for the oxidation of two model phenolic (caffeic acid and ferulic acid) pollutants of agricultural wastewaters, as olive mill wastewaters (OMWs). The biocatalyst was able to reach a 70% conversion within 15 min.



## 1. Introduction

Ordered mesoporous silica (OMS) is a promising material for several technological applications because of its outstanding features [1]. Among the different possible applications, OMSs are being used in nanomedicine [2,3], adsorption [4], inorganic catalysis [5], and biocatalysis [6]. In particular, the use of OMSs as enzyme supports for immobilized biocatalysts seems to be a very feasible application, as demonstrated by the huge number of papers and recent reviews [6–9]. Among the enzymes immobilized on OMSs, which retained their activity after the immobilization, there are: chloroperoxidase [10], lipase [11,12], cytochrome c [13], xylanase [13], lysozyme [14], myoglobin [15], laccase [16], subtilisin [17], and many others [18]. The easiest method to carry out enzyme immobilization is physical adsorption. For physically adsorbed enzymes immobilization conditions, i.e. pH [15], ionic strength and electrolyte type have been shown to affect both enzyme loading and activity [19]. In general covalently bound enzymes are more stable to harsh reaction conditions and can be reused for several reaction cycles [20].

Most of previous works investigated the immobilization and the catalytic activity of only one enzyme immobilized on OMS. Very less common is the immobilization of two enzymes which work sequentially [21]. For example, Hartmann and coworkers were likely the first to immobilize glucose oxidase and chloroperoxidase on SBA-15 OMS to obtain a “tandem biocatalyst” [22]. The importance of that approach is due to the fact that chloroperoxidase is known to be susceptible to oxidative deactivation by hydrogen peroxide. *In situ* $H_2O_2$ formation through enzymatic glucose oxidation, carried out by glucose oxidase immobilized on SBA-15, was indeed found to avoid this problem.

Glucose oxidase (GOx; E.C.1.1.3.4) [23] and Horseradish peroxidase (HRP; E.C. 1.11.1.7) [24] are two versatile redox enzymes which are being used in biosensing [25,26], tissue engineering [27], and are very promising candidates for green chemistry [28] and bioremediation applications [29]. GOx oxidizes glucose to gluconolactone and reduces oxygen to $H_2O_2$, using flavin adenin dinucleotide as the cofactor. HRP is a heme protein which uses $H_2O_2$ to oxidize various aromatic substrates. It has been shown that, similarly to chloroperoxidase, also HRP is a.

* Corresponding author.
*E-mail addresses:* monduzzi@unica.it (M. Monduzzi), asalis@unica.it (A. Salis).

http://dx.doi.org/10.1016/j.micromeso.2016.12.023
1387-1811/

"suicide" enzyme, that is inactivated by high concentrations of its own substrate ($H_2O_2$) [22,30–33]. Hence, HRP activity could be retained by producing *in situ* a controlled amount of $H_2O_2$. This suggests the combined use of GOx and HRP for the realization of a bienzymatic biocatalyst.

GOx and HRP enzymes have been immobilized on several supports [21]. Most of those works were interested to the realization of a glucose biosensor [34,35]. But a novel and interesting application might be their use in bioremediation. For example, Phuoc et al. used GOx and HRP encapsulated onto phospholipids–templated silica, for the removal of polycyclic aromatic hydrocarbons from wastewaters [29]. Another interesting application is the oxidation of recalcitrant phenolic compounds. These compounds are present in the aqueous effluents of some important agricultural processes like coffee [36] and olive oil production [37]. Phenolic compounds are highly pollutant substances which need to be removed before their release in the environment. Besides phenolic compounds, OMWs also contain carbohydrates, and glucose in particular [37]. This suggested us the possibility to use a GOx/HRP@OMS bienzymatic biocatalyst for the treatment of the recalcitrant phenolic compounds for bioremediation purposes in particular of OMWs which is a big issue in the Mediterranean area [16,37]. To the best of our knowledge, this application has not been proposed yet.

In the present work we wanted to reach the following two goals. First of all we investigated different strategies for the obtainment of an active bienzymatic biocatalyst constituted by GOx and HRP immobilized on SBA-15 OMS. To this purpose, SBA-15 was firstly synthesized and characterized through different physico-chemical techniques. According to what shown in Scheme 1, we investigated: i. the optimal enzymatic GOx:HRP mass ratio; ii. the catalytic activities of the co-immobilized (HRP/GOx@SBA-15) and of the singly immobilized (HRP@SBA-15 and GOx@SBA-15) enzymes; iii. the effect of the drying process on the enzymatic activity. The reuse of the biocatalyst for several reaction cycles was also demonstrated. The second goal was to give a "proof of concept" that the obtained active bienzymatic biocatalyst could be used for the detoxification of agricultural wastewaters, such as OMWs, which contain both glucose and recalcitrant phenolic compounds. To this purpose a model wastewater containing glucose and either caffeic acid or ferulic acid was used a substrate solution for the bienzymatic biocatalyst. Caffeic acid and ferulic acid are two model recalcitrant phenolic compounds, common pollutants of olive mill and coffee production wastewaters [16,29,36].

## 2. Materials and methods

### 2.1. Chemicals

Glucose oxidase (GOx) type VII from *Aspergillus niger* lyophilized (145 U $mg^{-1}$), Horseradish peroxidase (HRP) type I lyophilized salt free (250 U $mg^{-1}$), 2,2′-azinobis-(3-ethylbenzothiazoline-6-sulfonate) diammonium salt (ABTS, ≥98%), glutaraldehyde (50 wt % in $H_2O$), tetraethylorthosilicate (TEOS, 98%), pluronic copolymer P123, 3-aminopropyltrimethoxysilane (APTES, 97%), bovine serum albumin (BSA, 98%), Bradford reagent, sodium phosphate dibasic (ACS Grade, ≥99%), citric acid monohydrate (≥99%), ethanol (98%), were purchased from Sigma-Aldrich. Sodium phosphate monobasic monohydrate (≥99%) was purchased from J.T. Backer. Sodium citrate (ACS Grade ≥99%) was purchased from Aldrich. Glucose (ACS Grade ≥99%) was purchased from Carlo Erba. Ferulic acid ((*E*)-3-(4-hydroxy-3-methoxyphenyl)prop-2-enoic acid, >98.0%), caffeic acid ((*E*)-3-(3,4-dihydroxyphenyl)prop-2-enoic acid, >95.0%), were from Fluka (Milan, Italy). Milli-Q water (resistivity > 18.2 MΩ $cm^{-1}$ at 25 °C) was used for all buffer and enzymatic solutions. Phosphate buffer 0.1M pH 8, and 0.025M citrate buffer pH 5 were used for to prepare the enzymatic solutions for the immobilization process.

### 2.2. Synthesis and characterization of SBA-15 mesoporous silica

SBA-15 mesoporous silica was synthesized and functionalized with APTES according to the method described in previous works [20]. Small angle X-rays scattering (SAXS) patterns were recorded for 3600 s by means of a S3-MICRO SWAXS camera system (HECUS X-ray Systems, Graz, Austria). Cu-Kα radiation of wavelength 1.542 Å was provided by a GeniX X-rays generator, operating at 30 kV and 0.4 mA. A 1D-PSD-50M system (HECUS X-ray Systems, Graz, Austria) containing 1024 channels of width 54.0 μm was used for the detection of scattered X-rays in the small-angle region. Transmission electron microscopy (TEM) images were obtained on a JEOL 100S microscope. Finely ground samples were placed directly onto Formvar-coated electron microscopy nichel grids.

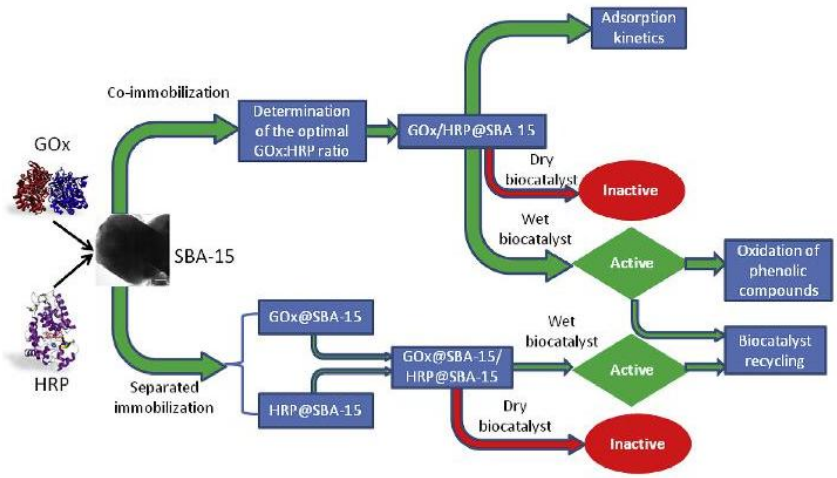


**Scheme 1.** Flow diagram of the experimental work.

Textural analysis was carried out using an ASAP2020 (Micromeritics), by determining the $N_2$ adsorption/desorption isotherms at 77 K. Before analysis, pure silica samples (SBA-15) were heated up to 250 °C at a rate of 1 °C/min under vacuum, while the functionalized samples (SBA-15-$NH_2$, GOx/HRP@SBA-15) were outgassed overnight at 40 °C. The specific surface area, and the pore size distribution were assessed by the Brunauer-Emmett-Teller (BET) and BJH methods, respectively.

Fourier Transform Infrared (FTIR) spectra were determined through a Bruker Tensor 27 spectrophotometer equipped with a diamond-ATR accessory and a DTGS detector. A number of 256 scans at a resolution of 2 $cm^{-1}$ were acquired in the range 4000–400 $cm^{-1}$.

### 2.3. Immobilization of GOx and HRP on SBA-15

#### 2.3.1. Covalent co-immobilization

The covalent co-immobilization of GOx and HRP on SBA-15, to obtain the GOx/HRP@SBA-15 biocatalyst, was carried out by putting in a 2 mL Eppendorf test tube 25 mg of amino functionalized SBA-15, 550 μL of 0.1 M phosphate buffer at pH 8, and 20 μL of glutaraldehyde solution (50 wt% in $H_2O$). The test tube was left under stirring for 30 min until the white silica particles became red. Then the excess of glutaraldehyde was removed through extensive washing of the functionalized sample with fresh buffer. Two separated solutions of GOx and HRP both, at the concentration 2 mg/mL, were prepared by dissolving the enzymatic powders in 0.1 M phosphate buffer at pH 8. The GOx solution (2 mg/mL) and the HRP solution (2 mg/mL) were suitably mixed together to obtain different mass ratios (GOx:HRP = 1:1; 2:1; 3:1; 5:1 7:1). Then, 1 mL of the resulting bi-enzymatic solution was added to an Eppendorf test tube containing the glutaraldehyde-activated silica support, and left under stirring in an Eppendorf thermomixer at 25 °C for 48h. The protein loading of the immobilized biocatalyst was determined according to what reported in the next paragraph. The bienzymatic biocatalyst was collected by centrifugation, washed three times, and dried overnight under vacuum at room temperature (dry biocatalyst). Alternatively, the samples were stored and then checked for activity without performing the drying step (wet biocatalyst).

#### 2.3.2. Separated covalent immobilization

The separated immobilization of GOx and HRP on SBA-15, to obtain the GOx@SBA-15/HRP@SBA-15 biocatalyst, was carried out by putting in a 2 mL Eppendorf test tube 5 mg of amino functionalized SBA-15, 550 μL of 0.1 M phosphate buffer at pH 8, and 20 μL of glutaraldehyde (50 wt% in $H_2O$). Then 200 μL of either a HRP solution (2 mg/mL in 0.1 M phosphate buffer at pH 8) or a GOx solution (2 mg/mL in 0.1 M phosphate buffer at pH 8) were added. The samples were left under stirring for 48 h. The dispersion was then centrifuged and the obtained solid was washed twice with fresh buffer. The immobilized biocatalysts were both kept wet, and collected together to get 10 mg of immobilized bienzymatic biocatalyst to be used for the activity measurements.

#### 2.3.3. Physical immobilization of HRP

The physical immobilization of HRP on SBA-15-$NH_2$ was carried out by adding to 5 mg of amino-functionalized support 200 μL of a 2 mg/mL HRP solution in either citrate buffer (0.025 M; pH 5) or phosphate buffer (0.1 M; pH 8). The samples were left under stirring for 48 h. The dispersion was then centrifuged and the obtained solid was washed twice with fresh buffer. After the immobilization step the obtained biocatalyst was dried under vacuum or left wet according to what described above.

All samples were prepared at least in triplicate.

### 2.4. Determination of protein loading

The protein loading of the immobilized biocatalysts was determined by measuring the protein concentration of the immobilizing solution at fixed times. The protein concentration was obtained by means of a spectrophtometric calibration line (λ = 595 nm) prepared using a Bradford microassay. BSA solutions in 0.0125 M phosphate buffer at pH 8 in the concentration range 0.5–8 μg/mL were used to build the calibration curve.

Unless differently specified, protein loading, $q$ ($mg_{protein} \times g^{-1}_{SBA\text{-}15}$) was calculated according to the equation [38]:

$$q = \frac{\left([P]_0 - [P]_f\right)V - [P]_w V_w}{m_{SBA-15}} \quad (1)$$

where, $[P]_0$ and $[P]_f$ are the protein concentration ($mg_{protein}/mL_{solution}$) at time t = 0 and t = 48h; V is the volume of the protein solution (mL), $m_{SBA\text{-}15}$ is the mass of SBA-15 (g).

The kinetics of loading process was investigated by measuring the protein concentration decrease at fixed times. Then different kinetic models were used to calculate the protein loading at equilibrium ($q_e$). According to a previous study [38], we fitted the kinetic data through the following equations:

$$q_t = \frac{q_e t}{a + t} \quad (2)$$

where, $q_t$ is the protein loading at time $t$.

Alternatively, kinetic data were analyzed by means of a pseudo-second order model [39]:

$$\frac{t}{q_t} = \frac{1}{k_2 q_e^2} + \frac{1}{q_e} t \quad (3)$$

where $k_2$ is the pseudo-second order rate constant (h g $mg^{-1}$).

Finally, data were also analyzed through an 'intraparticle diffusion' model [39]:

$$q_t = x_i + k_i t^{1/2} \quad (4)$$

where $k_i$ (mg $g^{-1}$ $h^{1/2}$) is the intraparticle diffusion constant, and $x_i$ is the intercept.

### 2.5. Activity assays

The enzymatic activities of the co-immobilized and singly immobilized biocatalysts were determined by UV/Vis spectrophotometry. A volume of 5600 μL of 25 mM citrate buffer pH5, 20–200 μL of glucose 0.5 M, and 20–200 μL of ABTS 0.02 M were added to 10 mg of immobilized bienzymatic biocatalyst. According to Scheme 2, GOx catalyzes the oxidation of glucose to gluconolactone which results in the *in situ* production of $H_2O_2$. The latter is used by HRP to oxidize ABTS. The formation of ABTS oxidized product as a function of time is followed by reading the absorbance at λ = 415 nm [40] (molar extinction coefficient, $\varepsilon_{ABTS} = 3.47 \times 10^4$ L $mol^{-1}$ $cm^{-1}$) [41]. Enzymatic activity is defined as the amount (μmoles) of ABTS transformed per minute ($\mu mol_{ABTS}$ $min^{-1}$). Specific activity defined as the enzymatic activity per mg of protein ($\mu mol_{ABTS}$ $min^{-1}$ $mg^{-1}$).

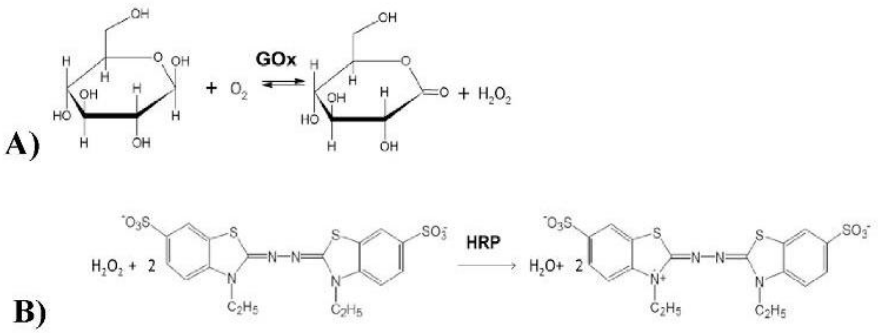


**Scheme 2.** Cascade reactions catalyzed by GOx and HRP. A) The oxidation of glucose to gluconolactone leads to *in situ* $H_2O_2$ production. B) The latter is a substrate for HRP which oxidizes $ABTS^{2-}$ to $ABTS^{\bullet-}$.

### 2.6. Stability of the immobilized bienzymatic biocatalyst

In order to investigate the thermal stability of the GOx/HRP@SBA-15 biocatalyst, a sample of 10 mg was suspended in 500 μL of 100 mM phosphate buffer at pH 8 in an Eppendorf test tube and incubated in an Eppendorf thermomixer for 1 h at the selected temperature (25, 30, 35, 40 and 50 °C). After that time, the sample was left to reach room temperature, and the liquid phase was removed after centrifugation. The enzymatic activity was then measured through the spectrophometric assay described in the paragraph 2.5. Each experiment at different temperature was done at least in triplicate.

The storage stability of the GOx/HRP@SBA-15 wet biocatalyst was investigated by measuring the enzymatic activity after 10 days storage at 4 °C by means of the activity assay described in paragraph 2.5. Experiments were done at least in triplicate.

Operational stability to recycling of the immobilized biocatalyst was studied by measuring the activity of the immobilized preparation according to what described in the paragraph 2.5 (1st cycle). Then the reaction suspension was centrifuged, the liquid phase removed and the assay repeated adding to the solid (biocatalyst) phase fresh buffer and substrates (see par. 2.5 for the quantities). This procedure was repeated 14 times.

### 2.7. Enzymatic removal of phenolic compounds

The enzymatic removal of the phenolic compounds, ferulic acid (FAc) and caffeic acid (CAc), was carried out by adding to 10 mg of immobilized bienzymatic biocatalyst 5 mL of a solution containing 1 mL of the phenolic compound at 5 mg/mL and 4 mL of glucose 0.5M at 298 K. The disappearance of the phenolic compounds was quantified spectrophometrically by means of suitable calibration curves obtained at $\lambda = 286$ nm and $\lambda = 310$ nm for FAc and CAc respectively.

## 3. Results and discussion

### 3.1. Synthesis and characterization of mesoporous SBA-15

SBA-15 mesoporous silica was firstly synthesized and characterized before to be used as a support for enzyme immobilization. Fig. 1 shows the structural characterization carried out through transmission electron microscopy (TEM, Fig. 1A) and small angle X-rays scattering (SAXS, Fig. 1B). Both techniques confirm that the synthesized sample has an ordered structure with a hexagonal array of parallel channels. Moreover, SAXS analysis permits to measure the lattice parameter $a = 11.7$ nm. The textural characterization was then carried out by determining $N_2$ adsorption/desorption isotherms. The physisorption curve (Fig. 1C) shows a type IV isotherm with a H1 hysteresis loop, typical of mesoporous materials with parallel channels. From the adsorption data a surface area of 880 $m^2\ g^{-1}$, and a pore volume of 1.25 $cm^3\ g^{-1}$ were estimated. A monomodal pore size distribution with a maximum at 6.7 nm (Fig. 1D) was calculated through the BJH model. Table 1 summarizes the textural and structural data of SBA-15. The SBA-15 sample was functionalized with aminopropyltriethoxysilane to obtain the amino functionalized SBA-15-$NH_2$ sample. This was needed for the covalent immobilization of the enzymes as described in the next paragraphs. The functionalization procedure does not change the structure as confirmed by SAXS (Fig. 1B) but affects the textural properties. Indeed, the surface area became 373 $m^2\ g^{-1}$, pore volume 0.65 $cm^3\ g^{-1}$, and pore size 5.5 nm (Table 1). A possible reason of the observed change of surface area and pore volume due to APTES functionalization is likely the filling of SBA-15 microporous volume. Indeed, if we look at the initial part (low p/p0 values) of the adsorption isotherm (Fig. 1C), we see a much lower volume of gas adsorbed for SBA-15-$NH_2$ with respect to SBA-15. However, these changes are consistent with what described in previous works [42–44].

ATR-FTIR spectroscopy was used for a further analysis (Fig. 1E). The spectrum shows the characteristic IR absorption bands for Si–O–Si asymmetric and symmetric stretching vibration at the wavenumbers of 1070 $cm^{-1}$ and 800 $cm^{-1}$ respectively. One intense band nearby 450 $cm^{-1}$ is due to Si–O–Si bending. The broad band around 3300 $cm^{-1}$ is due to the O–H stretching of adsorbed water. The functionalization with APTES causes the disappearance of the peak at 980 $cm^{-1}$, due to Si–OH vibration, whereas a weak peak at 1554 $cm^{-1}$ (Fig. 1F) is attributed to the asymmetric bending of $-NH_2$ groups in SBA-15-$NH_2$, and a weak band around 2940 $cm^{-1}$ is due to the stretching of C–H bond of the aminopropyl group (Fig. 1F).

### 3.2. Covalent co-immobilization of GOx and HRP on SBA-15 mesoporous silica

#### 3.2.1. Characterization of GOx/HRP@SBA-15 immobilized biocatalyst

The covalent co-immobilization GOx and HRP on amino functionalized SBA-15, using glutharaldheyde as the chemical linker, was firstly investigated. The obtained sample was characterized through SAXS, $N_2$ adsorption/desorption isotherms, and FTIR spectroscopy. The obtained results are the green curves shown in Fig. 1B–E. We observe in Fig. 1B that the structure of SBA-15-$NH_2$ is not affected by the enzyme immobilization process, as also

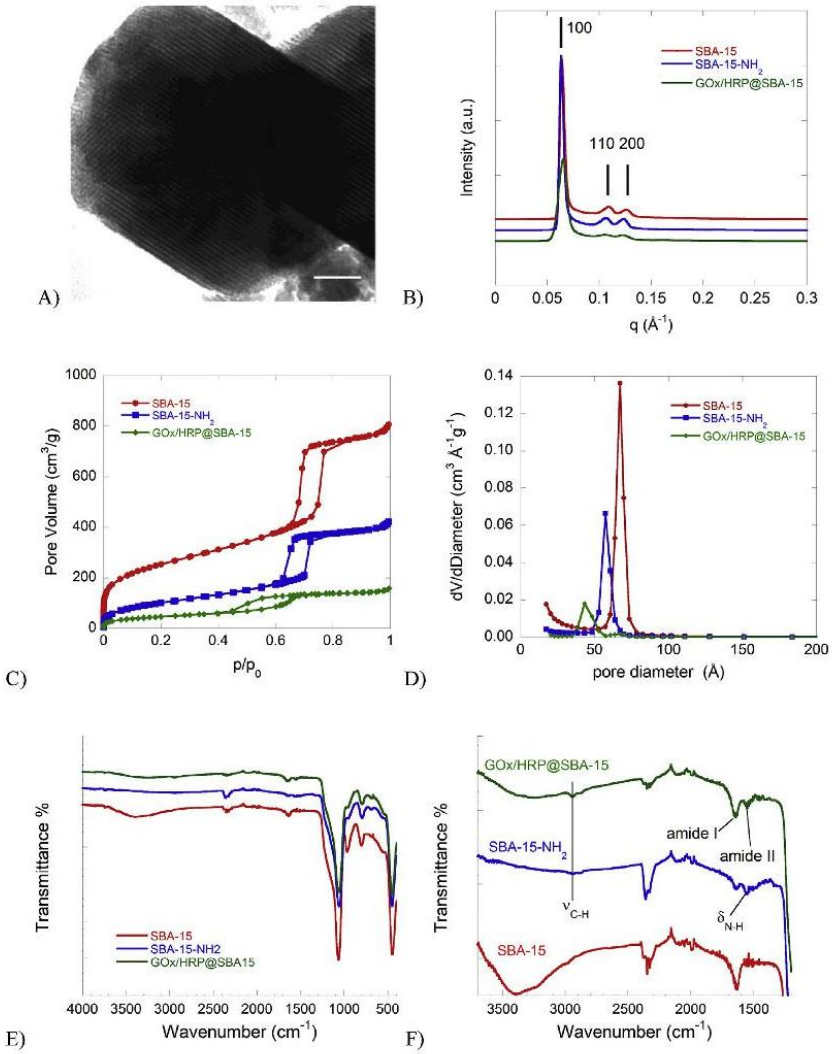


**Fig. 1.** Physico-chemical characterization of SBA-15 and SBA-15-$NH_2$; A) TEM image (Bar, 100 nm); B) SAXS pattern of SBA-15 (large panel) and SBA-15-$NH_2$ (small panel); C) $N_2$ adsorption-desorption isotherms at 77K; D) pore size distribution calculated from the desorption branch; E) ATR-FTIR spectrum.

**Table 1**
Textural and structural parameters of SBA-15 and SBA-15-$NH_2$.

| Sample | [a]$S_{BET}$ ($m^2$ $g^{-1}$) | [b]$V_p$ ($cm^3$ $g^{-1}$) | [c]$d_{BJH}$ (nm) | [d]$a$ (nm) |
|---|---|---|---|---|
| SBA-15 | 880 | 1.25 | 6.7 | 11.7 |
| SBA-15-$NH_2$ | 373 | 0.65 | 5.5 | 11.9 |
| GOx/HRP@SBA-15 | 166 | 0.24 | 3.6 | 11.9 |

[a] Specific surface area calculated by the BET method.
[b] Cumulative pore volume.
[c] Pore diameter calculated by applying BJH method to the data of the desorption branch.
[d] Lattice parameter.

confirmed by the same value of the lattice parameter, $a = 11.9$ nm, (Table 1). Textural characterization (Fig. 1C–D) instead, gave a surface area of 166 $m^2$ $g^{-1}$, a pore volume of 0.24 $cm^3$ $g^{-1}$, and a pore size of 3.6 nm. The reduction of these textural parameters, respect to the values of SBA-15-$NH_2$ sample, is consistent with enzyme immobilization within the pores of mesoporous silica (Table 1). FTIR analysis (Fig. 1F) confirms the successful enzyme immobilization due to the occurrence of the two peculiar peaks, amide I and amide II, at 1650 $cm^{-1}$ and 1550 $cm^{-1}$ respectively [45].

### 3.2.2. Immobilization kinetics

We then investigated the immobilization kinetics focusing on the effect of different GOx:HRP mass ratios. This was done because

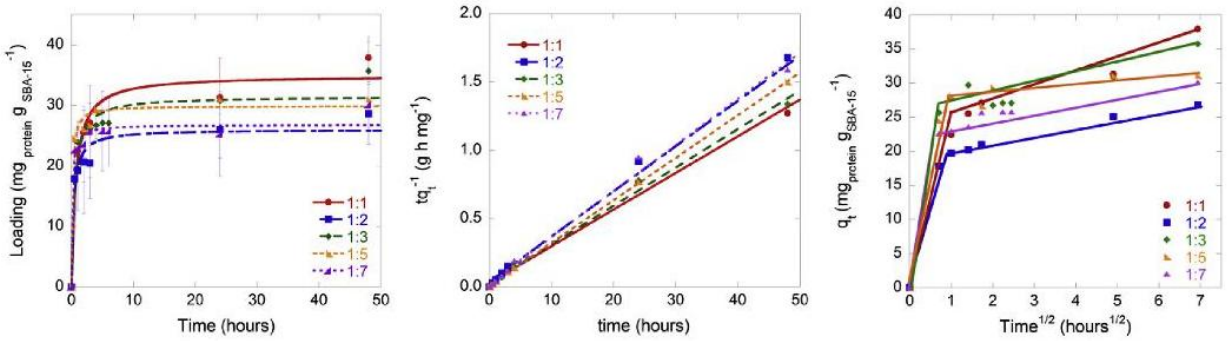


**Fig. 2.** Co-immobilization kinetics of GOx and HRP on SBA-15 mesoporous silica. A) Decrease of protein concentration in the immobilizing solution; B) increase of protein loading (mg of protein per g of SBA-15) for different GOx:HRP mass ratios; C) fitting of kinetic data with a pseudo-second order model (eq. (3)); D) fitting of kinetic data with an intraparticle diffusion model (eq. (4)).

a different enzyme mass ratio should result in a different instantaneous concentration of $H_2O_2$ available for ABTS oxidation. As shown in the next paragraph, this can either favor or disfavor the biocatalyst's performance.

Fig. 2 shows the effect of different GOx:HRP mass ratios on the adsorption kinetics. In particular Fig. 2A displays the increase of enzyme loading as a function of time. The protein concentration sharply decreased at initial times (t < 10 h), then reached the equilibrium after about 24 h. Longer times gave only a small loading increase (Fig. 2A). Among the used kinetic models - that is, the pseudo-second order (eq. (3); Fig. 2B) and the intraparticle diffusion model (eq. (4); Fig. 2C) - the latter is of particular interest since it can provide useful information about the mechanism of the adsorption process. In general, enzyme immobilization occurs through a multi-step mechanism. The plot of the intraparticle diffusion model reports $q_t$ (protein loading at time t) in the y axis versus $t^{1/2}$ in the x axis. Generally the data can be fitted through 2 or 3 straight lines having different slopes. Each slope is associated to one of the steps of the immobilization mechanism. The data shown in Fig. 2C are indeed consistent with a two step process. Table 2 lists the values of protein loading at equilibrium ($q_e$) obtained for the immobilization experiments. The $q_e$ values, expressed as $mg_{protein} \times g^{-1}_{SBA\text{-}15}$, range between 30 and 40 mg $g^{-1}$ for most GOx:HRP mass ratios. The loading values obtained through fitting procedures (using eq.s (2) and (3)), were consistent with those obtained by subtracting the protein amount at the times t = 0 h and t = 48 h (eq. (1)).

### 3.3. Catalytic activity of the immobilized biocatalyst

#### 3.3.1. Co-immobilized GOx/HRP@SBA-15

The different co-immobilized enzyme (dried) samples having different GOx:HRP ratios (2:1; 1:1; 1:2; and 1:3) were checked for enzymatic activity. Results in Fig. 3 show that for GOx/HRP@SBA-15 biocatalyst, the ratio GOx:HRP = 1:1 has the highest activity among those tested. Nevertheless, we noticed that the measured activity was very low if compared to that of the free enzymes, which was 26.1 $\mu mol_{ABTS} \times min^{-1}$ for the mass ratio GOx:HRP = 1:1 (data not shown). An activity loss due to the immobilization process is not a strange result since already observed in previous works [12]. Nevertheless, in order to understand the possible causes of such a low activity some qualitative experiments were carried out. The addition of suitable volumes of aqueous free GOx and free HRP solutions to two different test tubes containing the immobilized biocatalyst suspended in the substrate (glucose and ABTS) solution gave very interesting qualitative results. Indeed, the test tube containing the free GOx and the co-immobilized biocatalyst was inactive, whereas that containing the free HRP and the co-immobilized biocatalyst was highly active. This observation suggests that the immobilized HRP is inactive, whereas the immobilized GOx is still active.

3.3.2 Comparison between the separately immobilized GOx@SBA-15/HRP@SBA-15 and coimmobilized GOx/HRP@SBA-15 biocatalysts.

In order to try to increase the low biocatalyst activity we tried different immobilization strategies and compared the corresponding catalytic activities. More in detail, the covalent immobilization of GOx and HRP on SBA-15 was carried out separately to obtain GOx@SBA-15 and HRP@SBA-15 biocatalysts. In this experiment the immobilized biocatalysts were both dried under vacuum,

**Table 2**
Protein loading at equilibrium, $q_e$, obtained by different kinetic models forGOx:HRP enzymatic solutions at different mass ratios.

| GOx:HRP mass ratio | [a]$q_e$ (mg/g) | [b]$q_e$ (mg/g) | [c]$q_e$ (mg/g) |
|---|---|---|---|
| 2:1 | 24 ± 5 | – | – |
| 1:1 | 38 ± 3 | 34 ± 2 | 37 ± 2 |
| 1:2 | 30 ± 5 | 25 ± 2 | 30 ± 1 |
| 1:3 | 40 ± 4 | 30 ± 2 | 35 ± 1 |
| 1:5 | 31 ± 2 | 30 ± 1 | 31 ± 0 |
| 1:7 | 30 ± 4 | 27 ± 1 | 30 ± 1 |

[a] Protein loading at equilibrium calculated through eq. (1).
[b] Protein loading at equilibrium calculated through eq. (2) (Fig. 2B).
[c] Protein loading at equilibrium calculated through eq. (3) (Fig. 2C).

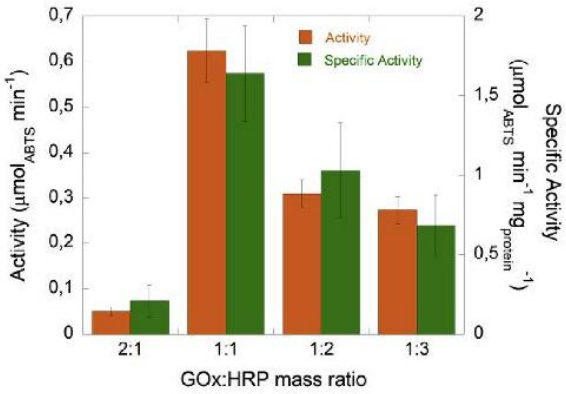


**Fig. 3.** Enzymatic activity of HRP/GOx@SBA-15 dried biocatalyst at four different GOx:HRP mass ratios.

**Table 3**
Loading and specific activity of the coimmobilized (GOx/HRP@SBA-15) or separately immobilized (GOx@SBA-15/HRP@SBA-15) biocatalysts.

| Sample | Loading[a] (mg $g^{-1}$) | Dry/wet | Specific activity (μmol $min^{-1}$ $mg^{-1}$) |
|---|---|---|---|
| GOx/HRP@SBA-15 | 38 ± 3 | Dry | 1.6 ± 0.3 |
| GOx/HRP@SBA-15 | 38 ± 3 | Wet | 116 ± 27 |
| GOx@SBA-15/HRP@SBA-15 | 27±1[b] | Dry/dry | 0.4 ± 0.1 |
| GOx@SBA-15/HRP@SBA-15 | 5±1[b,c] | Dry/dry | 0.20 ± 0.06 |
| GOx@SBA-15/HRP@SBA-15 | 21 ± 4[b,d] | Dry/dry | 1.2 ± 0.6 |
| GOx@SBA-15/HRP@SBA-15 | 21 ± 4[b,d] | Dry/wet | 18 ± 8 |

[a] Protein loading calculated by means of eq. (1).
[b] Loading of HRP on SBA-15. GOx loading on SBA-15 is 35 ± 2 mg $g^{-1}$.
[c] HRP was immobilized by physical adsorption at pH = 5.
[d] HRP was immobilized by physical adsorption at pH = 8.

and then mixed together after the immobilization. The activity was measured by adding a solution containing the mixture of glucose and ABTS substrates. Also for the separately immobilized enzymes, GOx@SBA-15/HRP@SBA-15 (Table 3), the specific activity was 0.4 ± 0.1 μmol $min^{-1}$ $mg^{-1}$ that is even lower than that measured for the co-immobilized biocatalyst GOx/HRP@SBA-15 (1.6 ± 0.3 μmol $min^{-1}$ $mg^{-1}$, Table 3). From previous and present results we found that the loss of activity is mainly imputable to the immobilized HRP. Indeed, HRP seems to be more sensitive to the covalent immobilization process than GOx which keeps its activity at a higher extent after immobilization both in the singly and in the co-immobilized biocatalysts. Although the covalent immobilization generally results in a more stable biocatalyst, it can result into the distortion of the enzyme structure which may lead to a partial or full inactivation. Then, in order to determine if the covalent binding to SBA-15 was critical for HRP, its physical adsorption at two different pH values (5 and 8) was carried out. Although the loading of HRP can be modulated by a change of pH in the physical immobilization process, the activity is again very low and comparable to that of the covalent immobilized GOx@SBA-15/HRP@SBA-15 biocatalyst (Table 3). Hence, the use of the separately immobilized bienzymatic biocatalyst does not give any advantage in terms of activity, regardless HRP is covalently or physically immobilized. The results above have demonstrated that the activity of the bienzymatic biocatalyst does not depend on the fact that the enzymes are co-immobilized or singly immobilized on SBA-15 mesoporous silica. Moreover, not even the type of immobilization (covalent versus physical) is responsible for the low activity of the biocatalyst.

#### 3.3.2. Activity of dry versus wet biocatalyst

Another possible reason for the low biocatalyst activity might be due to the water content of the immobilized preparation. For free enzymes it is well known that enzymes are better stored in solid rather than in liquid form [46]. In order to obtain a solid preparation, water needs to be removed for example through freeze-drying. This and similar processes are seen to result in a partial or total loss of enzyme activity which can be limited by the addition of stabilizers (i.e. carbohydrates) [46]. For immobilized enzymes, it is a common procedure to dry, usually under vacuum at room temperature, the obtained wet biocatalyst. This because a dried preparation can be weighed, manipulated, and stored more easily than a wet one. Similarly, to the case of free enzymes, it may happen that the drying process can result in the partial or full enzyme inactivation. In the literature there are contrasting information about this issue for GOx and HRP enzymes. Dai et al. prepared a modified glassy carbon electrode by dropping upon it a GOx-HRP/SBA-15 suspension. This modified electrode was used after drying for 3h in ambient conditions [34]. Yang et al. instead stored the immobilized bienzymatic system suspended in suitable buffer solutions [47]. Similarly [48], stored the enzymes in aqueous solution at pH 7 and 4 °C. Cao et al. stored the biocatalyst at 4 °C without specifying if it had been dried or not [35]. Hence, it is of fundamental importance to understand if the drying process is critical for the activity of GOx and HRP. For these reasons we measured the activity of the bienzymatic biocatalyst where GOx@SBA-15 was, as usual, dried under vacuum while HRP@SBA-15 was kept wet. The specific activity of the singly immobilized GOx@SBA-15/HRP@SBA-15 bienzymatic biocatalyst was 18 ± 8 μmol $min^{-1}$ $mg^{-1}$, that is about one order of magnitude higher than the bienzymatic biocatalyst where HRP@SBA-15 was dried (Table 3). Even more interesting is the fact that the activity of the wet co-immobilized biocatalyst was about two order of magnitude higher (116 ± 27 μmol $min^{-1}$ $mg^{-1}$) than that of the same type of dried biocatalyst. This means that although GOx is less sensitive to drying than HRP it has, anyway, a substantial benefit to remain hydrated instead of being dried.

### 3.4. Stability of the immobilized bienzymatic biocatalyst

#### 3.4.1. Thermal and storage stability

Once ascertained that the immobilized bienzymatic biocatalyst is active only if kept wet, it is important to check its thermal, storage and operational stability. Fig. 4A shows the specific activity of the immobilized GOx/HRP@SBA-15 biocatalyst after 1 h incubation at different temperatures in the range 25 °C–50 °C. The immobilized biocatalyst has a slight increase in activity at 30 °C, but already at 35 °C we observe a sudden activity decrease. Finally, the incubation at 50 °C results in a quasi full inactivation of the immobilized biocatalyst. Fig. 4B, instead shows, the storage stability of the immobilized biocatalyst. GOx/HRP@SBA-15 was stored for 10 days at 4 °C. The effect of storage was to decrease the specific activity of the immobilized bienzymatic biocatalyst from the initial value of 116 ± 27 μmol $min^{-1}$ $mg^{-1}$ to about 45 ± 9 μmol $min^{-1}$ $mg^{-1}$. Previous findings suggest that this low thermal and storage stability of the bienzymatic biocatalyst is likely imputable to HRP [49] rather than the more robust GOx enzyme.

#### 3.4.2. Operational stability: biocatalyst recycling

One of the main goals of immobilized enzymes is the possibility of their reuse. This because enzymes are generally very expensive respect to traditional chemical catalysts. Besides their high cost, enzymes are also highly unstable in their native, and active, conformation. For these reasons, enzyme immobilization permits to recover the biocatalyst particles (i.e. by filtration or centrifugation), and also to stabilize the enzyme in its active conformation. In addition, here we have seen that the hydration of the immobilized biocatalyst plays an important role to determine the activity. Fig. 5 displays the reuse of the immobilized biocatalyst for different reaction cycles. In particular, we compared the dry singly immobilized bienzymatic biocatalyst GOx@SBA-15/HRP@SBA-15 (dry/dry) with that where the immobilized HRP was kept wet (dry/wet), and

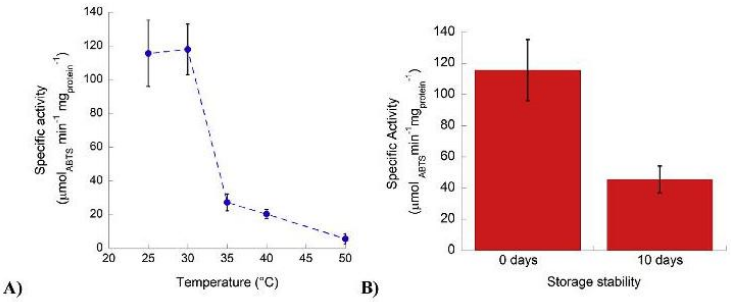


**Fig. 4.** Biocatalyst stability: A) thermal stability. B) storage stability.

the wet co-immobilized GOx/HRP@SBA-15 biocatalyst. The dry separately immobilized biocatalyst had a very low specific activity and became fully inactive at the 7th reaction cycle. The separately immobilized biocatalyst, where HRP@SBA-15 was kept wet, had a higher activity that was lost after the 6th reaction cycle. Finally the wet co-immobilized biocatalyst was very active and could be reused several times, keeping a specific activity of about 60 μmol $min^{-1}$ $mg^{-1}$ at the 14th reaction cycle. Hence, although the bienzymatic biocatalyst was not very stable to the thermal treatment and storage, its possible reuse for more than 14 reaction cycles is a remarkable result.

### 3.5. Enzymatic oxidation of recalcitrant phenolic compounds

A possible application of a bienzymatic biocatalyst could be the oxidation of water pollutants. For example [29] reported the oxidation of polycyclic aromatic hydrocarbons through an immobilized GOx/Hb (Hemoglobin) bienzymatic biocatalyst. Here, in order to test a potential application of the bienzymatic biocatalyst, we investigated the enzymatic oxidation of two phenolic

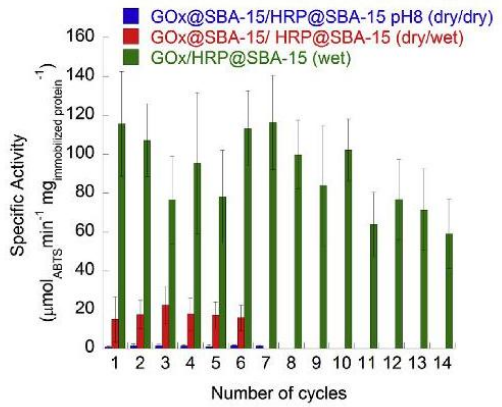


**Fig. 5.** Biocatalyst recycling performance. Blue columns refer to the separately immobilized GOx@SBA-15/HRP@SBA-15 dry biocatalyst (GOx was covalently immobilized on SBA-15; HRP was physically immobilized at pH 8 on SBA-15); red columns refer to the same separately immobilized biocatalyst but where GOx@SBA-15 was dried, whereas HRP@SBA-15 was kept wet; green columns refer to the activity of the covalent co-immobilized GOx/HRP@SBA-15 which was kept wet. (For interpretation of the references to colour in this figure legend, the reader is referred to the web version of this article.)

compounds contained in OMWs. OMWs have a complicated composition in phenolic compounds, carbohydrates, organic acids and minerals [37]. Although OMWs are rich in nutrients, their release in the environment is not possible due to the phytotoxic action of phenolic compounds. Hence, a way to overcome this problem is to firstly oxidize phenolic compounds contained in OMWs. A similar problem occurs in those geographical areas, i.e. Brasil, where coffee is produced. Torres et al. studied the enzymatic oxidation of caffeic acid, a recalcitrant phenolic pollutant, contained in wastewaters of coffee production [36]. They compared the action of peroxidases of different sources by adding different amounts of $H_2O_2$. As explained above a locally produced $H_2O_2$ is a key issue for "suicide" enzymes as peroxidases [30]. For this reason the sequential action of GOx and HRP in an immobilized bienzymatic biocatalyst seems to be a good option. Moreover, OMWs already contain carbohydrates and glucose in particular (from 4.8% to 13.4%) [37], thus there is no need to add external $H_2O_2$ as HRP substrate.

As a proof of concept of the possibility to use the bienzymatic biocatalyst for the degradation of phenolic compounds contained in OMWs we prepared two solutions containing glucose and either ferulic acid (FAc) or caffeic acid (CAc). The disappearance of the phenolic compounds was investigated spectrophotometrically at the wavelength of 286 nm (FAc) and 310 nm (CAc). Fig. 6A shows the decrease of ferulic and caffeic acid concentration due to the action of the immobilized bienzymatic biocatalyst. Fig. 6B shows that the two phenolic compounds reached a conversion of about 70% within 15 min. This result is better than what obtained by Torres et al. that at maximum reached 51% conversion of caffeic acid within 15 min [36] by means of peroxidase and external addition of $H_2O_2$. Thus, although the reaction did not reach completeness, it is nevertheless fast. Hence, the GOx/HRP@SBA-15 bienzymatic biocatalyst has a potential interest for environmental applications.

## 4. Conclusions

The present work investigated the realization of a bienzymatic biocatalyst constituted by GOx and HRP immobilized onto SBA-15 ordered mesoporous silica. Some important points about the activity of the obtained biocatalyst should be remarked. The activity of the bienzymatic biocatalyst does not depend on the fact that the system is constituted by a mixture of two singly immobilized enzymes, GOx@SBA-15/HRP@SBA-15, or by co-immobilized enzymes GOx/HRP@SBA-15. In fact, it is rather the drying process that constitutes the most critical issue. Indeed, although from one hand the drying permits an easy handling of the biocatalyst, on the other hand, it leads to the loss of most the enzymatic activity. In particular, the drying process inactivates HRP at a higher extent than GOx. We

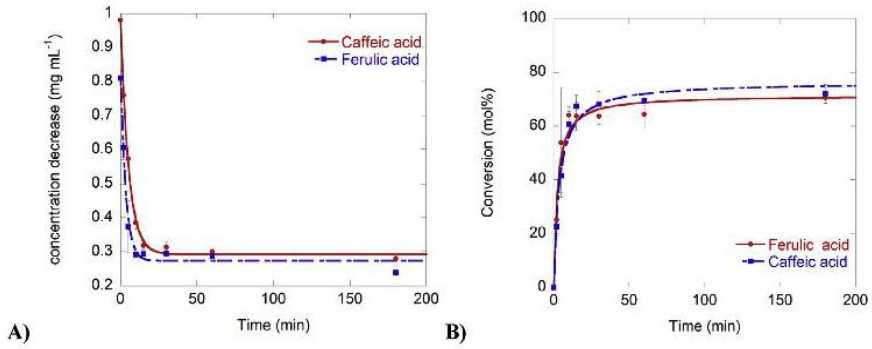


**Fig. 6.** Biocatalytic (wet GOx/HRP@SBA-15) oxidation of the recalcitrant phenolic compounds ferulic acid and caffeic acid. A) Concentration decrease and B) conversion of ferulic acid and caffeic acid as a function of reaction time.

also found that HRP is active when kept wet. This independently HRP is covalently or physically immobilized on SBA-15. The wet bienzymatic co-immobilized biocatalyst retained its activity for 14 reaction cycles. Finally, a possible application of the biocatalyst for bioremediation of OMWs was proposed. OMWs are highly pollutant by-product of olive oil production mainly based in the Mediterranean region. The phytotoxic nature of OMWs is due to the presence of recalcitrant phenolic compounds. But in the complex composition of OMWs also glucose occurs [37]. This suggested us the use of a GOx/HRP bienzymatic biocatalyst for the oxidation of phenolic compounds contained in OMWs. Hence, we modelled the biocatalytic treatment of OMWs by using a solution containing glucose and a phenolic compound, i.e. either caffeic or ferulic acid. The hydrogen peroxide produced by GOx-catalyzed glucose oxidation was used by HRP to oxidize ferulic acid and caffeic acid. The immobilized bienzymatic biocatalyst GOx/HRP@SBA-15 allowed to reach a conversion of about 70 mol% of the two phenolic compounds within only 15 min. To the best of our knowledge the use of a GOx/HRP bienzymatic system for the treatment of OMWs has not been proposed yet. These encouraging results require, nonetheless, a deeper investigation using more complex phenolic solutions and, ultimately, a test with a real OMWs sample.

## Acknowledgements

CSGI and CNBS are thanked for financial support. F.P. thanks Agenzia delle Dogane e dei Monopoli for financing her PhD scholarship. Prof. E. Sanjust is thanked for useful discussion and valuable advices.

## References

[1] B. Lebeau, A. Galarneau, M. Linden, Introduction for 20 years of research on ordered mesoporous materials, Chem. Soc. Rev. 42 (2013) 3661–3662, http://dx.doi.org/10.1039/c3cs90005c.
[2] V. Mamaeva, C. Sahlgren, M. Lindén, Mesoporous silica nanoparticles in medicine-recent advances, Adv. Drug Deliv. Rev. 65 (2013) 689–702, http://dx.doi.org/10.1016/j.addr.2012.07.018.
[3] M. Monduzzi, S. Lampis, S. Murgia, A. Salis, From self-assembly fundamental knowledge to nanomedicine developments, Adv. Colloid Interface Sci. 205 (2014) 48–67, http://dx.doi.org/10.1016/j.cis.2013.10.009.
[4] Z.X. Wu, D.Y. Zhao, Ordered mesoporous materials as adsorbents, Chem. Commun. 47 (2011) 3332–3338, http://dx.doi.org/10.1039/C0cc04909c.
[5] E.M. Usai, M.F. Sini, D. Meloni, V. Solinas, A. Salis, Sulfonic acid-functionalized mesoporous silicas: microcalorimetric characterization and catalytic performance toward biodiesel synthesis, Microporous Mesoporous Mater 179 (2013) 54–62, http://dx.doi.org/10.1016/j.micromeso.2013.05.008.
[6] J.M. Bolivar, I. Eisl, B. Nidetzky, Advanced characterization of immobilized enzymes as heterogeneous biocatalysts, Catal. Today 259 (2015) 66–80, http://dx.doi.org/10.1016/j.cattod.2015.05.004.
[7] M. Hartmann, X. Kostrov, Immobilization of enzymes on porous silicas–benefits and challenges, Chem. Soc. Rev. 42 (2013) 6277–6289, http://dx.doi.org/10.1039/c3cs60021a.
[8] N. Carlsson, H. Gustafsson, C. Thörn, L. Olsson, K. Holmberg, B. Åkerman, Enzymes immobilized in mesoporous silica: a physical–chemical perspective, Adv. Colloid Interface Sci. 205 (2014) 339–360, http://dx.doi.org/10.1016/j.cis.2013.08.010.
[9] E. Magner, Immobilisation of enzymes on mesoporous silicate materials, Chem. Soc. Rev. 42 (2013) 6213–6222, http://dx.doi.org/10.1039/c2cs35450k.
[10] Y.J. Han, J.T. Watson, G.D. Stucky, A. Butler, Catalytic activity of mesoporous silicate-immobilized chloroperoxidase, J. Mol. Catal. - B Enzym 17 (2002) 1–8, http://dx.doi.org/10.1016/S1381-1177(01)00072-8.
[11] H. Gustafsson, E.M. Johansson, A. Barrabino, M. Odén, K. Holmberg, Immobilization of lipase from Mucor miehei and Rhizopus oryzae into mesoporous silica - the effect of varied particle size and morphology, Colloids Surf, B. Biointerfaces 100 (2012) 22–30, http://dx.doi.org/10.1016/j.colsurfb.2012.04.042.
[12] A. Salis, D. Meloni, S. Ligas, M.F. Casula, M. Monduzzi, V. Solinas, et al., Physical and chemical adsorption of Mucor javanicus lipase on SBA-15 mesoporous silica. Synthesis, structural characterization, and activity performance, Langmuir 21 (2005) 5511–5516, http://dx.doi.org/10.1021/la047225y.
[13] S. Hudson, E. Magner, J. Cooney, B.K. Hodnett, Methodology for the immobilization of enzymes onto mesoporous materials, J. Phys. Chem. B 109 (2005) 19496–19506.
[14] A. Vinu, V. Murugesan, M. Hartmann, Adsorption of lysozyme over mesoporous molecular sieves MCM-41 and SBA-15: influence of pH and aluminum incorporation, J. Phys. Chem. B 108 (2004) 7323–7330, http://dx.doi.org/10.1021/jp037303a.
[15] H. Essa, E. Magner, J. Cooney, B.K. Hodnett, Influence of pH and ionic strength on the adsorption, leaching and activity of myoglobin immobilized onto ordered mesoporous silicates, J. Mol. Catal. B Enzym 49 (2007) 61–68, http://dx.doi.org/10.1016/j.molcatb.2007.07.005.
[16] A. Salis, M. Pisano, M. Monduzzi, V. Solinas, E. Sanjust, Laccase from Pleurotus sajor-caju on functionalised SBA-15 mesoporous silica: immobilisation and use for the oxidation of phenolic compounds, J. Mol. Catal. B Enzym 58 (2009) 175–180, http://dx.doi.org/10.1016/j.molcatb.2008.12.008.
[17] K. Murai, T. Nonoyama, T. Saito, K. Kato, Enzyme structure and catalytic properties affected by the surface functional groups of mesoporous silica, Catal. Sci. Technol. 2 (2012) 310–315, http://dx.doi.org/10.1039/c1cy00258a.
[18] Z. Zhou, M. Hartmann, Progress in enzyme immobilization in ordered mesoporous materials and related applications, Chem. Soc. Rev. 42 (2013) 3894–3912, http://dx.doi.org/10.1039/c3cs60059a.
[19] A. Salis, L. Medda, F. Cugia, M. Monduzzi, Effect of electrolytes on proteins physisorption on ordered mesoporous silica materials, Colloids Surf. B. Biointerfaces 137 (2016) 77–90, http://dx.doi.org/10.1016/j.colsurfb.2015.04.068.
[20] A. Salis, M.F. Casula, M.S. Bhattacharyya, M. Pinna, V. Solinas, M. Monduzzi, Physical and chemical lipase adsorption on SBA-15: effect of different interactions on enzyme loading and catalytic performance, ChemCatChem 2 (2010) 322–329, http://dx.doi.org/10.1002/cctc.200900288.
[21] F. Jia, B. Narasimhan, S. Mallapragada, Materials-based strategies for multi-enzyme immobilization and co-localization: a review, Biotechnol. Bioeng. 111 (2014) 209–222, http://dx.doi.org/10.1002/bit.25136.
[22] D. Jung, C. Streb, M. Hartmann, Oxidation of indole using chloroperoxidase and glucose oxidase immobilized on SBA-15 as tandem biocatalyst, Microporous Mesoporous Mater 113 (2008) 523–529, http://dx.doi.org/10.1016/j.micromeso.2007.12.009.
[23] H.J. Hecht, D. Schomburg, H. Kalisz, R.D. Schmid, The 3D structure of glucose oxidase from Aspergillus Niger. Implications for the use of GOD as a biosensor enzyme, Biosens. Bioelectron. 8 (1993) 197–203, http://dx.doi.org/10.1016/0956-5663(93)85033-K.

[24] N.C. Veitch, Horseradish peroxidase: a modern view of a classic enzyme, Phytochemistry 65 (2004) 249–259, http://dx.doi.org/10.1016/j.phytochem.2003.10.022.
[25] X. Yu, W. Lian, J. Zhang, H. Liu, Multi-input and -output logic circuits based on bioelectrocatalysis with horseradish peroxidase and glucose oxidase immobilized in multi-responsive copolymer films on electrodes, Biosens. Bioelectron. 80 (2016) 631–639, http://dx.doi.org/10.1016/j.bios.2016.02.010.
[26] M. Mathew, N. Sandhyarani, Detection of glucose using immobilized bienzyme on cyclic bisureas-gold nanoparticle conjugate, Anal. Biochem. 459 (2014) 31–38, http://dx.doi.org/10.1016/j.ab.2014.05.003.
[27] Q. Wei, M. Xu, C. Liao, Q. Wu, M. Liu, Y. Zhang, et al., Printable hybrid hydrogel by dual enzymatic polymerization with superactivity, Chem. Sci. 7 (2016) 2748–2752, http://dx.doi.org/10.1039/C5SC02234G.
[28] A. Ramanavicius, A. Kausaite-Minkstimiene, I. Morkvenaite-Vilkonciene, P. Genys, R. Mikhailova, T. Semashko, et al., Biofuel cell based on glucose oxidase from Penicillium funiculosum 46.1 and horseradish peroxidase, Chem. Eng. J. 264 (2015) 165–173, http://dx.doi.org/10.1016/j.cej.2014.11.011.
[29] L.T. Phuoc, P. Laveille, F. Chamouleau, G. Renard, J. Drone, B. Coq, et al., Bridging the gap in catalysis via multidisciplinary approaches Guest, Dalt. Trans. 39 (2010) 8511–8520, http://dx.doi.org/10.1039/C001146K.
[30] J. Rocha-Martin, S. Velasco-Lozano, J.M. Guisán, F. López-Gallego, Oxidation of phenolic compounds catalyzed by immobilized multi-enzyme systems with integrated hydrogen peroxide production, Green Chem. 16 (2014) 303, http://dx.doi.org/10.1039/c3gc41456f.
[31] K.J. Baynton, J.K. Bewtra, N. Biswas, K.E. Taylor, Inactivation of horseradish peroxidase by phenol and hydrogen peroxide: a kinetic investigation, Biochim. Biophys, Acta - Protein Struct. Mol. Enzymol. 1206 (1994) 272–278, http://dx.doi.org/10.1016/0167-4838(94)90218-6.
[32] J.A. Nice, H. Wright, A model of peroxidase activity with inhibition by hydrogen peroxide, Enzyme Microb. Technol. 229 (1997) 302–310.
[33] K. Chattopadhyay, S. Mazumdar, Structural and conformational stability of horseradish peroxidase: effect of temperature and pH, Biochemistry 39 (2000) 263–270, http://dx.doi.org/10.1021/bi990729o.
[34] Z. Dai, J. Bao, X. Yang, H. Ju, A bienzyme channeling glucose sensor with a wide concentration range based on co-entrapment of enzymes in SBA-15 mesopores, Biosens. Bioelectron. 23 (2008) 1070–1076, http://dx.doi.org/10.1016/j.bios.2007.10.015.
[35] X. Cao, Y. Li, Z. Zhang, J. Yu, J. Qian, S. Liu, Catalytic activity and stability of glucose oxidase/horseradish peroxidase co-confined in macroporous silica foam, Analyst 137 (2012) 5785–5791, http://dx.doi.org/10.1039/c2an36237f.
[36] J.A. Torres, P.M.B. Chagas, M.C. Silva, C.D. Dos Santos, A.D. Corrêa, Enzymatic oxidation of phenolic compounds in coffee processing wastewater, Water Sci. Technol. 73 (2016) 39–50, http://dx.doi.org/10.2166/wst.2015.332.
[37] S. Dermeche, M. Nadour, C. Larroche, F. Moulti-Mati, P. Michaud, Olive mill wastes: biochemical characterizations and valorization strategies, Process Biochem. 48 (2013) 1532–1552, http://dx.doi.org/10.1016/j.procbio.2013.07.010.
[38] D. Steri, M. Monduzzi, A. Salis, Ionic strength affects lysozyme adsorption and release from SBA-15 mesoporous silica, Microporous Mesoporous Mater 170 (2013) 164–172, http://dx.doi.org/10.1016/j.micromeso.2012.12.002.
[39] T.P.B. Nguyen, J.W. Lee, W.G. Shim, H. Moon, Synthesis of functionalized SBA-15 with ordered large pore size and its adsorption properties of BSA, Microporous Mesoporous Mater 110 (2008) 560–569, http://dx.doi.org/10.1016/j.micromeso.2007.06.054.
[40] Y. Lee, J. Yoon, U. Von Gunten, Spectrophotometric determination of ferrate (Fe(VI)) in water by ABTS, Water Res. 39 (2005) 1946–1953, http://dx.doi.org/10.1016/j.watres.2005.03.005.
[41] S. Scott, W. Chen, A. Bakac, J.H. Espenson, Spectroscopic parameters, electrode potential, acid ionization constants, and alectron exchange rates of the ABTS radicals and ions, J. Phys. Chem. 97 (1993) 6710–6714, http://dx.doi.org/10.1021/j100127a022.
[42] M. Vallet-Regí, F. Balas, M. Colilla, M. Manzano, Bone-regenerative bioceramic implants with drug and protein controlled delivery capability, Prog. Solid State Chem. 36 (2008) 163–191, http://dx.doi.org/10.1016/j.progsolidstchem.2007.10.002.
[43] M. Piludu, L. Medda, F. Cugia, M. Monduzzi, A. Salis, Silver enhancement for transmission electron microscopy imaging of antibody fragment–gold nanoparticles conjugates immobilized on ordered mesoporous silica, Langmuir 31 (2015) 9458–9463, http://dx.doi.org/10.1021/acs.langmuir.5b02830.
[44] F. Cugia, S. Sedda, F. Pitzalis, D.F. Parsons, M. Monduzzi, A. Salis, Are specific buffer effects the new frontier of Hofmeister phenomena? Insights Lysozyme Adsorpt. Ordered Mesoporous Silica 6 (2016) 94617–94621, http://dx.doi.org/10.1039/C6RA17356J.
[45] A. Salis, M.S. Bhattacharyya, M. Monduzzi, Specific ion effects on adsorption of lysozyme on functionalized SBA-15 mesoporous silica, J. Phys. Chem. B 114 (2010) 7996–8001, http://dx.doi.org/10.1021/jp102427h.
[46] D.A. Aniket, D.L. Gaul, J.T. Bitterfield, V.M. Su, I. Li, Singh, et al., Enzyme dehydration using microglassification preserves the Protein's structure and function, J. Pharm. Sci. 104 (2015) 640–651, http://dx.doi.org/10.1002/jps.24279.
[47] H. Yang, W. Wei, S. Liu, Monodispersed silica nanoparticles as carrier for co-immobilization of bi-enzyme and its application for glucose biosensing, Spectrochim. Acta - Part A Mol. Biomol. Spectrosc. 125 (2014) 183–188, http://dx.doi.org/10.1016/j.saa.2014.01.004.
[48] H. Gustafsson, A. Küchler, K. Holmberg, P. Walde, Co-immobilization of enzymes with the help of a dendronized polymer and mesoporous silica nanoparticles, J. Mater. Chem. B 3 (2015) 6174–6184, http://dx.doi.org/10.1039/C5TB00543D.
[49] W. Chouyyok, J. Panpranot, C. Thanachayanant, S. Prichanont, Effects of pH and pore characters of mesoporous silicas on horseradish peroxidase immobilization, J. Mol. Catal. B Enzym 56 (2009) 246–252, http://dx.doi.org/10.1016/j.molcatb.2008.05.009.

# Accepted article

**Pitzalis, F**.; Carucci,C., Naseri, M., Magner,E., Fotohui, L., Salis A. *"Lipases encapsulation onto ZIF-8. A comparison of biocatalysts obtained at low and high zinc:2methyl-imidazole mole ratio in aqueous medium"* ChemCatChem (2018) In Press
**DOI:** 10.1002/cctc.201701984

http://onlinelibrary.wiley.com/doi/10.1002/cctc.201701984/full

FULL PAPER WILEY-VCH

# Lipases encapsulation onto ZIF-8. A comparison between biocatalysts obtained at low and high zinc:2-methylimidazole molar ratio in aqueous medium

Federica Pitzalis[†][a],Cristina Carucci[†][b], Maryam Naseri[a,c], Lida Fotouhi[c], Edmond Magner*[b], Andrea Salis*[a]

**Abstract:** Lipase AK from *Pseudomonas fluorescens*, and Lipase RM from *Rhizomucor miehei* were encapsulated into a zeolite imidazolate framework (ZIF-8) via "one-pot" synthesis to obtain AK@ZIF-8 and RM@ZIF-8 biocatalysts. The effect of a high (1:40) and low (1:4) Zn:2-methylimidazole molar ratio on the biocatalysts synthesis was investigated. The different Zn:L ratios affected both the surface area, the loading and the specific activity of the biocatalysts. Samples synthesised using high Zn:L ratio had high values of surface area whereas those obtained using low Zn:L ratio had higher loadings and specific activities. The decrease of pH (from 11.6 to 9.4) during the synthesis at high Zn:L ratio produced ZIF-8 samples with features similar to those observed for low Zn:L ratio samples. The low Zn:L (1:4) ratio AK@ZIF-8 biocatalyst retained 99% activity after storage for 15 days at 5°C and 40% activity after 5 reaction cycles.

## 1. Introduction

Enzymes are generally active under mild conditions, i.e. room temperature and atmospheric pressure,[1] conditions that enable the development of environmentally friendly 'green' industrial processes. However, in contrast to conventional chemical catalysts, enzymes are expensive and unstable in e.g. non aqueous solutions and at extremes of pH. Immobilisation can overcome these disadvantages.[2] When an enzyme is immobilised on a solid support it generally retains its catalytic activity, enhances its stability, and can be reused for several reaction cycles.[3, 4] In the past 15 years ordered mesoporous silicates have widely been used for enzyme immobilisation due to their textural and structural features.[5–9] More recently, metal organic frameworks (MOFs) have emerged as a possible new family of enzyme supports. MOFs, first synthesised by Yaghi et al.[10] consist of metal ions coordinated with organic ligands to form a porous 3D network. Zeolite imidazolate frameworks (ZIFs) are an important MOF subclass containing a zeolite-like crystalline structure where $Zn^{2+}$ (or $Co^{2+}$) ions are coordinated by imidazole derivatives forming a tetrahedral network.[11–15] Systematic change of the organic ligand or the metal ion results in a variety of 3D structures, similar to those of natural zeolites.[16] ZIFs can be prepared in several ways, i.e. by solvothermal,[15–17] mechano-chemical,[18] sonochemical,[19] microwave-assisted,[20] or hydrothermal[12] synthetic methods. Among these, water synthesis is facile, rapid, and low cost.[12] Moreover, this is a very suitable way to obtain enzyme@ZIF conjugates.[21–23] ZIF-8 is a metal organic framework where $Zn^{2+}$ ions are coordinated by 2-methylimidazole (2-MIM) to form rhombic dodecahedral structures.[15] These structures are often referred to as "SOD-like" due to their similarity to those of the natural zeolite "sodalite". Although water synthesis is predominantly used for the immobilisation of single enzymes[21–24] or to obtain bienzymatic systems,[25] some critical aspects of the mechanism of formation remain unknown. The mechanism of crystallization,[20] porosity,[12] and the surface area[26] of pure ZIFs prepared in aqueous media are strongly influenced by the molar ratio between $Zn^{2+}$ ions and the alkyl-imidazole ligand, as well as by the water content.[26] Moreover, the addition of the enzyme to the reaction mixture during crystal nucleation can affect the crystal shape and morphology[22,24] and, consequently, the activity of the obtained immobilised biocatalyst.[22,24]

Lipases (E.C. 3.1.1.3 triacylglycerol acylhydrolases) are one of the most widely used enzymes for biotechnological applications,[27–29] such as the production of biodiesel,[28,30,31] as well as in the food,[32] and pharmaceutical[33,34] industries. To the best of our knowledge, only a limited number of works investigating the catalytic performance of lipases immobilised on MOFs in general[34–36] and on ZIFs in particular, have been reported. Very recently, Gascòn et al. immobilised lipase B from *Candida antarctica* on Basolite F-300 like materials.[37] Cao et al. measured the catalytic activity of *Bacillus subtilis* lipase immobilised on Cu-BTC MOF.[35] He et al. immobilised a thermophilic lipase from *Alcaligenes sp.* on ZIF-8, through a mechanochemical synthetic method.[38] Cheong et al. immobilised *Burkholderia cepacia* lipase in amino-functionalised ZIF-8 through physical adsorption, and measured both the hydrolytic and transesterification activity.[39] Shi et al. immobilised the lipase from *Candida rugosa* on ZIF-8 synthesised via a solvothermal method using methanol as the solvent.[40] Liang et al. immobilised several enzymes on ZIF-8, including a lipase (origin not specified).[24] Lyu et al. reported the in-situ immobilisation of lipase from *Thermomyces lanuginosus* on ZIF-8, using methanol as solvent and polyvinylpyrrolidone as a protective coating for the enzymes.[41] Finally, Huo et al. prepared a hierarchical magnetic ZIF-8/UiO-66/$Fe_3O_4$ support for the encapsulation of *Candida antarctica* lipase B.[42]

In this work the 'one-pot' water synthesis of ZIF-8 and the encapsulation of lipases from *Pseudomonas fluorescens* (lipase

[a] F. Pitzalis[†], Prof, Andrea Salis*
Department of Chemical and Geological Sciences, University of Cagliari, Cittadella Universitaria, SS 554 bivio Sestu, 09042 Monserrato (CA) (Italy)
E-mail: asalis@unica.it
[b] C. Carucci[†], Prof. E. Magner*
Department of Chemical Sciences, Synthesis and Solid State Pharmaceutical Centre and Bernal Institute, University of Limerick, Limerick, V94 T9PX, Ireland
E-mail: edmond.magner@ul.ie
[c] M. Naseri, Prof. L. Fotouhi
Department of Chemistry, Alzahra University, Tehran, Iran
E-mail: lfotouhi@alzahra.ac.ir

[†]These authors contributed equally to this work, *corresponding authors.
Supporting information for this article is given via a link at the end of the document.

AK) and *Rhizomucor miehei* (lipase RM), to obtain AK@ZIF-8 and RM@ZIF-8 biocatalysts, is reported. These lipases are well characterized.[43–46] Lipase RM has a molecular mass of 32kDa, with an isoelectric point, pI, of 3.8.[47] Lipase AK has a molecular mass of 33kDa and a pI = 4.[48] These lipases are very promising enzymes due to their good activity toward triglyceride transesterification for biodiesel production.[47,49–51] While they have mainly been immobilized on polymers of silica supports, to the best of our knowledge, no data is available about the immobilization of AK and RM lipases on ZIF-8.Here, two stoichiometric ratios of $Zn^{2+}$ and the 2-MIM ligand (L) i.e. Zn:L=1:40 [25] and Zn:L=1:4 [24] were used in previous reports. The Zn:L ratio affects both the texture of ZIF-8 and the activity of the obtained lipase@ZIF-8 biocatalyst. A similar effect on ZIF-8 structure and catalytic activity was obtained by changing the pH at which the biocatalysts were prepared. Finally, the storage stability and the ability to recycle of the most active lipase@ZIF-8 biocatalysts were examined.

## 2. Results and Discussion

### 2.1 Characterisation of ZIF-8 and lipase@ZIF-8 samples

ZIF-8 and lipase@ZIF-8 samples were synthesised by using two different $Zn^{2+}$:2-MIM (Zn:L) molar ratios. Samples named ZIF-$8_{HR}$ and lipase@ZIF-$8_{HR}$ were obtained by using a high Zn:L (1:40)[25] molar ratio, whereas samples ZIF-$8_{LR}$ and lipase@ZIF-$8_{LR}$ were obtained by using a low Zn:L (1:4)[24] molar ratio. All samples were characterised using a range of techniques i.e. X-ray diffraction (XRD), porosimetry, scanning electron microscopy (SEM), Fourier transform infrared spectroscopy (FTIR) and thermogravimetric analysis (TGA).

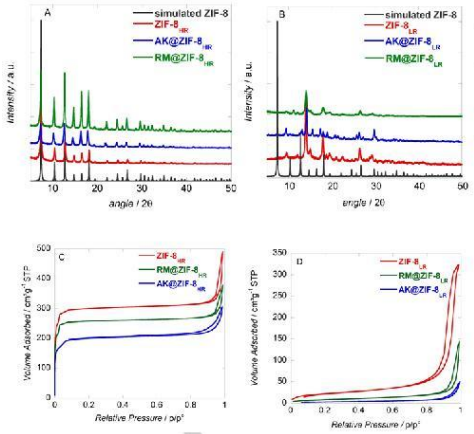


**Figure 1.** XRD patterns of ZIF-8 and lipase@ZIF-8 prepared using a Zn:L ratio of A) 1:40 and B) 1:4. $N_2$ adsorption and desorption isotherms of ZIF-8, AK@ZIF-8 and RM@ZIF-8 prepared using a Zn:L ratio of C) 1:40 and D) 1:4.

The XRD patterns of ZIF-$8_{HR}$ and lipase@ZIF-$8_{HR}$ (Figure 1A) are in good agreement with those of a ZIF-8 simulated pattern reported in the literature.[52,53] The diffractograms (Figure 1B) of ZIF-$8_{LR}$ and lipase@ZIF-$8_{LR}$ samples have different patterns. XRD patterns for ZIF-8 materials synthesised with various 2-MIM concentrations were previously observed in a variety of studies. Kida et al. observed the occurrence of a crystalline ZIF-8 SOD-like structure with high molar Zn:L ratios (1:40; 1:60; 1:80; 1:100), while, at lower ratios (Zn:L ratio 1:20) they observed the occurrence of mixed phases associated with the formation of $Zn(OH)_2$, $Zn(OH)NO_3$, and $Zn_5(OH)_8(NO_3)_2(H_2O)_2$.[26] Shi et al. synthesised a ZIF-8 sample (Zn:L ratio of 1:4) that had an XRD pattern which was assigned to an unknown mixed phase[54] while Liang et al. obtained a ZIF-8 sample with a typical SOD-like crystalline structure at a Zn:L ratio of 1:4.[24] The structure of ZIF-8 is affected by the presence of encapsulated protein. At a Zn:L ratio of 1:4 different–morphologies were observed for a wide range of proteins (i.e. nanoflowers for horseradish peroxidase, nanostars for trypsin etc.).[24] Similarly, Cui et al. observed a variety of XRD patterns and crystal morphologies for catalase@ZIF-8 samples obtained with Zn:L ratios in the range 1:1 - 1:20.[22] The concentration of protein concentration also affects the structure of ZIF-8. The peak intensity decreased with increasing concentration of BSA.[24] The XRD patterns of AK@ZIF-8 and RM@ZIF-8 samples showed different peak intensities (Figure 1A-B) suggesting an interaction between the enzyme molecules and the ZIF-8 material.[37,55] These findings demonstrate that the formation of pure ZIF-8 and lipase@ZIF-8 structures in aqueous solution is a complex process.

**Table 1.**Textural parameters obtained by the $N_2$ physisorption analysis of ZIF-8 and lipase@ZIF-8 samples

| Sample | Zn:L Ratio | $S_{BET}$ ($m^2g^{-1}$) | Pore volume ($cm^3g^{-1}$) |
|---|---|---|---|
| ZIF-$8_{HR}$ | 1:40 | 919 | n.a. |
| AK@ZIF-$8_{HR}$ | 1:40 | 615 | 39 |
| RM@ZIF-$8_{HR}$ | 1:40 | 790 | n.a. |
| ZIF-$8_{LR}$ | 1:4 | 79 | 0.50 |
| AK@ZIF-$8_{LR}$ | 1:4 | 4.4 | 0.049 |
| RM@ZIF-$8_{LR}$ | 1:4 | 30 | 0.22 |

Figures 1C-D show the textural characterisation of ZIF-8 and lipase@ZIF-8 samples performed by nitrogen physisorption. A ZIF-$8_{HR}$ sample displayed a typical type I isotherm associated with a microporous material (Figure 1 C) with a high surface area of 919 $m^2/g$ (Table 1).The small hysteresis present at $p/p_0 > 0.8$ may be due to the presence of mesopores in ZIF-$8_{HR}$ as well as in the lipase@ZIF-$8_{HR}$ samples. This was previously observed for other enzyme@ZIF-8.[22] The decrease in surface area for lipase@ZIF-8 (Table 1) is likely due to enzyme encapsulation into the ZIF-8 structure.[22,24,37,38] The $N_2$ adsorption/desorption isotherms obtained for the samples synthesised with the low Zn:L (1:4) ratio (Figure 1D), are significantly different. Low ratios of Zn:2-MIM ligand result in low surface areas (Table 1). This is consistent with the work of Kida et al. who investigated the textural parameters of ZIF-8 samples at different Zn:L ratios over the range 1:100 - 1:20.[26] They observed surface areas of over 1500 $m^2/g$ for SOD-type ZIF-8 at

high Zn:L ratios (from 1:40 to 1:100) and lower values of surface areas (from 1300 to 120 $m^2/g$) for the molar ratio 1:20.[26] Scanning electron microscopy (SEM) images of ZIF-8, AK@ZIF-8, and RM@ZIF-8 synthesised at a Zn:L=1:40 ratio and the corresponding samples synthesised at a Zn:L=1:4 ratio are shown in Figures S1A-C and Figure S1D-F (see Supporting Information file), respectively. Changes in particle size and morphology were observed in the presence and absence of enzyme. Figure 2 displays the FTIR spectra of the pure ZIF-8 and the lipase@ZIF-8 samples obtained at high (Figure 2A) and low (Figure 2B) Zn:L ratio. For ZIF-8, the C=N stretching mode shows a band at 1584 $cm^{-1}$. The band at 1420 $cm^{-1}$ is associated with a stretching mode of imidazole ring.[14] A strong band at 760 $cm^{-1}$ is due to out of plane bending of the imidazole aromatic ring, whereas the in-plane bending of the ring produces bands in the range 900 $cm^{-1}$ - 1350 $cm^{-1}$.[14] Finally, the characteristic band at 421 $cm^{-1}$ is associated with the Zn-N stretching mode.[14,56] For lipase@ZIF-8 samples the bands in the range 1644-1648 $cm^{-1}$, due to the C=O stretching of the amide I, confirm the successful encapsulation of lipase molecules in the ZIF-8.

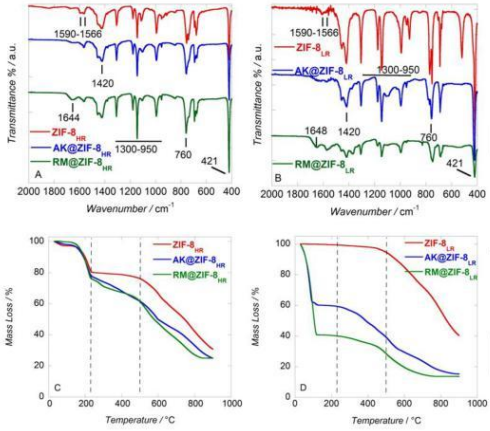


**Figure 2.** FTIR spectra of ZIF-8 and lipase@ZIF-8, A) high Zn:L (1:40) ratio; B) low Zn:L (1:4) ratio. TGA curves of ZIF-8 and lipase@ZIF-8 prepared by using the C) high Zn:L ratio, and D) low Zn:L ratio.

Thermogravimetric analysis (TGA) data show (Figure 2C-D) that ZIF-$8_{HR}$ and lipase@ZIF-$8_{HR}$ samples are stable up to 140°C. Both materials displayed a similar mass loss of ca. 20 % (see Table 2) in the temperature range140-230°C (Figure 2C), associated with the removal of water and unreacted reagents.[12] At higher temperatures, in the range 230°C - 500°C, a small mass loss was observed for pure ZIF-$8_{HR}$ (5.1 %), while lipase@ZIF-$8_{HR}$ biocomposites showed a gradual and continuous decomposition, with Δm of 17.0 % and 15.3 % for AK@ZIF-$8_{HR}$ and RM@ZIF-$8_{HR}$, respectively (Table 2). This mass loss is probably due to the decomposition of enzymes encapsulated in the ZIF-8 network.[25,38] At temperature greater than 500°C the mass loss is likely due to the decomposition of the ZIF-8 structure.[12] In the case of the samples synthesised at a low (1:4) ratio of Zn:L, the curves in Figure 2D follow different trends. ZIF-$8_{LR}$ sample has a small mass loss 4.7 % up to 500°C, similar to that of ZIF-$8_{HR}$. The steep mass loss above 500 °C is likely due to the thermal decomposition of the structure (Table 2). For the lipase@ZIF-$8_{LR}$ samples the initial mass loss (T < 130°C) is associated with the loss of water. Between 230-500°C, the decomposition of the enzymes occurs with mass losses of 7.3% and 11.4% for AK@ZIF-$8_{LR}$ and RM@ZIF-$8_{LR}$, respectively. The diversity in shape in Figures 2C and 2D are due to the different synthesis conditions.[22,26,37,57,58]

**Table 2.** Mass loss (Δm) of ZIF-8 and lipase@ZIF-8 samples at high (HR=1:40) and low (LR=1:4) Zn:L ratios.

| Sample | Δm (%) T<230°C | Δm (%) 230°C <T<500°C | Δm (%) T>500°C |
|---|---|---|---|
| ZIF-$8_{HR}$ | 18.8 | 5.1 | 76.1 |
| AK@ZIF-$8_{HR}$ | 21.5 | 17.0 | 61.6 |
| RM@ZIF-$8_{HR}$ | 23.3 | 15.3 | 36.6 |
| ZIF-$8_{LR}$ | 0.7 | 4.7 | 54.4 |
| AK@ZIF-$8_{LR}$ | 29.3 | 7.3 | 63.4 |
| RM@ZIF-$8_{LR}$ | 60.0 | 11.4 | 15.0 |

### 2.2 Loading and activity of AK@ZIF-8 and RM@ZIF-8 biocatalysts

Protein loading (Figure 3 A,B) and enzyme activity (Figure 3 C,D) of the lipase@ZIF-8 samples were quantified by the Bradford[59] and p-nitrophenyl butyrate assays,[60,61] respectively. Lipase@ZIF-8 samples obtained at a Zn:L ratio 1:4 had higher protein loadings than those obtained at a ratio of 1:40. The loadings were 138±13 mg/g (AK@ZIF-$8_{LR}$), 77±12 mg/g (RM@ZIF-$8_{LR}$), 40±10 mg/g (AK@ZIF-$8_{HR}$), and 12±6 mg/g (RM@ZIF-$8_{HR}$).

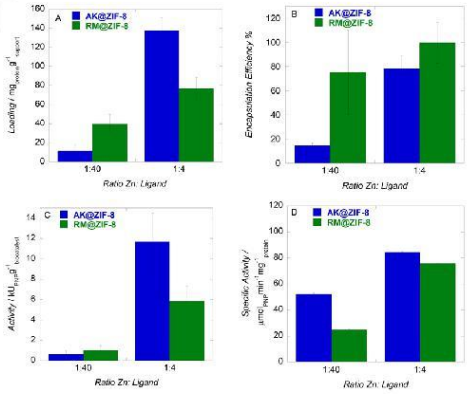


**Figure 3.** Comparison A) enzyme loading, B) encapsulation efficiency, C) enzymatic activity, and D) specific activity (PNP= p-nitrophenol) of lipase ZIF-8 prepared at Zn:L ratios of 1:40 and 1:4.

Moreover, the samples obtained using a ratio of 1:4 resulted in a very high encapsulation efficiency (EE%, the amount of immobilised protein relative to the total protein amount in the immobilising solution) (Figure 3B). Lipase RM in particular was completely immobilised in the ZIF-$8_{LR}$ material, with an EE% of 99% while, with lipase AK, an EE% of 78% was observed. The encapsulation efficiency for samples obtained by Zn:L=1:40 ratios was 14% and 75% for AK@ZIF-$8_{HR}$ and lipase RM@ZIF-$8_{HR}$ respectively (Figure 3B). The catalytic activities of lipase@ZIF-8 samples are shown in Figures 3C-D. Specific activities ($\mu mol_{PNP}\ min^{-1}\ mg_{protein}^{-1}$ = U/mg) were 84.5±0.3 U/mg (AK@ZIF-$8_{LR}$), 75.8±0.4 U/mg (RM@ZIF-$8_{LR}$), 52.2±2 U/mg (AK@ZIF-$8_{HR}$) and 24.9±0.7 U/mg (RM@ZIF-$8_{HR}$). Although samples obtained at the low Zn:L (1:4) molar ratio had low surface areas (Table 1), they resulted in higher loadings, encapsulation efficiencies and specific activities than samples synthesised with a high (1:40) ratio. This means that lipases are better adapted to the ZIF-$8_{LR}$ than to ZIF-$8_{HR}$ structures.

### 2.3 Effect of pH on lipase@ZIF-$8_{HR}$ samples

The two procedures used to synthesise ZIF-8 and lipase@ZIF-8 samples differ in terms of Zn:L ratio and in the pH of the synthesis solution. The pH was 11.6 at a Zn:L ratio of 1:40 and 10.6 for a ratio of 1:4. This pH difference might be responsible of at least part of the observed differences of surface area, loading and catalytic activity between the two types of samples. Thus, samples at a Zn:L=1:40 were prepared, but changing the pH of the synthesis solution (from 11.6 to 10.2, 9.8, 9.4) by adding HCl. The effect of the selected pH on surface area, protein loading, encapsulation efficiency and specific activity of the lipase@ZIF-$8_{HR}$ biocatalysts was then examined. As shown in Figure 4, a change of pH of the synthesis solution (Zn:L=1:40) affects the surface area of lipase@ZIF-$8_{HR}$ samples. Although the isotherms of the samples obtained at different pH values have similar shapes, the amount of adsorbed nitrogen decreases at decreasing pH for AK@ZIF-$8_{HR}$ (Figure 4A) resulting in a decrease in the surface area (Figure 4C). On the contrary, for RM lipase the highest surface area was obtained with samples synthesised at pH 10.2. At pH 9.4 the surface area decreased dramatically for both AK@ZIF-$8_{HR}$ and RM@ZIF-$8_{HR}$. At this pH the isotherms are similar to those obtained for the samples with Zn:L=1:4 ratio (Figure 1C), prepared at a pH of 10.6. These data clearly show the effect of pH on the surface area of lipase@ZIF-$8_{HR}$ samples. The $pK_a$ of 2-methylimidazole is 7.85.[62] As the pH of the ligand solution is lowered to values closer to the $pK_a$ of 2-MIM, the concentration of the protonated form of the ligand increases. This may affect the formation of the structure of lipase@ZIF-$8_{HR}$ samples. At pH 9 no solid sample could be collected by centrifugation after a synthesis time of 24 h. Moreover, the isotherms obtained at a ratio Zn:L=1:4 (Figure 1D) are similar to those obtained at a ratio of Zn:L=1:40 at pH 9.4 (Figures 4A and 4B) suggesting that a decrease of pH produces an effect similar to the decrease of the ratio of Zn:L. That hypothesis is supported by the data reported in Figure 4C, and in Table S1, where the comparison among surface areas obtained with the two synthesis conditions is shown. At ratio Zn:L=1:40, the highest surface area was achieved at pH 10.2 for AK@ZIF-$8_{HR}$ (618 $m^2/g$) and RM@ZIF-$8_{HR}$ (923 $m^2/g$) samples. Conversely, at pH 9.4 the surface areas of AK@ZIF-$8_{HR}$ (33 $m^2/g$) and RM@ZIF-$8_{HR}$ (43 $m^2/g$) were similar to those of the corresponding biocatalysts obtained at Zn:L=1:4 (4.4 $m^2/g$ and 30 $m^2/g$). These data show that, in addition to pH, the type of enzyme influences the properties of lipase@ZIF-8.

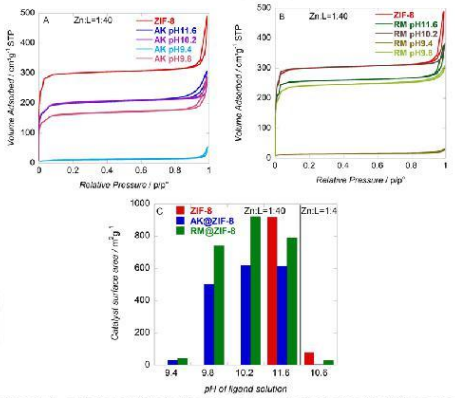


**Figure 4.** $N_2$ ads-desorption isotherms and comparison among surface areas obtained at different pH conditions of synthesis. A) AK@ZIF-8 and B) RM@ZIF-8, obtained by means of a Zn:L=1:40 controlling the pH during the synthesis. and; C) influence of pH on the surface area of all lipase@ZIF-8 samples at all synthesis conditions tested.

The effect of the synthesis pH on protein loading and catalytic activity was then investigated. Figure 5A shows that protein loading increases by decreasing the pH of the synthesis solution. This applies to both lipases, although the loading is always higher for lipase RM than for lipase AK. At pH 9.4 a loading of 102±10 mg/g and 55±6 mg/g was obtained for RM@ZIF-$8_{HR}$ and AK@ZIF-$8_{HR}$ samples, respectively. It should be noticed that the highest protein loading obtained at pH 9.4 is lower than that obtained with a Zn:L ratio of 1:4 (Figure 3A). Similarly, the highest encapsulation efficiency was reached for the samples obtained by the Zn:L=1:40 ratio at pH 9.4. EE% was 71% for RM@ZIF-$8_{HR}$ and only 34% for AK@ZIF-$8_{HR}$. These values were, however, lower than those obtained for Zn:L= 1:4 ratio (Figure S3B).

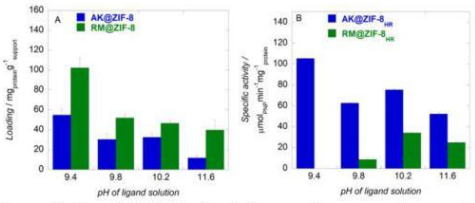


**Figure 5.** Lipase@ZIF-8 biocatalyst. A comparison among the samples obtained with Zn:L=1:40 ratio at different synthesis solution pH. A) Loading and B) catalytic activity.

The specific activities of the immobilised biocatalysts obtained by means of a Zn:L=1:40 ratio at different pH are shown in Figure 5B. AK@ZIF-$8_{HR}$ samples increased their specific activity by decreasing the synthesis pH from 11.6 to pH 9.4. The specific activity measured for RM@ZIF-$8_{HR}$ instead, was always lower than that of AK@ZIF-$8_{HR}$ in the investigated pH range. Moreover the specific activity was about zero for RM@ZIF-$8_{HR}$ samples synthesised at pH 9.4 (Figure 5B). It has been reported that *Mucor miehei* lipases display the maximal activity at pH 8.[47] Thus, we expect RM lipase to be less active in highly alkaline conditions (pH > 9.4) required for ZIF-8 formation. From these results we may argue that pH affects the synthesis of ZIF-8 and the consequent biocatalyst in a manner that cannot be ignored. A final comparison between the effect of pH and that of Zn:L ratio deserves notice. For the synthesis at Zn:L=1:4 ratio - whose initial pH of ligand solution was 10.6 - the biocatalysts are generally more active than those obtained at different pH tested at Zn:L=1:40 ratio (see par. 2.2). This suggests that the concentration of the 2-MIM ligand plays a more important role than pH on affecting the specific activity of the lipase@ZIF-8 biocatalysts.

### 2.4 Stability of lipase@ZIF-$8_{LR}$ biocatalysts

The stability to store and to reuse an enzyme is a key issue for the development of a suitable immobilised biocatalyst. Free enzymes are generally quite expensive and unstable particularly in terms of long-term storage and harsh reaction conditions such as extremes of temperature or pH. Hence, a high storage stability allows the design of a large-scale biocatalyst production, while recycling allows for a reduction of operational costs. Figure 6 shows the storage stability and the recycling of lipase@ZIF-$8_{LR}$ biocatalysts (Zn:L=1:4 ratio). These samples were chosen because, respect to those synthesised with the Zn:L=1:40 ratio, they reached the highest enzyme loading and specific activity. The biocatalysts were stored at 4°C for 15 days. An activity retention of 88% and 99% was obtained for RM@ZIF-$8_{LR}$ and AK@ZIF-$8_{LR}$, respectively (Figure 6A). This demonstrates that, the investigated storage conditions do not significantly affect the relative activity of both biocatalysts. He et al. investigated the long-term stability and recycling of the thermophilic lipase from *Alcaligenes sp.* immobilised on ZIF-8.[38]

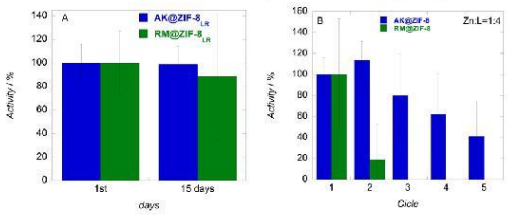


**Figure 6.** Stability and recycling of lipase ZIF-$8_{LR}$ (Zn:L=1:4 ratio) biocatalyst. A) residual activity of the catalyst after 15 days and B) recycling.

After 5 days storage of the immobilised lipases at two different temperatures, they obtained an activity retention of 20.3% (37°C) and 6.0% (60°C). The operational stability to recycling of the two biocatalysts was then investigated (Figure 6B). RM@ZIF-$8_{LR}$ biocatalyst retained only a 30% of its initial activity in the second reaction cycle, and became fully inactive in the third cycle. Instead, AK@ZIF-$8_{LR}$ biocatalyst displayed a better performance, since it could be reused 5 times with activity retention of 40% at the 5$^{th}$ reaction cycle (Figure 6B). He et al. could recycle their biocatalyst 10 times with 75.7% retention of activity after the 10$^{th}$ reaction cycle.[38] Hence, although our and He et al. experimental conditions were not exactly the same, AK@ZIF-$8_{LR}$ was less stable to recycling but more stable to storage than *Alcaligenes* lipase immobilised on ZIF-8. From these measurements it is difficult to discern the cause of the observed activity loss. Nonetheless, due to the fact that the enzyme is encapsulated within ZIF-8 structure it is more likely that deactivation rather than leaching is the cause of the observed trends.

## 3. Conclusions

Two synthetic methods differing for the ratio between zinc ion and 2-MIM ligand were compared for the preparation of lipase@ZIF-8 biocatalysts. A high Zn:L (1:40) ratio[25] and a low (1:4) ratio[24] gave lipase@ZIF-$8_{HR}$ and lipase@ZIF-$8_{LR}$ samples, respectively. The structural and textural features of ZIF-8 and lipase@ZIF-8 samples are both affected by Zn:L ratio. ZIF-$8_{HR}$ samples had very high surface areas compared with ZIF-$8_{LR}$ samples (Table 1). However, the latter samples had higher enzyme loadings and higher specific activities (Figure 3). The effect of decreasing the solution pH during the synthesis of lipase@ZIF-$8_{HR}$ samples was then investigated. The obtained samples had lower surface areas (Figure 4) but higher loadings and specific activities (Figure 5), mimicking the behaviour of lipase@ZIF-$8_{LR}$ samples. This observation, to the best of our knowledge, had not already been reported. AK@ZIF-$8_{LR}$ and RM@ZIF-$8_{LR}$ retained high levels of activity after 15 days storage at 4°C. Finally, AK@ZIF-$8_{LR}$ could be recycled 5 times with activity retention of 40% at the 5$^{th}$ reaction cycle. This last biocatalyst might be a good candidate for further studies as, for example, the synthesis of biodiesel.[50]

## Experimental Section

### 4.1 Chemicals

Lipase AK from *Pseudomonas fluorescens* (LAKGO751641) was purchased from Amano Enzymes, Japan. Lipase RM (2000 U $g^{-1}$) from *Rhizomucor Miehei* fungi was purchased from Sigma. Both lipases were used without any further purification. p-nitrophenyl butyrate, zinc nitrate hexahydrate (98%), 2-methylimidazole (99%), 2-propanol, bovine serum albumin (BSA, 98%), Bradford reagent, sodium phosphate dibasic (ACS Grade, ≥99%), magnesium nitrate (ACS Grade, ≥99%), were purchased

from Sigma-Aldrich. Sodium phosphate monobasic monohydrate (≥99%) was purchased from J.T. Backer.

**4.2 Synthesis of ZIF-8 and lipase@ZIF-8 samples with a low Zn:2-MIM ratio (Zn:L=1:4).**

For the preparation of ZIF-8,[24] a volume of 50 mL of an aqueous solution of zinc nitrate (40mM corresponding to 0.60 g and 2 mmol of $Zn(NO_3)_2 \times 6H_2O$) was quickly added under stirring to 50 mL of an aqueous solution of 2-methylimidazole (160 mM corresponding to 0.66 g and 8 mmol, pH 10.6). The reaction mixture was aged overnight at 25°C. Then the ZIF-8 sample was collected by centrifugation and washed three times with milliQ water. For the preparation of lipase@ZIF-8 biocatalyst, 0.4 g of lipase AK or 8mL (corresponding to 9.2 g of the commercial liquid preparation) of lipase RM were dissolved in the 2-methylimidaziole aqueous solution (160 mM). The resulting lipase/2-methylimidazole solution (pH=10.2) was quickly mixed under stirring to 50 mL the 40 mM zinc nitrate solution. Then the synthesis of Lipase@ZIF-8 was carried out with the same procedure followed for ZIF-8 sample (Zn:L=1:4).

**4.3 Synthesis of ZIF-8 and lipase@ZIF-8 samples with a high Zn:2-MIM ratio (Zn:L=1:40).**

For the preparation of ZIF-8,[12,25] 0.60 g of zinc nitrate (2mmol) were dissolved in 4 g of milliQ water and quickly added under stirring to 40 g of an aqueous solution containing 6.63 g (80 mmol) of 2-methylimidazole. The reaction mixture was left under continuous stirring for 10 minutes. Then the solution was aged overnight at 25°C. The ZIF-8 sample was recovered by centrifugation and washed three times with milliQ water. For the preparation of lipase@ZIF-8, 0.4 g of lipase AK or 8mL of lipase RM (corresponding to 9.2 g of the commercial liquid preparation) were dissolved into 40 g of an aqueous solution containing 6.63 g (80 mmol) of 2-methylimidazole aqueous solution. The resulting lipase/2-methylimidazole solution (pH=11.2) was quickly mixed under stirring to 4 g of the zinc nitrate solution. Then the synthesis of Lipase@ZIF-8 was carried out with the same procedure followed for ZIF-8 sample (Zn:L=1:40).The effect of pH on the synthesis of lipase@ZIF-8 samples was also investigated. To this purpose 4 additional lipase@ZIF-8 samples were prepared by decreasing the pH of 2-methylimidazole solution - before the addition of the lipases - from the initial value 11.6 to 10.2, 9.8, 9.4 and 9.0, by means of HCl addition. Then the synthesis proceeded as described above.

**4.4 Characterization of ZIF-8 samples**

A X'PERT Pro PANalytical diffractometer was used for X-ray diffraction (XRD) experiments with Cu-Kα radiation. The data were collected with a two theta step size of 0.02° from 5 to 50° and an accumulation time 20 s. The experimental XRD patterns were compared (Fig. 1A,B) with simulated patterns obtained using a deposited cif.file[53] and plotted with Mercury software. Thermogravimetric analysis (TGA) analysis was carried out by means of a TGA 4000 Perkin Elmer. The temperature range was from 30 °C to 900 °C, the ramp rate selected was 10 °C per min, under nitrogen flow (flow rate=20 mL $min^{-1}$). Scanning electron microscopy (SEM) analysis was performed at various magnifications, by a HITACHI SU-70 equipment at 10 kV. Fourier transform infrared (FTIR) analysis was conducted with a Bruker Tensor 27 spectrophotometer, equipped with a diamond-ATR accessory and a DTGS detector. A number of 256 scans at a resolution of 2 $cm^{-1}$ were averaged from wave number 4000 to 400 $cm^{-}1$. An ASAP 2020 (Micromeritics), was used to investigate the textural characteristics of all the samples. The $N_2$ adsorption/desorption isotherms were recorded at 77 K. Before the analysis, ZIF-8 (lipase@ZIF-8) samples were out-gassed under vacuum for 12 h at 200°C (120°C). The Brunauer-Emmett-Teller[63] (BET), and the Barret-Joyner-Halenda[64] (BJH) methods were used to determine specific surface area, the pore volume and the pore size distribution.

**4.5 Determination of enzyme loading and encapsulation efficiency**

Protein loading and the encapsulation efficiency of lipase@ZIF-8 samples were calculated by measuring the protein concentration in the initial and final immobilising solutions. The protein concentration was obtained spectrophotometrically (λ= 595 nm) through the Bradford Assay.[59] Encapsulation efficiency (EE%) is the percent ratio between the amount of immobilised protein and the amount of protein in the immobilising solution:

$$EE\% = (1 - [P]_f / [P]_0) \times 100\%$$

Where $[P]_0$ and $[P]_f$ are the initial and the final protein concentrations in the immobilising solution.[65]

Protein loading ($mg_{protein}/g_{ZIF-8}$) is the amount of immobilised protein per g of support.[66,67]

$$loading = \frac{[P]_0 V_0 - [P]_f V_f - [P]_w V_w}{m_{ZIF-8}}$$

Where, $[P]_0$, $[P]_f$ and $[P]_w$are the protein concentrations (mg/mL) in the initial, final and washing solutions; $V_0$ and $V_f$ (mL) are the initial and final volumes of the immobilising solution; and $V_w$ (mL) is the volume of washing solution; $m_{ZIF-8}$ is the mass (g) of ZIF-8 support.

**4.6 Determination of biocatalysts activity and stability**

The activity of free and immobilised lipases was measured by means of a Varian Cary 60 UV-VIS spectrophotometer, equipped with an optical fibre probe with the p-nitro phenylbutyrate (PNPB )assay.[60,68,69] The activity of free lipases (AK and RM) was measured by adding 5 µL of the lipase aqueous solution to 2 mL of 0.1 M phosphate buffer pH 7, 200

µL of PNPB (0.02 M in 2-propanol) solution and 200 µL of 2-propanol. The activity of immobilised lipases was measured by adding 5 mg of lipase@ZIF-8 samples to 5 mL of 0.1 M phosphate buffer pH 7, 500 µL of PNPB solution and 500 µL of 2-propanol. The (free and immobilised) lipases catalyse the formation of p-nitrophenol which was quantified at λ=400 nm (molar extinction coefficient of p-nitrophenol, ε=9396.1 $M^{-1}cm^{-1}$) at room temperature. The lipase activity (µmol p-nitrophenol × $min^{-1}$) was corrected by subtracting the amount of p-nitrophenol formed in the absence of lipases. Storage and recycling stabilities were carried out by means of the PNPB assay, as described above. For storage tests, the wet biocatalyst was stored at 4°C and dried under vacuum the day before the activity measurements. For recycling tests, the used biocatalyst (5 mg) was recovered by centrifugation and washed with 1 mL of 0.1 M phosphate buffer pH 7 before the addition of the fresh substrate solution. All activity and stability measurements were carried out at least in triplicate.

## Acknowledgements

AS thanks FIR 2017 and Fondazione di Sardegna and Regione Autonoma Sardegna (F72F16003070002) and MIUR (FFABR 2017) for financial support. FP is grateful to the "Agenzia delle Dogane e dei Monopoli" for funding her PhD. Synthesis and Solid State Pharmaceutical Centre (SSPC), funded by Science Foundation Ireland (SFI) under grant 12/RC/2275 is thanked for financial support. This work was also supported by the Iran National Science Foundation: INSF (Grant no. 93043395).

**Keywords:** Lipase•encapsulation•biocatalysis•ZIF 8•MOF

[1] S. Jemli, D. Ayadi-Zouari, H. Ben Hlima, S. Bejar, *Crit. Rev. Biotechnol.* **2016**, *36*, 246–258.
[2] R. DiCosimo, J. McAuliffe, A. J. Poulose, G. Bohlmann, *Chem. Soc. Rev.* **2013**, *42*, 6437.
[3] J. M. Blamey, F. Fischer, H.-P. Meyer, F. Sarmiento, M. Zinn, in *Biotechnol. Microb. Enzym.*, Elsevier, **2017**, pp. 347–403.
[4] I. Eş, J. D. G. Vieira, A. C. Amaral, *Appl. Microbiol. Biotechnol.* **2015**, *99*, 2065–2082.
[5] E. Magner, *Chem. Soc. Rev.* **2013**, *42*, 6213.
[6] M. Hartmann, X. Kostrov, *Chem. Soc. Rev.* **2013**, *42*, 6277.
[7] N. Carlsson, H. Gustafsson, C. Thörn, L. Olsson, K. Holmberg, B. Åkerman, *Adv. Colloid Interface Sci.* **2014**, *205*, 339–360.
[8] A. Salis, L. Medda, F. Cugia, M. Monduzzi, *Colloids Surf. B. Biointerfaces* **2016**, *137*, 77–90.
[9] M. Piras, A. Salis, M. Piludu, D. Steri, M. Monduzzi, *Chem. Commun.* **2011**, *47*, 7338.
[10] O. M. Yaghi, H. Li, *J. Am. Chem. Soc.* **1995**, *117*, 10401–10402.
[11] W. Morris, C. J. Stevens, R. E. Taylor, C. Dybowski, O. M. Yaghi, M. A. Garcia-Garibay, *J. Phys. Chem. C* **2012**, *116*, 13307–13312.
[12] Y. Pan, Y. Liu, G. Zeng, L. Zhao, Z. Lai, *Chem. Commun.* **2011**, *47*, 2071.
[13] T. D. Bennett, D. A. Keen, J. C. Tan, E. R. Barney, A. L. Goodwin, A. K. Cheetham, *Angew. Chemie - Int. Ed.* **2011**, *50*, 3067–3071.
[14] Y. Hu, H. Kazemian, S. Rohani, Y. Huang, Y. Song, *Chem. Commun. (Camb).* **2011**, *47*, 12694–6.
[15] K. S. Park, Z. Ni, A. P. Côté, J. Y. Choi, R. Huang, F. J. Uribe-Romo, H. K. Chae, M. O'keeffe, O. M. Yaghi, *Proc. Natl. Acad. Sci. U. S. A.* **2006**, *103*, 10186.
[16] S. Bhattacharjee, M.-S. Jang, H.-J. Kwon, W.-S. Ahn, *Catal. Surv. from Asia* **2014**, *18*, 101–127.
[17] S. K. Nune, P. K. Thallapally, A. Dohnalkova, C. Wang, J. Liu, G. J. Exarhos, *Chem. Commun.* **2010**, *46*, 4878–80.
[18] P. J. Beldon, L. Fábián, R. S. Stein, A. Thirumurugan, A. K. Cheetham, T. Friščić, *Angew. Chemie - Int. Ed.* **2010**, *49*, 9640–9643.
[19] H. Y. Cho, J. Kim, S. N. Kim, W. S. Ahn, *Microporous Mesoporous Mater.* **2013**, *169*, 180–184.
[20] Q. Bao, Y. Lou, T. Xing, J. Chen, *Inorg. Chem. Commun.* **2013**, *37*, 170–173.
[21] K. Liang, C. J. Coghlan, S. G. Bell, C. Doonan, P. Falcaro, *Chem. Commun.* **2016**, *52*, 473–476.
[22] J. Cui, Y. Feng, T. Lin, Z. Tan, C. Zhong, S. Jia, *ACS Appl. Mater. Interfaces* **2017**, *9*, 10587–10594.
[23] E. Gkaniatsou, C. Sicard, R. Ricoux, J.-P. Mahy, N. Steunou, C. Serre, *Mater. Horiz.* **2017**, *4*, 55–63.
[24] K. Liang, R. Ricco, C. M. Doherty, M. J. Styles, S. Bell, N. Kirby, S. Mudie, D. Haylock, A. J. Hill, C. J. Doonan, et al., *Nat. Commun.* **2015**, *6*, 7240.
[25] X. Wu, J. Ge, C. Yang, M. Hou, Z. Liu, *Chem. Commun.* **2015**, *51*, 13408–13411.
[26] K. Kida, M. Okita, K. Fujita, S. Tanaka, Y. Miyake, *CrystEngComm* **2013**, *15*, 1794.
[27] W. Shuai, R. K. Das, M. Naghdi, S. K. Brar, M. Verma, *Biotechnol. Appl. Biochem.* **2017**, *64*, 496–508.
[28] Z. Amini, Z. Ilham, H. C. Ong, H. Mazaheri, W. H. Chen, *Energy Convers. Manag.* **2017**, *141*, 339–353.
[29] M. L. Verma, M. Puri, C. J. Barrow, *Crit. Rev. Biotechnol.* **2014**, *8551*, 1–12.
[30] A. Salis, M. S. Bhattacharyya, M. Monduzzi, V. Solinas, *J. Mol. Catal. B Enzym.* **2009**, *57*, 262–269.
[31] A. Salis, M. Pinna, M. Monduzzi, V. Solinas, *J. Mol. Catal. B Enzym.* **2008**, *54*, 19–26.
[32] J. Trbojevic Ivic, D. Velickovic, A. Dimitrijevic, D. Bezbradica, V. Dragacevic, M. Gavrovic Jankulovic, N. Milosavic, *J. Sci. Food Agric.* **2016**, 4281–4287.
[33] P. Choudhury, B. Bhunia, *Biopharm J.* **2015**, *1*, 41–47.
[34] W.-L. Liu, N.-S. Yang, Y.-T. Chen, S. Lirio, C.-Y. Wu, C.-H. Lin, H.-Y. Huang, *Chem. - A Eur. J.* **2015**, *21*, 115–119.
[35] Y. Cao, Z. Wu, T. Wang, Y. Xiao, Q. Huo, Y. Liu, *Dalt. Trans.* **2016**, *45*, 6998–7003.
[36] S. Jung, Y. Kim, S.-J. Kim, T.-H. Kwon, S. Huh, S. Park, *Chem. Commun. (Camb).* **2011**, *47*, 2904–2906.
[37] V. Gascón, C. Carucci, M. B. Jiménez, R. M. Blanco, M. Sánchez-Sánchez, E. Magner, *ChemCatChem* **2017**, *9*, 1182–1186.
[38] H. He, H. Han, H. Shi, Y. Tian, F. Sun, Y. Song, Q. Li, G. Zhu, *ACS Appl. Mater. Interfaces* **2016**, *8*, 24517–24524.
[39] L.-Z. Cheong, Y. Wei, H. Wang, Z. Wang, X. Su, C. Shen, *J. Nanoparticle Res.* **2017**, *19*, 280.
[40] J. Shi, X. Wang, S. Zhang, L. Tang, Z. Jiang, *J. Mater. Chem. B* **2016**, *4*, 2654–2661.
[41] F. Lyu, Y. Zhang, R. N. Zare, J. Ge, Z. Liu, *Nano Lett.* **2014**, *14*, 5761–5765.
[42] J. Huo, J. Aguilera-Sigalat, S. El-Hankari, D. Bradshaw, *Chem. Sci.* **2015**, *6*, 1938–1943.
[43] A. M. Brzozowski, U. Derewenda, Z. S. Derewenda, G. G. Dodson, D. M. Lawson, J. P. Turkenburg, F. Bjorkling, B. Huge-Jensen, S. A. Patkar, L. Thim, *Nature* **1991**, *351*, 491–494.
[44] M. Adamczak, W. Bednarski, *Process Biochem.* **2004**, *39*, 1347–1361.
[45] C. Angkawidjaja, D. ju You, H. Matsumura, K. Kuwahara, Y. Koga, K. Takano, S. Kanaya, *FEBS Lett.* **2007**, *581*, 5060–5064.
[46] G. Fernández-Lorente, J. M. Palomo, M. Fuentes, C. Mateo, J. M. Guisán, R. Fernández-Lafuente, *Biotechnol. Bioeng.* **2003**, *82*, 232–237.
[47] H. Gustafsson, E. M. Johansson, A. Barrabino, M. Odén, K. Holmberg, *Colloids Surf. B. Biointerfaces* **2012**, *100*, 22–30.
[48] Y. Kojima, S. Shimizu, *J. Biosci. Bioeng.* **2003**, *96*, 219–226.
[49] M. Garmroodi, M. Mohammadi, A. Ramazani, M. Ashjari, J. Mohammadi, B. Sabour, M. Yousefi, *Int. J. Biol. Macromol.* **2016**, *86*, 208–215.
[50] A. Salis, M. F. Casula, M. S. Bhattacharyya, M. Pinna, V. Solinas, M. Monduzzi, *ChemCatChem* **2010**, *2*, 322–329.
[51] A. Salis, M. Pinna, M. Monduzzi, V. Solinas, *J. Biotechnol.* **2005**, *119*, 291–299.
[52] D. W. Lewis, A. R. Ruiz-Salvador, A. Gomez, L. M. Rodriguez-Albelo, F.-X. Coudert, B. Slater, A. K. Cheetham, C. Mellot-Draznieks, *CrystEngComm* **2009**, *11*, 2272–2276.
[53] D. Fairen-Jimenez, S. A. Moggach, M. T. Wharmby, P. A. Wright, S. Parsons, T. Düren, *J. Am. Chem. Soc.* **2011**, *133*, 8900–8902.
[54] Q. Shi, Z. Chen, Z. Song, J. Li, J. Dong, *Angew. Chemie - Int. Ed.* **2011**, *50*, 672–675.
[55] V. Gascón, E. Castro-Miguel, M. Díaz-García, R. M. Blanco, M. Sanchez-Sanchez, *J. Chem. Technol. Biotechnol.* **2017**, *92*, 2583–

2593.
[56] M. Jian, B. Liu, G. Zhang, R. Liu, X. Zhang, *Colloids Surfaces A Physicochem. Eng. Asp.* **2015**, *465*, 67–76.
[57] P. Chulkaivalsucharit, X. Wu, J. Ge, *RSC Adv.* **2015**, *5*, 101293–101296.
[58] M. Sanchez-Sanchez, I. de Asua, D. Ruano, K. Diaz, *Cryst. Growth Des.* **2015**, *15*, 4498–4506.
[59] M.M.Bradford, *Anal. Biochem.* **1976**, *72*, 248–254.
[60] F. Beisson, A. Tiss, C. Rivière, R. Verger, *Eur. J. Lipid Sci. Technol.* **2000**, *102*, 133–153.
[61] S. H. Sterri, B. A. Johnsen, F. Fonnum, *Biochem. Pharmacol.* **1985**, *34*, 2779–2785.
[62] B. Lenarcik, P. Ojczenasz, *J.heterocyclic Chem.* **2002**, *39*, 287.
[63] S. Brunauer, P. H. Emmett, E. Teller, *J. Am. Chem. Soc.* **1938**, *60*, 309–319.
[64] E. P. Barrett, L. G. Joyner, P. P. Halenda, *J. Am. Chem. Soc.* **1951**, *73*, 373–380.
[65] S. Yang, J. Chen, D. Zhao, D. Han, X. Chen, *Int. J. Pharm.* **2012**, *434*, 155–160.
[66] D. Steri, M. Monduzzi, A. Salis, *Microporous Mesoporous Mater.* **2013**, *170*, 164–172.
[67] F. Pitzalis, M. Monduzzi, A. Salis, *Microporous Mesoporous Mater.* **2017**, *241*, 145–154.
[68] J. Amoah, S. H. Ho, S. Hama, A. Yoshida, A. Nakanishi, T. Hasunuma, C. Ogino, A. Kondo, *Bioresour. Technol.* **2016**, *211*, 224–230.
[69] D. Gilham, R. Lehner, *Methods* **2005**, *36*, 139–147.

## FULL PAPER

*Rhizomucor miehei* and *Pseudomonas fluorescens* lipases were encapsulated on ZIF-8 support via a "one-pot" aqueous synthesis. The effect of two different Zinc:Ligand molar ratios on enzyme loading and activity was investigated.

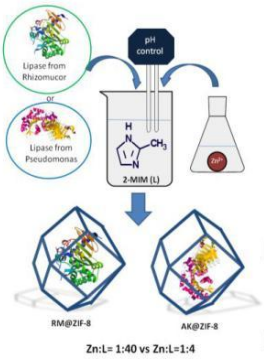


*Federica Pitzalis*[†[a]], *Cristina Carucci*[†[b]], *Maryam Naseri*[[a,c]], *Lida Fotouhi*[[c]], *Edmond Magner*[*[b]], *Andrea Salis*[*[a]]

***Page No. – Page No.***

**Lipases encapsulation onto ZIF-8. A comparison between biocatalysts obtained at low and high zinc:2-methylimidazole molar ratio in aqueous medium**

# Supporting information of the accepted article

# Lipases encapsulation onto ZIF-8. A comparison of biocatalysts obtained at low and high zinc:2methyl-imidazole mole ratio in aqueous medium

Federica Pitzalis,[1] Cristina Carucci[2], Maryam Naseri[1,3], Lida Fotouhi,[3] Edmond Magner,[2] Andrea Salis[1]

[1]Department of Chemical and Geological Sciences, University of Cagliari-CSGI and CNBS, Cittadella Universitaria, S.S. 554 bivio Sestu, 09042 Monserrato, Cagliari, Italy

[2] Department of Chemical Sciences, Bernal Institute, University of Limerick, Limerick, Ireland

[3] Department of Chemistry, University of Alzahara, Teheran, Iran

**Supporting information**

**Table S1.** Textural parameters of samples prepared by means of ratio Zn:L=1:40, at different pH conditions.

| Sample | pH of ligand solution | Surface area ($m^2g^{-1}$) | Pore volume ($cm^3g^{-1}$) |
|---|---|---|---|
| ZIF-8 | 11.6 | 919 | 0.76 |
| AK@ZIF-8 | 11.6 | 615 | 0.47 |
| AK@ZIF-8 | 10.2 | 618 | 0.44 |
| AK@ZIF-8 | 9.8 | 504 | 0.45 |
| AK@ZIF-8 | 9.4 | 33 | 0.087 |
| RM@ZIF-8 | 11.6 | 790 | 0.58 |
| RM@ZIF-8 | 10.2 | 923 | 0.59 |
| RM@ZIF-8 | 9.8 | 742 | 0.48 |
| RM@ZIF-8 | 9.4 | 43 | 0.048 |

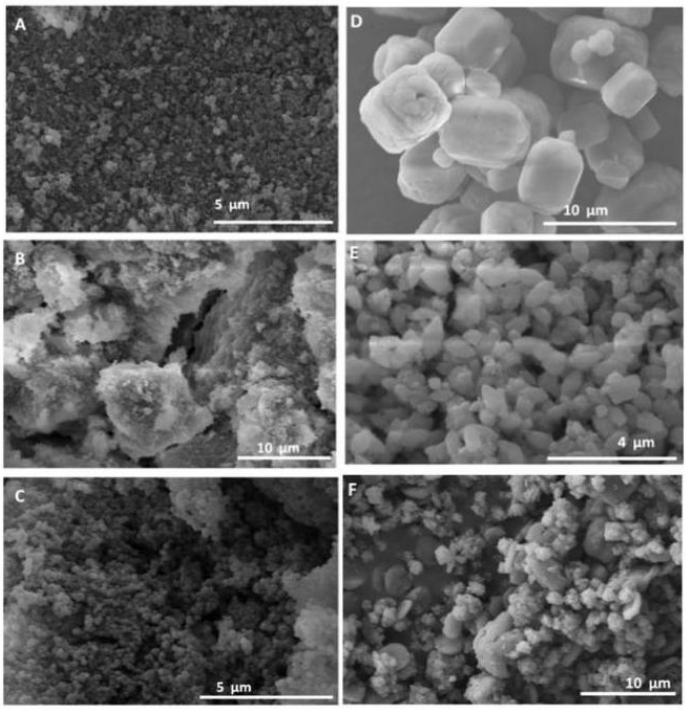


**Figure S1.** Scanning electron microscopy (SEM). On the left, SEM images of A) ZIF-8; B) AK@ZIF-8; C) RM@ZIF-8 samples obtained by using a Zn:L=1:40 ratio. On the right, SEM images of D) ZIF-8; E) AK@ZIF-8; F) RM@ZIF-8 samples obtained by using a Zn:L=1:4 ratio.

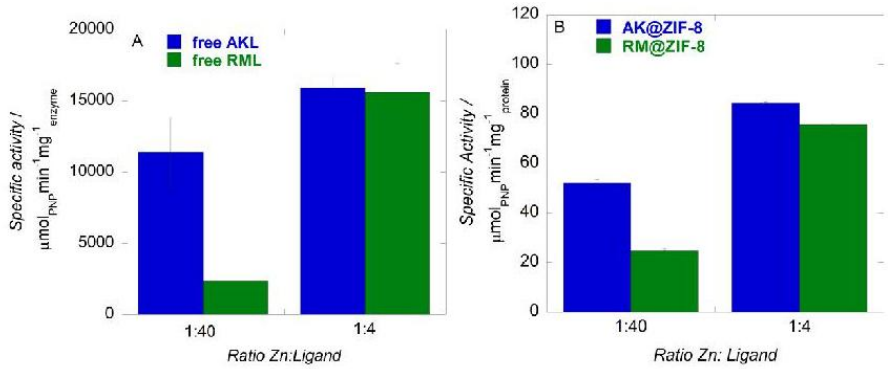


**Figure S2.** Specific activity. A) free enzymes, AKL and RML, of initial solutions with ratio Zn:L=1:40 and Zn:L=1:4 and B) corresponding immobilized biocatalysts.

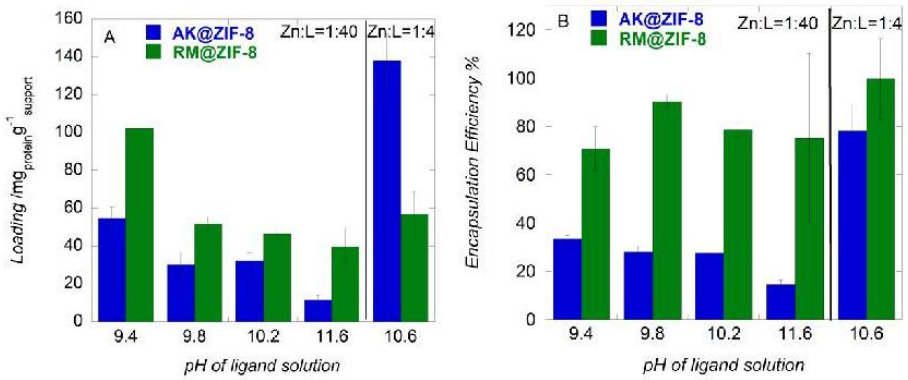


**Figure S3.** A comparison among all immobilised enzymes, AK@ZIF-8 and RM@ZIF-8 synthesised by means of a ratio Zn:L=1:40 and Zn:L=1:4 and at controlled initial pH of ligand solution. A) Loading and B) Encapsulation Efficiency.

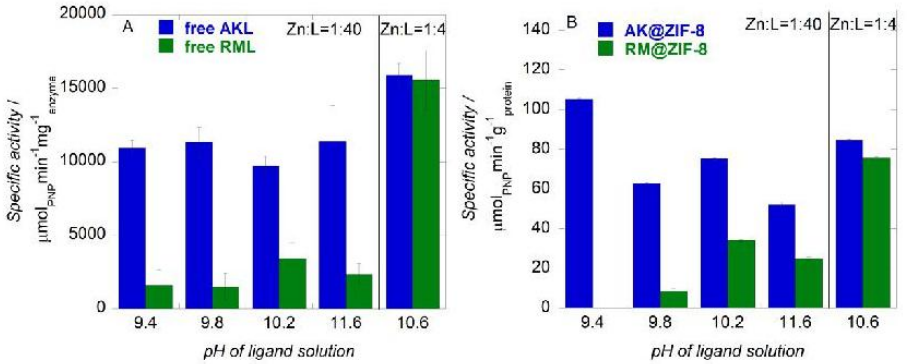


**Figure S4.** Specific activity. A) free enzymes, AKL and RML, of initial solutions with ratio Zn:L=1:40 and Zn:L=1:4 and at controlled initial pH of ligand solution. B) specific activity of AK@ZIF-8 and RM@ZIF-8 synthesized by means of a ratio Zn:L=1:40 and Zn:L=1:4, a comparison among all the biocatalysts.

# Conclusions

The efforts made by researchers to create new stable immobilized enzymes and to improve the stability and the reusability of biocatalysts is of great importance because biocatalysis is taking on a key role in the design of new industrial processes, according to a green and sustainable approach. The aim of this work was to investigate some of the strategies adopted in the current literature for the development of new immobilized enzymes that could be interesting for industrial applications. To this purpose, the choice of enzymes was made among those that have a significant commercial and industrial interest.

LYZ, is an important model enzyme, widely used in food industry as a preservative. GOx is widely used for biosensing in glycemia detection, and HRP is useful in various fields, among which biosensing and bioremediation. Particularly, the combined use of HRP and GOx is raising a wide scientific interest for the development of new promising glucose detectors. Lipase was chosen for its importance in the field of renewable feedstock, for biodiesel production. The choice of supports was another important factor: SBA-15 is inert, stable, with tunable porosity, and can be easily synthesized and functionalized. ZIF-8 is a new promising host material for enzymatic immobilization because of its high thermal stability, and its easy and quick synthesis. Three immobilization methods were investigated: physical adsorption, covalent anchoring and in situ encapsulation. The main conclusions outlined for this work are listed below.

SBA-15 mesoporous silica was synthesized and functionalized with APTES via a post synthesis procedure. The characterization of the SBA-15 and the amino-modified SBA-15-$NH_2$ was carried out with the following techniques: SAXS, TEM and $N_2$ physisorption, which were used to estimate the mesoporosity, FTIR, which was used to confirm the functionalization, and ELS which were used to estimate the zeta potential of both enzyme and silica. The physical adsorption of LYZ was carried out on SBA-15 and SBA-15-$NH_2$.

The loading obtained in different buffers, all at the fixed pH = 7.15, and in presence of strong electrolytes, was measured. The loading of LYZ on SBA-15 and the electrophoretic mobility of the free enzyme, SBA-15, and SBA-15-$NH_2$ were influenced by both buffers and salts. This is in agreement with recent works that propose that Hofmeister effects can occur for weak electrolytes also.

The covalent immobilization of GOx and HRP was carried out on SBA-15-$NH_2$ using glutaraldehyde as a linker. The characterization of the support and of the immobilized enzymes was carried out with SAXS, TEM, $N_2$ physisorption, and FT-IR. Simultaneous and separated immobilization of the two enzymes were investigated and compared, towards a combined covalent (GOx)/physical (HRP) separated immobilization, in terms of loading and specific activity. High loadings were obtained in the covalent conditions (around 38 mg/g for the simultaneous covalent immobilization, and 35 *vs* 27 mg/g for GOx and HRP, respectively). The combined immobilization resulted in different loadings for HRP (5 mg/g at pH 5 and 21 mg/g at pH 8). The trend of the specific activities resulted more significantly influenced by the drying procedure rather than by the loading or the simultaneous *vs* separated immobilization. Indeed, the most remarkable conclusion of this work, was the comparison of the two biocatalysts obtained by means of the covalent and simultaneous immobilization that differ only in the drying procedure. For both biocatalysts the loading is the same (around 38 mg/g), but specific activity is around 1.6 (μmol/ min×mg) for the dried biocatalyst, around 116 μmol/(min×mg) for the wet biocatalyst. This suggests that the activity of biocatalysts can be strongly influenced by the drying process. Another interesting conclusion can be pointed out from the tests concerning the separated immobilization. That is, some enzymes can be more or less robust towards procedures such as the drying. Indeed, the separated and dried biocatalyst in all immobilization conditions were all almost inactive. While the separated biocatalyst, where GOx was dried and HRP was wet, displayed a discrete activity (around 18 μmol/min×mg). The most active biocatalyst, namely the wet

biocatalyst obtained by simultaneous and covalent immobilization, exhibited also the best recycling performance, as it retained around the 50 percent of its activity at the 14$^{th}$ reaction cycle. A possible application of the wet GOx/HRP@SBA-15-$NH_2$ biocatalyst was suggested for the degradation of phenolic compounds. Thus, the kinetic of degradation of ferulic and caffeic acid was finally followed. Remarkably a conversion of 70 percent for both molecules was obtained in 15 minutes.

The hydrothermal synthesis of ZIF-8 was investigated, making a comparison with two synthesis condition, namely using two zinc: ligand (Zn:L) ratios: 1:4 and 1:40. The characterization of the material was carried out by means of SEM, XRD, N2 physisorption and FTIR. The molar ratio immediately emerged as a crucial factor that influences the crystal structure and the surface area of the support. The in situ encapsulation of lipase AK from *Pseudomonas fluorescens* (AKL) and lipase from *Rhizomucor miehei* (RML) on ZIF-8 was carried out by means of the same synthetic conditions tested for pure ZIF-8, namely Zn:L ratios = 1:4 and 1:40. For the latter ratio, several synthesis were carried out by controlling the pH before the dissolution of the enzyme in the ligand solution. Similarly to the pure ZIF-8, the biocatalysts were characterized by means of SEM, XRD, $N_2$ physisorption and FTIR. The loading and the activity were measured and compared. The main result to be pointed out in this work, is that the Zn:L ratio significantly influences the structure of both the support and of the biocatalysts. Consequently, also the loading and the activity of the biocatalysts are affected by the chosen synthesis condition. The biocatalysts obtained by Zn:L ratio 1:40 exhibited high crystallinity and a typical SOD-like structure, but poor loading and activity. Conversely, the biocatalysts obtained by Zn:L ratio 1:4 resulted in higher activity, although the crystalline phase was not associated to the typical SOD-like ZIF-8 structure. Thus, the latter biocatalysts were chosen for stability and recycling tests. It is worth remarking that, although the AK@ZIF-8 and RM@ ZIF-8 were obtained with the same reaction conditions, namely the Zn:L ratio 1:4, the recycling efficiency for the two

biocatalysts was not similar. Indeed AK@ZIF-8 was recycled five times, while RM@ ZIF-8 only twice. This suggests that also the type of enzyme can be more or less suitable for the immobilization on a certain kind of support. Clearly, the interaction between the immobilized enzyme and the support should carefully be considered when engineering a biocatalyst and choosing the strategies for its preparation.

# Bibliography


[1] V. Gold, in *IUPAC Compend. Chem. Terminol.*, IUPAC, Research Triagle Park, NC, **2014**, p. 1670.
[2] P. Anastas, N. Eghbali, *Chem. Soc. Rev.* **2010**, *39*, 301–312.
[3] B. D. Ribeiro, M. A. Z. Coelho, A. Machado de Castro, in *Princ. Green Chem. White Biotechnol.*, **2015**, pp. 1–8.
[4] A. J. J. Anthonsen, T. . In Adlercreutz, Patrick; Straathof, in (Ed.: Taylor & Francis.), Applied Biocatalysis, 2nd Edn. Academic, Amsterdam, **2000**, pp. 18–59.
[5] R. A. Sheldon, *Chem. - A Eur. J.* **2016**, *22*, 12984–12999.
[6] J. M. Blamey, F. Fischer, H.-P. Meyer, F. Sarmiento, M. Zinn, in *Biotechnol. Microb. Enzym.*, Elsevier, **2017**, pp. 347–403.
[7] L. P. Christopher, Hemanathan Kumar, V. P. Zambare, *Appl. Energy* **2014**, *119*, 497–520.
[8] S. Riva, *Trends Biotechnol.* **2006**, *24*, 219–226.
[9] P. Choudhury, B. Bhunia, *Biopharm J.* **2015**, *1*, 41–47.
[10] H.-P. Meyer, E. Eichhorn, S. Hanlon, S. Lütz, M. Schürmann, R. Wohlgemuth, R. Coppolecchia, *Catal. Sci. Technol.* **2013**, *3*, 29–40.
[11] I. Eş, J. D. G. Vieira, A. C. Amaral, *Appl. Microbiol. Biotechnol.* **2015**, *99*, 2065–2082.
[12] V. Ferreira-Leitão, M. Cammarota, E. Gonçalves Aguieiras, L. Vasconcelos de Sá, R. Fernandez-Lafuente, D. Freire, *Catalysts* **2017**, *7*, 9.
[13] J. M. Salgado, L. Abrunhosa, A. Venâncio, J. M. Domínguez, I. Belo, *Int. Biodeterior. Biodegrad.* **2016**, *110*, 16–23.
[14] C. R. Holkar, A. J. Jadhav, D. V. Pinjari, N. M. Mahamuni, A. B. Pandit, *J. Environ. Manage.* **2016**, *182*, 351–366.
[15] R. DiCosimo, J. McAuliffe, A. J. Poulose, G. Bohlmann, *Chem. Soc. Rev.* **2013**, *42*, 6437.
[16] S. M. Douglas, *Science (80-. ).* **2017**, *355*, 1261–1262.
[17] S. Pagani, M. Duranti, *Enzimologia: Dai Fondamenti Alle Applicazioni, Piccin Editore*, Piccin, **1998**.
[18] D. Voet, J. G. Voet, *John Wiley Sons* **2004**, *1*, 591.
[19] D. Voet, J. G. Voet, *Biochem. ed Stiefel J (Wiley, New York)* **1990**, 342–344.
[20] A. H. Blair, *Clin. Biochem.* **1976**, *9*, 155–159.
[21] A. G. McDonald, K. F. Tipton, *FEBS J.* **2014**, *281*, 583–592.
[22] NC-IUB, *Eur. J. Biochem.* **1979**, *97*, 319–320.
[23] Z. Amini, Z. Ilham, H. C. Ong, H. Mazaheri, W. H. Chen, *Energy Convers. Manag.* **2017**, *141*, 339–353.
[24] J. Polaina, A. P. MacCabe, *Industrial Enzymes*, Springer Netherlands, Dordrecht, **2007**.
[25] S. Sharma, S. S. Kanwar, *Sci. World J.* **2014**, *2014*, 1–15.
[26] L. Brady, A. M. Brzozowski, Z. S. Derewenda, E. Dodson, G. Dodson, S. Tolley, J. P. Turkenburg, L. Christiansen, B. Huge-Jensen, L. Norskov, et al., *Nature* **1990**, *343*, 767–770.
[27] A. S. Rose, A. R. Bradley, Y. Valasatava, J. M. Duarte, A. Prlić, P. W. Rose, *Proc. 21st Int. Conf. Web3D Technol. - Web3D '16* **2016**, 185–186.
[28] A. S. Rose, P. W. Hildebrand, *Nucleic Acids Res.* **2015**, *43*, W576–W579.
[29] K. Kakugawa, M. Shobayashi, O. Suzuki, T. Miyakawa, *Biosci. Biotechnol. Biochem.* **2002**, *66*, 978–985.
[30] K.-E. Jaeger, S. Ransac, H. B. Koch, F. Ferrato, B. W. Dijkstra, *FEBS Lett.* **1993**, *332*,

143–149.
[31] C. Angkawidjaja, D. ju You, H. Matsumura, K. Kuwahara, Y. Koga, K. Takano, S. Kanaya, *FEBS Lett.* **2007**, *581*, 5060–5064.
[32] C. Maldarelli, R. K. Jain, I. B. Ivanov, E. Ruckenstein, *J. Colloid Interface Sci.* **1980**, *78*, 118–143.
[33] D. J. Ericsson, A. Kasrayan, P. Johansson, T. Bergfors, A. G. Sandström, J. E. Bäckvall, S. L. Mowbray, *J. Mol. Biol.* **2008**, *376*, 109–119.
[34] G. Fernández-Lorente, J. M. Palomo, M. Fuentes, C. Mateo, J. M. Guisán, R. Fernández-Lafuente, *Biotechnol. Bioeng.* **2003**, *82*, 232–237.
[35] R. Verger, M. C. E. Mieras, G. H. De Haas, *J. Biol. Chem.* **1973**, *248*, 4023–4034.
[36] A. M. Brzozowski, U. Derewenda, Z. S. Derewenda, G. G. Dodson, D. M. Lawson, J. P. Turkenburg, F. Bjorkling, B. Huge-Jensen, S. A. Patkar, L. Thim, *Nature* **1991**, *351*, 491–494.
[37] A. Rauwerdink, R. J. Kazlauskas, *ACS Catal.* **2015**, *5*, 6153–6176.
[38] A. L. Paiva, V. M. Balcão, F. X. Malcata, *Enzyme Microb. Technol.* **2000**, *27*, 187–204.
[39] W. Shuai, R. K. Das, M. Naghdi, S. K. Brar, M. Verma, *Biotechnol. Appl. Biochem.* **2017**, *64*, 496–508.
[40] A. Salis, M. Pinna, M. Monduzzi, V. Solinas, *J. Mol. Catal. B Enzym.* **2008**, *54*, 19–26.
[41] C. Cai, Y. Gao, Y. Liu, N. Zhong, N. Liu, *Food Chem.* **2016**, *212*, 205–212.
[42] M. Adamczak, W. Bednarski, *Process Biochem.* **2004**, *39*, 1347–1361.
[43] H. Gustafsson, E. M. Johansson, A. Barrabino, M. Odén, K. Holmberg, *Colloids Surf. B. Biointerfaces* **2012**, *100*, 22–30.
[44] Y. Kojima, S. Shimizu, *J. Biosci. Bioeng.* **2003**, *96*, 219–226.
[45] B. Vasel, H. J. Hecht, R. D. Schmid, D. Schomburg, *J. Biotechnol.* **1993**, *28*, 99–115.
[46] X. Y. Wu, S. JÄÄskelÄinen, W.-Y. Linko, *Appl. Biochem. Biotechnol.* **1996**, *59*, 145–158.
[47] M. Garmroodi, M. Mohammadi, A. Ramazani, M. Ashjari, J. Mohammadi, B. Sabour, M. Yousefi, *Int. J. Biol. Macromol.* **2016**, *86*, 208–215.
[48] A. Salis, M. F. Casula, M. S. Bhattacharyya, M. Pinna, V. Solinas, M. Monduzzi, *ChemCatChem* **2010**, *2*, 322–329.
[49] A. Salis, M. Pinna, M. Monduzzi, V. Solinas, *J. Biotechnol.* **2005**, *119*, 291–299.
[50] H. Dan, X. Dong, X. Lu, Y. Ding, *J. Sol-Gel Sci. Technol.* **2017**, *81*, 782–790.
[51] S. Mine, S. Tate, T. Ueda, M. Kainosho, T. Imoto, *Analysis* **1999**, 1547–1565.
[52] T. Imoto, T. Ueda, T. Tamura, Y. Isakari, Y. Abe, M. Inoue, T. Miki, K. Kawano, H. Yamada, *Protein Eng. Des. Sel.* **1994**, *7*, 743–748.
[53] M. S. Weiss, J. Gottfried, R. Hilgenfeld, **2000**, 952–958.
[54] D. J. Vocadlo, G. J. Davies, R. Laine, S. G. Withers, *Nature* **2001**, *412*, 835–838.
[55] A. L. Bowman, I. M. Grant, A. J. Mulholland, *Chem. Commun.* **2008**, 4425.
[56] C. C. F. Blake, L. N. Johnson, G. A. Mair, A. C. T. North, D. C. Phillips, V. R. Sarma, *Proc. R. Soc. London. Ser. B, Biol. Sci.* **1967**, *167*, 378–388.
[57] C. Corradini, I. Alfieri, A. Cavazza, C. Lantano, A. Lorenzi, N. Zucchetto, A. Montenero, *J. Food Eng.* **2013**, *119*, 580–587.
[58] S. Bhatia, A. Bharti, *J. Food Sci. Technol.* **2015**, *52*, 3504–3512.
[59] V. A. Proctor, F. E. Cunningham, D. Y. C. Fung, *C R C Crit. Rev. Food Sci. Nutr.* **1988**, *26*, 359–395.
[60] D. P. dos Santos, T. L. M. Alves, J. C. Pinto, *Polímeros* **2016**, *26*, 282–290.
[61] G. Merlini, V. Bellotti, *Clin. Chim. Acta* **2005**, *357*, 168–172.
[62] I. Arcan, A. Yemenicioğlu, *Food Res. Int.* **2013**, *51*, 208–216.
[63] F. Cugia, S. Sedda, F. Pitzalis, D. F. Parsons, M. Monduzzi, A. Salis, *RSC Adv.* **2016**, *6*, 94617–94621.

[64] A. Salis, M. S. Bhattacharyya, M. Monduzzi, *J. Phys. Chem. B* **2010**, *114*, 7996–8001.
[65] D. Steri, M. Monduzzi, A. Salis, *Microporous Mesoporous Mater.* **2013**, *170*, 164–172.
[66] J. Wang, L. Tang, P. Somasundaran, W. Fan, G. Zeng, Y. Deng, Y. Zhou, J. Wang, Y. Shen, *J. Colloid Interface Sci.* **2017**, *503*, 131–141.
[67] K. Liang, R. Ricco, C. M. Doherty, M. J. Styles, S. Bell, N. Kirby, S. Mudie, D. Haylock, A. J. Hill, C. J. Doonan, et al., *Nat. Commun.* **2015**, *6*, 7240.
[68] S. B. Bankar, M. V. Bule, R. S. Singhal, L. Ananthanarayan, *Biotechnol. Adv.* **2009**, *27*, 489–501.
[69] H. J. Hecht, H. M. Kalisz, J. Hendle, R. D. Schmid, D. Schomburg, *J. Mol. Biol.* **1993**, *229*, 153–172.
[70] H. J. Hecht, D. Schomburg, H. Kalisz, R. D. Schmid, *Biosens. Bioelectron.* **1993**, *8*, 197–203.
[71] J. J. O'Malley, J. L. Weaver, *Biochemistry* **1972**, *11*, 3527–3532.
[72] J. H. Pazur, K. Kleppe, *Biochemsitry* **1964**, *3*, 578–583.
[73] C. Chen, Q. Xie, D. Yang, H. Xiao, Y. Fu, Y. Tan, S. Yao, *RSC Adv.* **2013**, *3*, 4473.
[74] C. Desmet, C. A. Marquette, L. J. Blum, B. Doumèche, *Biosens. Bioelectron.* **2016**, *76*, 145–163.
[75] D. W. S. Wong, *Appl. Biochem. Biotechnol.* **2009**, *157*, 174–209.
[76] D. Jung, C. Streb, M. Hartmann, *Int. J. Mol. Sci.* **2010**, *11*, 762–778.
[77] D. Jung, C. Streb, M. Hartmann, *Microporous Mesoporous Mater.* **2008**, *113*, 523–529.
[78] A. Mallardi, V. Angarano, M. Magliulo, L. Torsi, G. Palazzo, *Anal. Chem.* **2015**, *87*, 11337–11344.
[79] M. Khan, S.-Y. Park, *J. Colloid Interface Sci.* **2015**, *457*, 281–8.
[80] N. Caro-Jara, R. Mundaca-Uribe, C. Zaror-Zaror, J. Carpinelli-Pavisic, M. Aranda-Bustos, C. Peña-Farfal, *Electroanalysis* **2013**, *25*, 308–315.
[81] X. Yu, W. Lian, J. Zhang, H. Liu, *Biosens. Bioelectron.* **2016**, *80*, 631–639.
[82] B. C. Lai Truong Phuoc, Paco Laveille, Françoise Chamouleau, Gilbert Renard, Jullien Drone, François Fajula and Anne, ¸ Galarneau*, *Dalton Trans.* **2010**, *39*, 8511–8520.
[83] L. Banci, *J. Biotechnol.* **1997**, *53*, 253–263.
[84] G. S. Zakharova, I. V. Uporov, V. I. Tishkov, *Biochem.* **2011**, *76*, 1391–1401.
[85] N. C. Veitch, *Phytochemistry* **2004**, *65*, 249–259.
[86] G. I. Berglund, G. H. Carlsson, A. T. Smith, H. Szöke, A. Henriksen, J. Hajdu, *Nature* **2002**, *417*, 463–468.
[87] G. N. La Mar, G. Hernandez, J. S. de Ropp, *Biochemistry* **1992**, *31*, 9158–9168.
[88] P. R. Ortiz de Montellano, in *Heme Peroxidases*, **2016**, pp. 1–30.
[89] T. L. Poulos, *Chem. Rev.* **2014**, *114*, 3919–3962.
[90] E. P. Cipolatti, M. J. A. Silva, M. Klein, V. Feddern, M. M. C. Feltes, J. V. Oliveira, J. L. Ninow, D. de Oliveira, *J. Mol. Catal. B Enzym.* **2014**, *99*, 56–67.
[91] M. M. Vdovenko, C. C. Lu, F. Y. Yu, I. Y. Sakharov, *Food Chem.* **2014**, *158*, 310–314.
[92] X. Cheng, L. Challier, A. Etcheberry, V. Noël, H. Perez, *Int. J. Electrochem. Sci.* **2012**, *7*, 6247–6264.
[93] Y. Wang, B. Zhou, S. Wu, K. Wang, X. He, *Talanta* **2015**, *134*, 712–717.
[94] J. Heo, *Anal. Sci.* **2014**, *30*, 991–997.
[95] J. Yu, L. Ge, P. Dai, S. Ge, S. Liu, *Biosens. Bioelectron.* **2010**, *25*, 2065–2070.
[96] M. Hartmann, X. Kostrov, *Chem. Soc. Rev.* **2013**, *42*, 6277.
[97] M. Marguet, C. Bonduelle, S. Lecommandoux, *Chem. Soc. Rev.* **2013**, *42*, 512–529.
[98] H. Tan, S. Guo, N.-D. Dinh, R. Luo, L. Jin, C.-H. Chen, *Nat. Commun.* **2017**, *8*, 663.
[99] X. Wu, J. Ge, C. Yang, M. Hou, Z. Liu, *Chem. Commun.* **2015**, *51*, 13408–13411.
[100] X. Lian, Y.-P. Chen, T.-F. Liu, H.-C. Zhou, *Chem. Sci.* **2016**, *7*, 6969–6973.

[101] W. Wang, F. Wang, Y. Yao, S. Hu, K. K. Shiu, *Electrochim. Acta* **2010**, *55*, 7055–7060.
[102] X. Lian, Y. Fang, E. Joseph, Q. Wang, J. Li, S. Banerjee, C. Lollar, X. Wang, H.-C. Zhou, *Chem. Soc. Rev.* **2017**, *46*, 3386–3401.
[103] T. P. B. Nguyen, J. W. Lee, W. G. Shim, H. Moon, *Microporous Mesoporous Mater.* **2008**, *110*, 560–569.
[104] W.-D. Chen, X.-Y. Dong, Y. Sun, *J. Chromatogr. A* **2002**, *962*, 29–40.
[105] Q. Sun, L. Yang, *Water Res.* **2003**, *37*, 1535–1544.
[106] M. Jian, B. Liu, G. Zhang, R. Liu, X. Zhang, *Colloids Surfaces A Physicochem. Eng. Asp.* **2015**, *465*, 67–76.
[107] A. W. Marczewski, M. Seczkowska, A. Deryło-Marczewska, M. Blachnio, *Adsorption* **2016**, *22*, 777–790.
[108] K. Cai, X. He, Z. Song, Q. Yin, Y. Zhang, F. M. Uckun, C. Jiang, J. Cheng, *J. Am. Chem. Soc.* **2015**, *137*, 3458–3461.
[109] S. Yang, J. Chen, D. Zhao, D. Han, X. Chen, *Int. J. Pharm.* **2012**, *434*, 155–160.
[110] K. M. El-Say, *Drug Des. Devel. Ther.* **2016**, *10*, 825–839.
[111] W. A. Khan, *Sci. Appl. Tailored Nanostructures, one Cent. Press* **2016**, 50–67.
[112] G. L. Hornyak, J. J. Moore, H. F. Tibbals, J. Dutta, *Fundamentals of Nanotechnology*, CRC Press, **2008**.
[113] C. Buzea, I. I. Pacheco, K. Robbie, *Biointerphases* **2007**, *2*, MR17-MR71.
[114] A. Salis, L. Medda, F. Cugia, M. Monduzzi, *Colloids Surf. B. Biointerfaces* **2016**, *137*, 77–90.
[115] L. Medda, B. Barse, F. Cugia, M. Boström, D. F. Parsons, B. W. Ninham, M. Monduzzi, A. Salis, *Langmuir* **2012**, *28*, 16355–16363.
[116] F. Cugia, M. Monduzzi, B. W. Ninham, A. Salis, *RSC Adv.* **2013**, *3*, 5882.
[117] E. Magner, *Chem. Soc. Rev.* **2013**, *42*, 6213.
[118] Z. Zhou, M. Hartmann, *Chem. Soc. Rev.* **2013**, *42*, 3894.
[119] J. Mehta, N. Bhardwaj, S. K. Bhardwaj, K.-H. Kim, A. Deep, *Coord. Chem. Rev.* **2016**, *322*, 30–40.
[120] E. Gkaniatsou, C. Sicard, R. Ricoux, J.-P. Mahy, N. Steunou, C. Serre, *Mater. Horiz.* **2017**, *4*, 55–63.
[121] S. Hudson, E. Magner, J. Cooney, B. K. Hodnett, *J. Phys. Chem. B* **2005**, *109*, 19496–19506.
[122] P. Atkins, J. Paula, *Physical Chemistry*, **2006**.
[123] J. N. Israelachvili, *Intermolecular and Surface Forces*, Elsevier, **2011**.
[124] S. Velasco-Lozano, F. López-Gallego, J. C. Mateos-Díaz, E. Favela-Torres, *Biocatalysis* **2016**, *1*, 166–177.
[125] X. Cui, W.-C. Zin, W.-J. Cho, C.-S. Ha, *Mater. Lett.* **2005**, *59*, 2257–2261.
[126] A. Salis, D. Meloni, S. Ligas, M. F. Casula, M. Monduzzi, V. Solinas, E. Dumitriu, *Langmuir* **2005**, *21*, 5511–6.
[127] J. M. Rosenholm, T. Czuryszkiewicz, F. Kleitz, J. B. Rosenholm, M. Lindén, *Langmuir* **2007**, *23*, 4315–4323.
[128] J. M. Rosenholm, M. Lindén, *Chem. Mater.* **2007**, *19*, 5023–5034.
[129] A. Yamaguchi, M. Namekawa, T. Kamijo, T. Itoh, N. Teramae, *Anal. Chem.* **2011**, *83*, 2939–2946.
[130] A. Salis, B. W. Ninham, *Chem. Soc. Rev.* **2014**, *43*, 7358–7377.
[131] A. Salis, D. F. Parsons, M. Boström, L. Medda, B. Barse, B. W. Ninham, M. Monduzzi, *Langmuir* **2010**, *26*, 2484–2490.
[132] J. Kim, R. J. Desch, S. W. Thiel, V. V. Guliants, N. G. Pinto, *J. Chromatogr. A* **2011**, *170*, 6697–6704.
[133] L. Medda, M. F. Casula, M. Monduzzi, A. Salis, *Langmuir* **2014**, *30*, 12996–13004.

[134] M. Lundqvist, C. Cabaleiro-Lago, *J. Colloid Interface Sci.* **2017**, *504*, 78–85.
[135] H. N. Po, N. M. Senozan, *J. Chem. Educ.* **2001**, *78*, 1499–1503.
[136] A. Liese, L. Hilterhaus, *Chem. Soc. Rev.* **2013**, *42*, 6236.
[137] F. Hoffmann, M. Cornelius, J. Morell, M. Fröba, *Angew. Chemie - Int. Ed.* **2006**, *45*, 3216–3251.
[138] M. Vallet-Regí, F. Balas, M. Colilla, M. Manzano, *Prog. Solid State Chem.* **2008**, *36*, 163–191.
[139] S. Sadjadi, M. M. Heravi, *RSC Adv.* **2017**, *7*, 30815–30838.
[140] I. Migneault, C. Dartiguenave, M. J. Bertrand, K. C. Waldron, *Biotechniques* **2004**, *37*, 790–802.
[141] H. Yang, W. Wei, S. Liu, *Spectrochim. Acta - Part A Mol. Biomol. Spectrosc.* **2014**, *125*, 183–188.
[142] R. A. Sheldon, S. van Pelt, *Chem. Soc. Rev.* **2013**, *42*, 6223–6235.
[143] H. Maleki, L. Durães, A. Portugal, *J. Non. Cryst. Solids* **2014**, *385*, 55–74.
[144] V. I. Lozinsky, I. Y. Galaev, F. M. Plieva, I. N. Savina, H. Jungvid, B. Mattiasson, *Trends Biotechnol.* **2003**, *21*, 445–451.
[145] M. B. Majewski, A. J. Howarth, P. Li, M. R. Wasielewski, J. T. Hupp, O. K. Farha, *CrystEngComm* **2017**, *19*, 4082–4091.
[146] K. Liang, J. J. Richardson, C. J. Doonan, X. Mulet, Y. Ju, J. Cui, F. Caruso, P. Falcaro, *Angew. Chemie - Int. Ed.* **2017**, *5005*, 8510–8515.
[147] J. J. Richardson, K. Liang, F. Lisi, M. Björnmalm, M. Faria, J. Guo, P. Falcaro, *Eur. J. Inorg. Chem.* **2016**, *2016*, 4499–4504.
[148] N. Rueda, J. C. S. dos Santos, C. Ortiz, R. Torres, O. Barbosa, R. C. Rodrigues, Á. Berenguer-Murcia, R. Fernandez-Lafuente, *Chem. Rec.* **2016**, *16*, 1436–1455.
[149] P. Lòpez-Serrano, L. Cao, F. Van Rantwijk, R. A. Sheldon, *Biotechnol. Lett.* **2002**, *24*, 1379–1383.
[150] J. L. Paris, M. Colilla, I. Izquierdo-Barba, M. Manzano, M. Vallet-Regí, *J. Mater. Sci.* **2017**, *52*, 8761–8771.
[151] V. Nairi, L. Medda, M. Monduzzi, A. Salis, *J. Colloid Interface Sci.* **2017**, *497*, 217–225.
[152] D. Montes, E. Tocuyo, E. Gonzaĺez, D. Rodriǵuez, R. Solano, R. Atencio, M. A. Ramos, A. Moronta, *Microporous Mesoporous Mater.* **2013**, *168*, 111–120.
[153] J. Liang, Z. Liang, R. Zou, Y. Zhao, *Adv. Mater.* **2017**, *29*, 1–21.
[154] N. Lashgari, A. Badiei, G. M. Ziarani, *Nanochemistry Res.* **2016**, *1*, 127–141.
[155] J. S. Beck, J. C. Vartuli, W. J. Roth, M. E. Leonowicz, C. T. Kresge, K. D. Schmitt, C. T. W. Chu, D. H. Olson, E. W. Sheppard, S. B. McCullen, et al., *J. Am. Chem. Soc.* **1992**, *114*, 10834–10843.
[156] D. Zhao, J. Feng, Q. Huo, N. Melosh, G. Fredrickson, B. Chmelka, G. Stucky, *Science* **1998**, *279*, 548–52.
[157] T. Jesionowski, J. Zdarta, B. Krajewska, *Adsorption* **2014**, *20*, 801–821.
[158] N. Carlsson, H. Gustafsson, C. Thörn, L. Olsson, K. Holmberg, B. Åkerman, *Adv. Colloid Interface Sci.* **2014**, *205*, 339–360.
[159] F. Di Renzo, H. Cambon, R. Dutartre, *Microporous Mater.* **1997**, *10*, 283–286.
[160] P. F. Fulvio, **2005**, 5049–5053.
[161] S.-H. Wu, C.-Y. Mou, H.-P. Lin, *Chem. Soc. Rev.* **2013**, *42*, 3862.
[162] Q. Huo, D. I. Margolese, U. Ciesla, D. G. Demuth, P. Feng, T. E. Gier, P. Sieger, A. Firouzi, B. F. Chmelka, F. Schüth, et al., *Chem. Mater.* **1994**, *6*, 1176–1191.
[163] J. S. Kresge, C.T. , Leonowicz, M.E. , Roth, W.J., Vartuli, J.C., Beck, *Lett. to Nat.* **1992**, *359*, 710–712.
[164] S. Kerkhofs, T. Willhammar, H. Van Den Noortgate, C. E. A. Kirschhock, E. Breynaert, G. Van Tendeloo, S. Bals, J. A. Martens, *Chem. Mater.* **2015**, *27*, 5161–

5169.
[165] P. Yuan, J. Yang, X. Bao, D. Zhao, J. Zou, C. Yu, *Langmuir* **2012**, *28*, 16382–16392.
[166] I. W. Hamley, *Nanotechnology* **2003**, *39*, 39–54.
[167] C. J. Brinker, Y. Lu, A. Sellinger, H. Fan, *Adv. Mater.* **1999**, *11*, 579–585.
[168] S. P. Naik, S. Yamakita, M. Ogura, T. Okubo, *Microporous Mesoporous Mater.* **2004**, *75*, 51–59.
[169] D. Carboni, A. Pinna, H. Amenitsch, M. F. M. F. Casula, D. Loche, L. Malfatti, P. Innocenzi, *Phys. Chem. Chem. Phys.* **2015**, *17*, 10679–86.
[170] P. Innocenzi, L. Malfatti, G. J. a a Soler-Illia, *Chem. Mater.* **2011**, *23*, 2501–2509.
[171] H. Zhang, X. Li, *J. Chem.* **2016**, *2016*, 1–16.
[172] J. Liu, Q. Yang, L. Zhang, D. Jiang, X. Shi, J. Yang, H. Zhong, C. Li, *Adv. Funct. Mater.* **2007**, *17*, 569–576.
[173] P. Schmidt-winkel, W. W. Lukens, D. Zhao, P. Yang, B. F. Chmelka, G. D. Stucky, V. Uni, S. Barbara, *J. Am. Chem. Soc.* **1999**, *121*, 254–255.
[174] J. S. Lettow, Y. J. Han, P. Schmidt-winkel, P. Yang, D. Zhao, G. D. Stucky, J. Y. Ying, **2000**, *4*, 8291–8295.
[175] M. Schoeffel, N. Brodie–Linder, F. Audonnet, C. Alba–Simionesco, *J. Mater. Chem.* **2012**, *22*, 557–567.
[176] O. M. Yaghi, H. Li, *J. Am. Chem. Soc.* **1995**, *117*, 10401–10402.
[177] H. He, H. Han, H. Shi, Y. Tian, F. Sun, Y. Song, Q. Li, G. Zhu, *ACS Appl. Mater. Interfaces* **2016**, *8*, 24517–24524.
[178] Y. Pan, Y. Liu, G. Zeng, L. Zhao, Z. Lai, *Chem. Commun.* **2011**, *47*, 2071.
[179] A. D. Katsenis, A. Puškarić, V. Štrukil, C. Mottillo, P. A. Julien, K. Užarević, M.-H. Pham, T.-O. Do, S. A. J. Kimber, P. Lazić, et al., *Nat. Commun.* **2015**, *6*, 1–8.
[180] K. Liang, C. J. Coghlan, S. G. Bell, C. Doonan, P. Falcaro, *Chem. Commun.* **2016**, *52*, 473–476.
[181] W. Jiang, X. Wang, J. Chen, Y. Liu, H. Han, Y. Ding, Q. Li, J. Tang, *ACS Appl. Mater. Interfaces* **2017**, *9*, 26948–26957.
[182] K. Liang, R. Ricco, C. M. Doherty, M. J. Styles, P. Falcaro, *CrystEngComm* **2016**, *18*, 4264–4267.
[183] X. Wang, J. Shi, S. Zhang, H. Wu, Z. Jiang, C. Yang, Y. Wang, L. Tang, A. Yan, *J. Mater. Chem. B* **2015**, *3*, 6587–6598.
[184] F. Lyu, Y. Zhang, R. N. Zare, J. Ge, Z. Liu, *Nano Lett.* **2014**, *14*, 5761–5765.
[185] W. Ma, Q. Jiang, P. Yu, L. Yang, L. Mao, *Anal. Chem.* **2013**, *85*, 7550–7557.
[186] C. Tudisco, G. Zolubas, B. Seoane, H. R. Zafarani, M. Kazemzad, J. Gascon, P.-L. Hagedoorn, L. Rassaei, *RSC Adv.* **2016**, *6*, 108051–108055.
[187] X. C. Huang, Y. Y. Lin, J. P. Zhang, X. M. Chen, *Angew. Chemie - Int. Ed.* **2006**, *45*, 1557–1559.
[188] K. S. Park, Z. Ni, A. P. Cô Té, J. Y. Choi, R. Huang, F. J. Uribe-Romo, H. K. Chae, M. O 'keeffe, O. M. Yaghi, *Proc. Natl. Acad. Sci. U. S. A.* **2006**, *103*, 10186.
[189] Q. Shi, Z. Chen, Z. Song, J. Li, J. Dong, *Angew. Chemie - Int. Ed.* **2011**, *50*, 672–675.
[190] D. W. Lewis, A. R. Ruiz-Salvador, A. Gomez, L. M. Rodriguez-Albelo, F.-X. Coudert, B. Slater, A. K. Cheetham, C. Mellot-Draznieks, *CrystEngComm* **2009**, *11*, 2272–2276.
[191] C. Baerlocher, L. B. McCusker, in *From Zeolites to Porous MOF Mater. - 40th Anniv. Int. Zeolite Conf.* (Eds.: R. Xu, Z. Gao, J. Chen, W. Yan), Elsevier, **2007**, pp. 657–665.
[192] S. Bhattacharjee, M.-S. Jang, H.-J. Kwon, W.-S. Ahn, *Catal. Surv. from Asia* **2014**, *18*, 101–127.
[193] Y. Pan, D. Heryadi, F. Zhou, L. Zhao, G. Lestari, H. Su, Z. Lai, *CrystEngComm* **2011**, *13*, 6937.
[194] Y.-R. Lee, M.-S. Jang, H.-Y. Cho, H.-J. Kwon, S. Kim, W.-S. Ahn, *Chem. Eng. J.* **2015**, *271*, 276–280.

[195] K. Kida, M. Okita, K. Fujita, S. Tanaka, Y. Miyake, *CrystEngComm* **2013**, *15*, 1794.
[196] T. Hikov, C. A. Schröder, J. Cravillon, M. Wiebcke, K. Huber, *Phys. Chem. Chem. Phys.* **2012**, *14*, 511–521.
[197] O. Delgado-Friedrichs, M. O'Keeffe, O. M. Yaghi, *Acta Crystallogr. Sect. A Found. Crystallogr.* **2006**, *62*, 350–355.
[198] O. Delgado-Friedrichs, M. O'Keeffe, O. M. Yaghi, *Phys. Chem. Chem. Phys.* **2007**, *9*, 1035–1043.
[199] J. T. Hughes, T. D. Bennett, A. K. Cheetham, A. Navrotsky, *J. Am. Chem. Soc.* **2013**, *135*, 598–601.
[200] L. T. L. Nguyen, K. K. A. Le, H. X. Truong, N. T. S. Phan, *Catal. Sci. Technol.* **2012**, *2*, 521–528.
[201] G. Liu, Y. Xu, Y. Han, J. Wu, J. Xu, H. Meng, X. Zhang, *Dalt. Trans.* **2017**, *46*, 2114–2121.
[202] J. Shi, X. Wang, S. Zhang, L. Tang, Z. Jiang, *J. Mater. Chem. B* **2016**, *4*, 2654–2661.
[203] S. Jemli, D. Ayadi-Zouari, H. Ben Hlima, S. Bejar, *Crit. Rev. Biotechnol.* **2016**, *36*, 246–258.
[204] R. Fernandez-Lafuente, *Molecules* **2017**, *22*, 1–5.
[205] W.-L. Liu, N.-S. Yang, Y.-T. Chen, S. Lirio, C.-Y. Wu, C.-H. Lin, H.-Y. Huang, *Chem. - A Eur. J.* **2015**, *21*, 115–119.
[206] S. S. Nadar, V. K. Rathod, *Enzyme Microb. Technol.* **2018**, *108*, 11–20.
[207] L.-Z. Cheong, Y. Wei, H. Wang, Z. Wang, X. Su, C. Shen, *J. Nanoparticle Res.* **2017**, *19*, 280.
[208] X. Zhang, Y. Zeng, A. Zheng, Z. Cai, A. Huang, J. Zeng, X. Liu, J. Liu, *Microchim. Acta* **2017**, *184*, 1933–1940.
[209] Y. Wang, C. Hou, Y. Zhang, F. He, M. Liu, X. Li, *J. Mater. Chem. B* **2016**, *4*, 3695–3702.
[210] F.-K. Shieh, S.-C. Wang, C.-I. Yen, C.-C. Wu, S. Dutta, L.-Y. Chou, J. V. Morabito, P. Hu, M.-H. Hsu, K. C. W. Wu, et al., *J. Am. Chem. Soc.* **2015**, *137*, 4276–4279.
[211] Y. Du, J. Gao, L. Zhou, L. Ma, Y. He, Z. Huang, Y. Jiang, *Chem. Eng. J.* **2017**, *327*, 1192–1197.
[212] J. Huo, J. Aguilera-Sigalat, S. El-Hankari, D. Bradshaw, *Chem. Sci.* **2015**, *6*, 1938–1943.
[213] J. Cui, Y. Feng, T. Lin, Z. Tan, C. Zhong, S. Jia, *ACS Appl. Mater. Interfaces* **2017**, *9*, 10587–10594.
[214] L. Wen, A. Gao, Y. Cao, F. Svec, T. Tan, Y. Lv, *Macromol. Rapid Commun.* **2016**, *37*, 551–557.
[215] Y. Yin, C. Gao, Q. Xiao, G. Lin, Z. Lin, Z. Cai, H. Yang, *ACS Appl. Mater. Interfaces* **2016**, *8*, 29052–29061.
[216] H. Cheng, L. Zhang, J. He, W. Guo, Z. Zhou, X. Zhang, S. Nie, H. Wei, *Anal. Chem.* **2016**, *88*, 5489–5497.
[217] P. Chulkaivalsucharit, X. Wu, J. Ge, *RSC Adv.* **2015**, *5*, 101293–101296.
[218] V. Mamaeva, C. Sahlgren, M. Lindén, *Adv. Drug Deliv. Rev.* **2013**, *65*, 689–702.
[219] F. Sevimli, A. Yilmaz, *Microporous Mesoporous Mater.* **2012**, *158*, 281–291.
[220] A. Salis, M. Fanti, L. Medda, V. Nairi, F. Cugia, M. Piludu, V. Sogos, M. Monduzzi, *ACS Biomater. Sci. Eng.* **2016**, *2*, 741–751.
[221] J. Gao, Y. Wang, Y. Du, L. Zhou, Y. He, L. Ma, L. Yin, W. Kong, Y. Jiang, *Chem. Eng. J.* **2017**, *317*, 175–186.
[222] Z. Ali, L. Tian, B. Zhang, N. Ali, M. Khan, Q. Zhang, *Enzyme Microb. Technol.* **2017**, *103*, 42–52.
[223] Z. Ali, L. Tian, P. Zhao, B. Zhang, N. Ali, M. Khan, Q. Zhang, *J. Mol. Catal. B Enzym.* **2016**, *134*, 129–135.

[224] M. Karimi, *Biocatal. Agric. Biotechnol.* **2016**, *8*, 182–188.
[225] A. Sadighi, S. F. Motevalizadeh, M. Hosseini, A. Ramazani, L. Gorgannezhad, H. Nadri, B. Deiham, M. R. Ganjali, A. Shafiee, M. A. Faramarzi, et al., *Appl. Biochem. Biotechnol.* **2017**, *182*, 1371–1389.
[226] C. M. Maroneze, G. P. dos Santos, V. B. de Moraes, L. P. da Costa, L. T. Kubota, *Biosens. Bioelectron.* **2016**, *77*, 746–751.
[227] N. Balistreri, D. Gaboriau, C. Jolivalt, F. Launay, *J. Mol. Catal. B Enzym.* **2016**, *127*, 26–33.
[228] P. Majumdar, A. Y. Khan, R. Bandyopadhyaya, *Biochem. Eng. J.* **2016**, *105*, 489–496.
[229] M. Kalantari, M. Yu, Y. Yang, E. Strounina, Z. Gu, X. Huang, J. Zhang, H. Song, C. Yu, *Nano Res.* **2017**, *10*, 605–617.
[230] M. Babaki, M. Yousefi, Z. Habibi, M. Mohammadi, P. Yousefi, J. Mohammadi, J. Brask, *Renew. Energy* **2016**, *91*, 196–206.
[231] J. Pang, G. Zhou, R. Liu, T. Li, *Mater. Sci. Eng. C* **2016**, *59*, 35–42.
[232] W. Xie, X. Zang, *Food Chem.* **2016**, *194*, 1283–1292.
[233] S. Hüttner, M. Zezzi Do Valle Gomes, L. Iancu, A. Palmqvist, L. Olsson, *Bioresour. Technol.* **2017**, *239*, 57–65.
[234] A. Arca-Ramos, V. V. Kumar, G. Eibes, M. T. Moreira, H. Cabana, *Environ. Sci. Pollut. Res.* **2016**, *23*, 8929–8939.
[235] Y. Yang, Y. Xu, Y. Yang, H. Yang, H. Yuan, Y. Huang, X. Liu, *Russ. J. Phys. Chem. A* **2016**, *90*, 2044–2054.
[236] H. Li, S. Li, P. Tian, Z. Wu, Z. Li, *Molecules* **2017**, *22*, 377.
[237] P. Corell Escuin, A. García-Bennett, J. V. Ros-Lis, A. Argüelles Foix, A. Andrés, *Food Chem.* **2017**, *217*, 360–363.
[238] J. Li, L. S. Li, L. Xu, *Mater. Lett.* **2017**, *193*, 67–69.
[239] A. Y. Khan, S. B. Noronha, R. Bandyopadhyaya, *Adv. Powder Technol.* **2016**, *27*, 85–92.
[240] H. Dai, S. Ou, Z. Liu, H. Huang, *Carbohydr. Polym.* **2017**, *169*, 504–514.
[241] J. Gao, H. Yu, L. Zhou, Y. He, L. Ma, Y. Jiang, *Biochem. Eng. J.* **2017**, *117*, 92–101.
[242] J. Li, L. S. Li, L. Xu, *Microporous Mesoporous Mater.* **2016**, *231*, 147–153.
[243] L. Boldon, F. Laliberte, L. Liu, *Nano Rev.* **2015**, *6*, 25661.
[244] H. Schnablegger, Y. Singh, *The SAXS Guide: Getting Acquainted with the Principles*, **2013**.
[245] H. Ma, K. Shieh, T. X. Qiao, *Nat. Sci.* **2006**, *4*, 14–22.
[246] D. McMullan, *Scanning* **1995**, *17*, 175–185.
[247] S. Brunauer, P. H. Emmett, E. Teller, *J. Am. Chem. Soc.* **1938**, *60*, 309–319.
[248] K. S. W. Sing, *Pure Appl. Chem.* **1982**, *54*, 2201–2218.
[249] C. M. Earnest, *Anal. Chem.* **1984**, *56*, 1471–1486.
[250] Y. Hu, H. Kazemian, S. Rohani, Y. Huang, Y. Song, *Chem. Commun. (Camb).* **2011**, *47*, 12694–6.
[251] M.M.Bradford, *Anal. Biochem.* **1976**, *72*, 248–254.
[252] F. Hasan, A. A. Shah, A. Hameed, *Biotechnol. Adv.* **2009**, *27*, 782–98.
[253] B. R. E. Childs, W. G. Bardsley, *Biochem. J.* **1975**, *145*, 93–103.